Université de Neuchâtel
Institut de Microtechnique

Thin film coated submicron gratings: theory, design, fabrication and application

Thèse

Présentée à la Faculté des sciences
pour obtenir le grade docteur ès sciences

par

Claus Heine

Neuchâtel, novembre 1996

IMPRIMATUR POUR LA THÈSE

Réseaux de diffraction couverts de couches minces :
théorie, conception, fabrication et application.

de M. Claus Heine

UNIVERSITÉ DE NEUCHÂTEL

FACULTÉ DES SCIENCES

La Faculté des sciences de l'Université de Neuchâtel sur le rapport des membres du jury,

Messiers R. Dändliker (directeur de thèse), O. Besson, J.-P. Turunen (Finlande), R. Morf (Zürich) et M. Gale (Zürich)

autorise l'impression de la présente thèse.

Neuchâtel, le 17 décembre 1996

Le doyen:

R. Dändliker

R. Dändliker

IN MEMORIAM

Alena Heine

1993 - 1995

ABSTRACT

The realization of new applications of submicron grating structures requires efficient theoretical methods and elaborate fabrication techniques. In this work rigorous diffraction theory for one-dimensional gratings has been investigated and optimization techniques, based on methods used in thin film optics, have been developed. Submicron gratings embossed in polycarbonate have been fabricated and characterized. This includes transmission measurements which are in good agreement with theoretical calculations. Designs for a wide range of optical filters, which lead to improved optical and mechanical properties, are presented. This has been demonstrated for broadband antireflection structures for solar energy applications, based on MgF_2-coated gratings.

LIST OF PUBLICATIONS

This thesis is an overview of the author's work in the field of submicron grating structures for optical applications. It consists of a detailed description of the methods developed and used for design and fabrication. The thesis includes the author's publications in this field.

I C. Heine and R.H. Morf, "Legendre- and Chebychev polynomial expansions, optimized for rigorous calculations of stacks of lamellar gratings," to be submitted to *J. Opt. Soc. Am. A.*

II C. Heine and R.H. Morf, "Submicrometer gratings for solar energy applications," *Appl. Opt.* **34**, 2476-2482, (1995).

III C. Heine, R.H. Morf, and M.T. Gale, "Coated submicron gratings for broadband antireflection in solar energy applications," *J. Mod. Opt.* **43**, 1371-1377, (1996).

IV C. Heine, R.H. Morf and M.T. Gale, "Submicron gratings with dielectric overcoat: performance and stability," in *Diffractive Optics and Micro-Optics: Testing & Evaluation,* OSA Topical Meeting, 304-307, April 29-May 2, 1996, Boston, Massachusetts, USA.

Throughout the overview, these papers will be referred to by Roman numerals.

CONTENTS

1. Introduction

> 'In 1873, the work of James Clerk Maxwell '*A Treatise on Electricity and Magnetism*' [1] was published, and in his system of equations we have all the basic theory for the analysis of thin-film optical problems.' [2].

It took more than 50 years until a rapid development in this field marked the beginnings of modern thin-film optical coatings. According to [2] '*the most important factor in this sudden expansion of thin film optical coatings was the manufacturing process*'. Since then a tremendous amount of work has been dedicated to the design and the fabrication of thin film optical filters.

In the same system of Maxwell's equations we have all the basic theory for the analysis of submicron grating diffraction problems, and we are in a period of development, in which processes for mass-production of devices with such small structures are being realized.

Parallel to this experimental progress, extensive work has been put in the theoretical investigation of diffraction gratings [3-8]. It is only recently that the main problems, such as poor calculation-efficiency and numerical instabilities [9] could be overcome [10, 11]. It is now possible to employ methods for the design and fabrication of complicated grating structures such as thin-film coated surface gratings or microstructured thin films.

The background of the present thesis is the search for (diffraction grating-) designs to solve problems, for which the performance of thin film solutions is not sufficient or their fabrication is too expensive. This work provides efficient methods to analyze and optimize such structures in theory. It does not pretend to present an overview of the various, more or less efficient methods for solving the diffraction problem. It is exclusively based on the rigorous method developed by R. Morf [10]. New is the implementation of Morf's method for arbitrary one-dimensional gratings, including thin film coated structures. In this thesis we investigate some basic convergence properties of the theory. This leads to an increased efficiency of the numerical calculations.

Design, fabrication and characterization of coated grating structures are described, mainly based on well established methods as they are known in thin-film optics. These methods are used to investigate theoretically and experimentally new applications for thin-film submicron grating structures.

The theory is described in detail in chapter 2, starting from Maxwell's equations. Rigorous diffraction theory has to be used in the regime, where the structural feature size is of the order of wavelength of light. We also provide an instructive physical picture for the transition from the rigorous regime to the scalar regime (low-frequency gratings) and to the regime, where effective medium theory can be applied (dielectric high-frequency gratings).

In thin film optics, many efficient design methods, both analytical and statistical, have been developed. In chapter 3 we show how some of these methods can be useful for the optimization of microstructured thin films. Based on these techniques we optimize the profile for a broadband antireflection surface grating as well as the layer thicknesses of a structured 'quarter-wave stack'.

In chapter 4 we compare theoretical calculations to experimental reality. Our investigations are based on grating structures embossed polycarbonate. The fabrication of such surface structures, using holographic exposure and hot embossing is well established and documented [12-14]. We therefore keep the description of the fabrication short and focus more on the experimental analysis of the grating profile. We compare theoretical and experimental results for transmission spectra of uncoated and coated gratings.

In chapters 2 to 4 the basic instruments for efficient design methods, leading to realistic submicron grating structures, have been prepared. In chapter 5 these instruments are used to design devices for various applications. Some of them, such as broadband antireflection structures for solar energy applications, asymmetric gratings and superimposed antireflection structures are investigated experimentally.

We conclude in chapter 6 and list the devices we investigated, as well as some of their main properties. With a short outlook we try to explain, what we expect for the further development of coated grating structures and microstructured thin films.

2. Rigorous theory for one-dimensional diffraction gratings

The solution of diffraction problems is a challenge whenever the dimensions of the diffracting objects are of the same order of magnitude as the wavelength of the diffracted fields. Approximations, assuming very small or very large objects are not valid any more and resonance phenomena are likely to appear.

In the case of electromagnetic waves, Maxwell's equations have to be solved directly. Only for very special geometries it is possible to find the analytical solution of the diffraction problem. In general, numerical methods have to be used. We call a calculation method rigorous, if for the investigated problem, within the electromagnetic theory, the possible accuracy is limited only by numerical restrictions.

The rigorous diffraction theory we investigate is based on Ref. [10]. We compare this to the method of finite elements. Different variations on Morf's method are tested, which leads us to simple rules, how to maximize the benefits from the advantageous convergence properties of the method.

In this chapter we give a detailed description of the method we investigated. The different sections contain the following:

1. The basic wave-equations describing the diffraction problem are well known. However their derivation, starting from Maxwell's equations is used to introduce the restrictions and to define the problem completely.

2. We approximate the grating with a stack of lamellar grating layers. This is the reason why the method is rigorous only for lamellar stacks. The modal expansion of the fields inside each layer, found by solving the Helmholtz-equation, is then rigorous.

3. Investigation of the eigenmodes and the eigenvalues of the grating layers leads to an instructive description of the transition to regimes, where approximations, such as effective medium theory and scalar theory, can be applied.

4. Matching the fields between the lamellar grating layers is the final step to solve the diffraction problem.

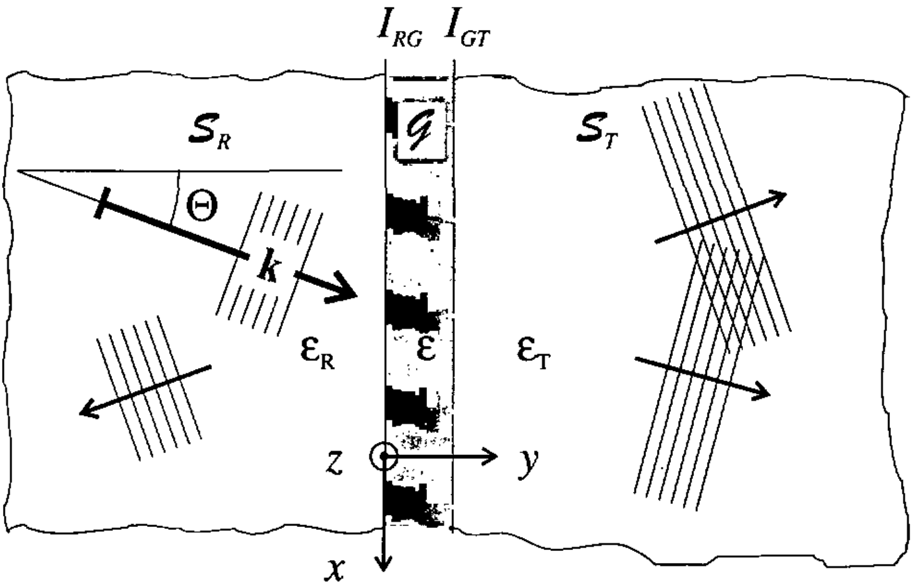

Fig. 1. Geometry of the diffraction problem.

2.1. Grating diffraction problem

Given are two optical homogeneous halfspaces $\mathcal{S}_R$ and $\mathcal{S}_T$, separated by a grating region $\mathcal{G}$. The situation is illustrated in Fig. 1. An electromagnetic wave is incident from $\mathcal{S}_R$ onto the grating region. Part of the light is transmitted into $\mathcal{S}_T$ (where T stands for transmitted) and part of the light is reflected back to $\mathcal{S}_R$ (where R stands for reflected). $\mathcal{S}_R$ and $\mathcal{G}$ are separated by the interface I_{RG}. The interface I_{GT} separates the grating region $\mathcal{G}$ from $\mathcal{S}_T$.

The general grating diffraction problem investigates the electromagnetic field in both halfspaces as well as in the grating region with arbitrary grating features. In this work we do not investigate the problem with such generality and we try to motivate some of the restrictions we introduce.

It is instructive to start from Maxwell's equations in macroscopic media:

$$\nabla \times \mathcal{E} = -\partial_t \mathcal{B} \tag{1}$$

$$\nabla \times \mathcal{H} = \mathcal{J} + \partial_t \mathcal{D} \tag{2}$$

$$\nabla \mathcal{D} = \rho \tag{3}$$

$$\nabla \mathcal{B} = 0. \tag{4}$$

Here $\mathcal{E}$ is the macroscopic electric field, $\mathcal{H}$ is the magnetic field, $\mathcal{J}$ is the current density, $\mathcal{D}$ is the displacement and $\mathcal{B}$ is the macroscopic magnetic induction. The charge density ρ and the current density are macroscopic averages of the charge and current densities in the medium. The averages are performed over a "*volume large compared to the volume occupied by a single atom or molecule*" [15]. Although it is possible today to fabricate structures having feature sizes as small as a molecule, most of the application relevant devices do not include such structures.

For the material equations we set:

$$\mathcal{D} = \varepsilon_r \, \mathcal{E} \tag{5}$$

$$\mathcal{J} = \sigma_0 \, \mathcal{E} \tag{6}$$

$$\mathcal{B} = \mu \, \mathcal{H}. \tag{7}$$

Here ε_r is the real dielectric constant, μ is the permeability and σ_0 is the conductivity. In the equations above it is already assumed, that we only investigate isotropic materials with no nonlinearities.

Using (1) and (2) together with the material equations we can write for the electric field

$$\nabla \times \nabla \times \mathcal{E} = -\mu \sigma_0 \partial_t \mathcal{E} - \mu \varepsilon_r \partial_t^2 \mathcal{E}. \tag{8}$$

We assume the permeability to be equal to one, neglecting magnetic effects, and proceed with a separation Ansatz for the time

$$\mathcal{E}(\mathbf{x}, t) = \mathbf{E}(\mathbf{x}) e(t), \tag{9}$$

where **x** is the space vector and t is the time.

This leads to the well known harmonic fields with

$$e(t) = \exp(\pm i \omega t), \tag{10}$$

so that equation (8) becomes

$$\nabla \times \nabla \times \mathbf{E}(\mathbf{x}) = \frac{\omega^2}{c^2}\left\{\varepsilon_r \mp i \frac{\sigma_0}{\omega \varepsilon_r}\right\}\mathbf{E}(\mathbf{x}). \tag{11}$$

At this point we introduce the complex dielectricity

$$\varepsilon = \varepsilon_r + i \frac{\sigma_0}{\omega \varepsilon_r}. \tag{12}$$

Note that this fixes the sign in equation (10) as well as in equation (11). Both, ε_r and σ_0 are constant in time but vary in space. The dielectricity will be a complex function, only depending on $\mathbf{x}$.

Inserting this in equation (11) and application of some vector identities leads to

$$\Delta(\mathbf{E}(\mathbf{x})) + \nabla\left(\frac{\mathbf{E}(\mathbf{x})\nabla\varepsilon(\mathbf{x})}{\varepsilon(\mathbf{x})}\right) + k_0^2 \varepsilon(\mathbf{x})\mathbf{E}(\mathbf{x}) = 0, \tag{13}$$

where k_0 is the vacuum wavenumber defined as $k_0 = \omega/c$, when c is the velocity of light in free space.

For the magnetic field similar arguments lead to the equation

$$\Delta(\mathbf{H}(\mathbf{x})) + \left(\frac{\nabla\varepsilon(\mathbf{x})}{\varepsilon(\mathbf{x})} \times \nabla \times \mathbf{H}(\mathbf{x})\right) + k_0^2 \varepsilon(\mathbf{x})\mathbf{H}(\mathbf{x}) = 0, \tag{14}$$

where we defined $\mathbf{H}(\mathbf{x})$ by using the separation Ansatz

$$\mathcal{H}(\mathbf{x}, t) = \mathbf{H}(\mathbf{x}) e(t). \tag{15}$$

It is now necessary to specify the properties of the incident light. In the two homogeneous halfspaces the solutions of equations (13) and (14) can be expanded in plane waves. Let the light incident be a plane wave which is given by

$$\mathbf{E}_{inc}(\mathrm{x}) = \left(\frac{\mathbf{k}\times\mathbf{e}}{|\mathbf{k}\times\mathbf{e}|}\right) E\exp(i\mathbf{kx}), \tag{16 a}$$

where **e** is a unity vector and **k** defines the direction of propagation. The absolute value of **k** is given by

$$\mathrm{k} = \frac{2\pi}{\sqrt{\varepsilon_R}\lambda_0}, \tag{17}$$

where λ_0 is the vacuum wavelength and ε_R is the dielectric constant in $\mathcal{S}_R$. The vector **k** and the normal on the interface I_{RG} define the plane of incidence (see Fig. 1).

We choose a Cartesian coordinate-system and place the origin in the interface I_{RG}. The y-axis is parallel to the normal on the interface I_{RG}, pointing in the direction of the halfspace of transmission. The z-axis is chosen to be normal on the plane of incidence. Therefore **k** has no component in the z-direction. The incident plane wave (16 a) can then be written as

$$\mathbf{E}_{inc}(\mathbf{x}) = E_s\mathbf{e}_z\exp(i\mathbf{kx}) + E_p\left(\frac{\mathbf{k}}{|\mathbf{k}|}\times\mathbf{e}_z\right)\exp(i\mathbf{kx}). \tag{16 b}$$

Here E_s and E_p are the complex amplitudes of the corresponding s- and p-polarized electrical field components of the incident wave and $\mathbf{e}_z$ is the unity vector in z-direction.

It is difficult to find the solutions of Maxwell's equations inside the grating region. With general $\varepsilon(\mathbf{x})$ equations (13) and (14) are rather complicated to solve, due to the different components of the fields being coupled. Responsible is the term

$$\nabla\left(\frac{\mathbf{E}\nabla\varepsilon}{\varepsilon}\right) = \nabla\left[\frac{1}{\varepsilon}\left(E_x\partial_x\varepsilon + E_y\partial_y\varepsilon + E_z\partial_z\varepsilon\right)\right] \tag{18}$$

in equation (13).

If we restrict ourselves to one-dimensional gratings and nonconical incidence,

then $$\varepsilon(\mathbf{x}) = \varepsilon(x,y) \qquad \forall\,\mathbf{x}, \tag{19}$$

and the term $E_z\,\partial_z\varepsilon$ always vanishes and s- and p-polarization are decoupled.

The incident plane wave can then be written as

$$\mathbf{E}_{inc}(\mathbf{x}) = E_z\mathbf{e}_z\exp(i\mathbf{kx}) + (\mathbf{k}\times H_z\mathbf{e}_z)\exp(i\mathbf{kx}). \tag{20}$$

It is therefore sufficient to find the solutions of equations (13) and (14) for the z-components. This is of advantage as we only have to calculate with fields with tangential components at all interfaces, and the boundary conditions are then particularly easy to handle.

Equation (13) reduces to

$$\partial_x^2 E_z(x,y) + \partial_y^2 E_z(x,y) + k_0^2\varepsilon(x,y)E_z(x,y) = 0, \tag{21}$$

and equation (14) can be written as

$$\begin{aligned}\partial_x^2 H_z(x,y) + \partial_y^2 H_z(x,y) - \frac{1}{\varepsilon(x,y)}\left(\partial_x\varepsilon(x,y)\partial_x H_z(x,y)\right)\\ - \frac{1}{\varepsilon(x,y)}\left(\partial_y\varepsilon(x,y)\partial_y H_z(x,y)\right) + k_0^2\varepsilon(x,y)H_z(x,y) = 0\,.\end{aligned} \tag{22}$$

Here we introduce the grating period. The question whether rigorous calculations have to be performed is connected to this parameter in combination with the wavelength of the incident light. The periodicity of the grating is chosen by the relation

$$\varepsilon(x+\Lambda, y) = \varepsilon(x,y),$$

where Λ is the grating period.

2.2. Separation of the variables and solution of the Helmholtz equation

In some practical cases the modulation of the dielectricity is realized by using diffusion effects as for example ion exchange [16, 17]. Here the dielectricity is a continuous periodic function of x, and for solving equation (13) it is useful to expand the x-dependent functions in Fourier series. However, in most cases the gratings are fabricated by some etching, embossing and coating technique.

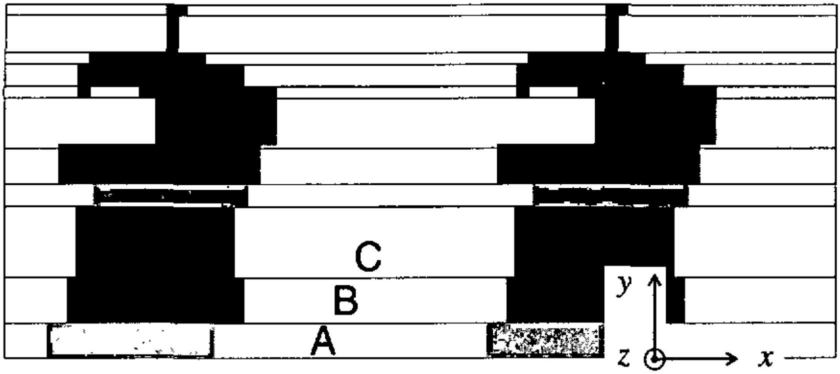

Fig. 2. Approximation of the grating region $\mathcal{G}$ with a stack of lamellar gratings.

Therefore, for fixed y, the dielectric function will be piecewise constant in x and a different approach, as described in [10], is expected to have improved convergence properties.

Throughout this work we will use this method of high order polynomial expansions. We will approximate the grating region by slicing it in layers A, B, C, ... The approximation is illustrated in Fig. 2.

The dielectric function inside each layer is assumed to have no y-dependence

$$\varepsilon(x,y) = \varepsilon^B(x) \qquad \forall \quad y \in \text{layer B}. \tag{23}$$

Suppose B(x,y) is a solution of equation (21) or equation (22) in layer B

$$\mathrm{B}(\mathrm{x},\mathrm{y}) \in \{E_z, H_z\}, \tag{24}$$

then

$$\partial_x^2 \mathrm{B}(x,y) + \partial_y^2 \mathrm{B}(x,y) - \frac{\delta_{pol\,H}}{\varepsilon^B(x)} \left(\partial_x \varepsilon^B(x) \partial_x \mathrm{B}(x,y)\right) + k_0^2 \varepsilon^B(x) \mathrm{B}(x,y) = 0\,. \tag{25}$$

The $\delta_{pol\,H}$ denotes the Kronecker symbol which is zero for the case of E-polarization and one for the case of H-polarization.

Now we apply a separation Ansatz

$$\mathrm{B}(x,y) = B(x)b(y), \tag{26}$$

which leads to

$$\partial_x^2 B(x) + \frac{\delta_{pol\,H}}{\varepsilon^B(x)}\left(\partial_x \varepsilon^B(x)\partial_x B(x)\right) + k_0^2 \varepsilon^B(x)B(x) = \mu^B B(x) \tag{27}$$

and
$$\partial_y^2 b(y) = -\mu^B b(y). \tag{28}$$

The eigenfunctions $B_m(x)$ and eigenvalues μ^B of equation (27) can be found in the following way: We know that $\varepsilon^B(x)$ is a piecewise constant function of x. Throughout this work an interval I_D of constant dielectric properties will be called domain D. The first or at least the second derivatives of the eigenfunctions are discontinuous functions at the boundaries of these domains. Expansion of these functions in terms of analytic functions over the complete period therefore leads to a Gibbs phenomenon [18]. For example if the Fourier basis is used for the expansion of the eigenfunctions of equation (27), the discontinuities are not treated correctly and the eigenvalues converge only algebraically to the exact eigenvalues.

However, inside each domain the fields are infinitely many times differentiable. Approximating the eigenfunctions within each domain with an expansion of orthogonal polynomials P_l, according to

$$B_m(x) = \sum_{l=0}^{M_D^B} b_{l,m}^D P_l(\xi(x)) \qquad x \in I_D, \tag{29}$$

leads to exponential convergence of the approximations to the exact eigenfunctions, if the correct boundary conditions between two adjacent domains are imposed. The approximation is illustrated in Fig. 3.

In expansion (29), $M^B{}_D$ is the order of the expansion in each domain. Aspects concerning this expansion are discussed in paper I. We only review some of the important results: We are free in the choice of the order of expansion in each domain. This has the advantage, that the spatial resolution within each domain can be adjusted independently. However, there is the danger to choose a very accurate description in one domain while the approximation in the other domain is rather poor.

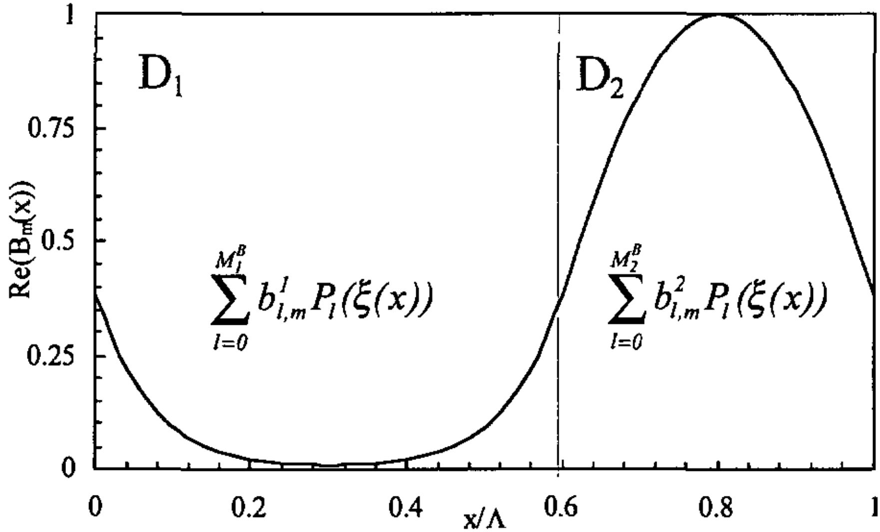

Fig. 3. In each domain we expand the eigenfunction $B_m(x)$ in orthogonal polynomials. The highest two orders are used for matching the functions at the boundaries of the domains according to the boundary conditions. Therefore no Gibbs phenomenon appears and the approximation exhibits exponential convergence.

As shown in paper I for dielectric gratings and normal incidence, the best way to distribute the expansion orders over the domains of the grating layer is given by

$$M_D^B(p) = \max\left\{\sqrt{k_0^2\varepsilon_D^B + p^2}\,\Delta x_D, \frac{\sqrt{k_0^2\varepsilon_{\max}^B + k_0^2\varepsilon_D^B}}{2}\Delta x_D\right\}. \tag{30}$$

Hereby p is a parameter that determines the order of approximation in the layer, $\varepsilon^B{}_{max}$ is the largest dielectricity in layer B and Δx_D is the width of the domain.

We have the possibility to subdivide the homogeneous domains in further subdomains. We could increase their number and fix the polynomial order within the subdomains. This corresponds to a method of finite elements. However, additional subdomains turn out to be disadvantageous in view of the convergence properties of the eigenfunctions. For purely dielectric gratings it is best to use Legendre polynomials as an orthogonal set. For metallic gratings it can be an advantage to use Chebyshev polynomials in the metallic domains. This is shown in paper I, where the convergence properties of the eigenvalues are investigated.

At the boundary x_D of the domains we have to fulfil the boundary conditions

$$B(x_D^-) = B(x_D^+) \tag{31}$$

and $$\left(\frac{1}{\varepsilon_D^B}\right)^{\delta_{pol\,H}} \partial_x B(x)\bigg|_{x_D^-} = \left(\frac{1}{\varepsilon_{D+1}^B}\right)^{\delta_{pol\,H}} \partial_x B(x)\bigg|_{x_D^+}. \tag{32}$$

In addition we have two equations due to the pseudo-periodicity of the Blochfunctions $B(x)$. We insert the expansion (29) in equation (27) and use the orthogonal properties of the polynomials. As a result we have as many equations as we have unknowns and the eigenvalue problem can be solved. A more detailed description is given in [10].

Once the eigenvalue problem is solved we are allowed to write for each domain D and for each eigenfunction

$$\partial_x^2 B_m(x) + \left(k_0^2 \varepsilon_D^B - \mu_m^B\right) B_m(x) = 0, \tag{33}$$

where m denotes the number of the eigenfunction.

It is instructive to investigate the behaviour of the solutions of this equations. In paper I this was done in order to find the criterion (30). In the following section we will investigate approximations such as effective medium theory and scalar theory.

2.3. Approximations for very high and very low frequency gratings

For normal incident light, inside each domain (D) the eigenfunctions have the form

$$B_m(x) = B_{si} \sin\left(\sqrt{k_0^2 \varepsilon_B^D - \mu_m^B}\, x\right) + B_{co} \cos\left(\sqrt{k_0^2 \varepsilon_B^D - \mu_m^B}\, x\right) \quad \forall\, x \in D, \tag{34}$$

as can be seen from equation (33). These eigenfunctions have to fulfil the boundary conditions at the interfaces of the different domains. This is performed by the complexe amplitudes B_{si} and B_{co}. Therefore, in the case of dielectric gratings the maximum eigenvalue μ_1^B cannot be larger than $k_0^2 \varepsilon^B_{max}$, because with larger eigenvalues the corresponding solutions would be hyperbolic functions in every domain. It would then not be possible any more to match the functions at the domain boundary in the required way.

Ultrahigh-frequency gratings

Zero order gratings with a grating period much smaller than the wavelength of light ($\Lambda << \lambda$) only have one propagating mode. They can be used to design and fabricate artificial index materials [19]. Theoretically such gratings can be modelled by effective medium theory [20]. Here the grating region is treated as a homogeneous dielectric layer with an artificial index n_{art}. We try to explain this in the following way:

Suppose a plane wave (propagating in y-direction, normal incidence) falls on a dielectric film with index of refraction n_{art}. The field due to the plane wave inside the dielectric film still is not x- or z-dependent and propagates according to its wavenumber $k_0 n_{art}$. For zero order gratings, we know that the wavenumber for the (only) propagating mode inside the grating is given by μ_1, as can be seen from equation (28). Therefore, we define the artificial dielectric index of refraction as

$$n_{art} = \frac{\sqrt{\mu_1}}{k_0}. \tag{35}$$

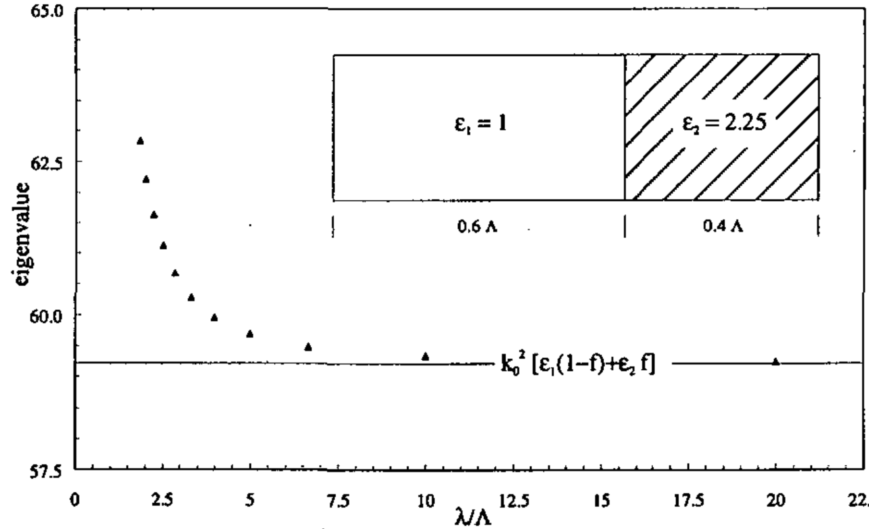

Fig. 4a. Largest eigenvalue as a function of reduced wavelength for a dielectric grating layer with two domains. The inlay shows the geometry of the grating layer. Note that we keep the wavelength constant and decrease the grating period.

The symbols in Fig. 4a indicate the largest eigenvalue of a lamellar grating layer with two domains as a function of the reduced wavelength λ/Λ. The first domain has a dielectric constant of $\varepsilon_1 = 1$ and a width of $\Delta x_1 = 0.6\Lambda$, the second domain has a dielectric constant of $\varepsilon_2 = 2.25$ and a relative width of $\Delta x_2 = 0.4\Lambda$ (cf. Fig 4a). The relative width $f = \Delta x_2/\Lambda$ is known as the duty-cycle of the grating structure. Please note that for $\lambda/\Lambda \to \infty$ the eigenvalue approximates a constant. This constant is equal to $k_0\varepsilon_{art}$, when ε_{art} is calculated according to

$$\varepsilon_{art} = (1-f)\varepsilon_1 + f\varepsilon_2, \tag{36}$$

using zero order effective medium theory for E-polarized light. We conclude that the propagation inside the high frequency grating can be described as propagation in a thin film with an artificial index.

The diffraction angles of a one-dimensional grating structure for nonconical incidence are give by the grating equation

$$n_i \sin\Theta_i - n_e \sin\Theta_e = m\frac{\lambda}{\Lambda}, \tag{37}$$

where n_i is the refractive index of the material filling the halfspace of incidence and Θ_i is the angle of incidence. n_e and Θ_e are the corresponding values for the transmitted or reflected light. The integer m denotes the diffraction order. The propagating mode in the zero order gratings is connected to $m = 0$. Therefore, Snell's law is fulfilled for this artificial thin film layer as well.

It remains to show that the eigenfunction $B_1(x)$, corresponding to the eigenvalue μ_1, describes a plane wave inside the grating layer, i.e. the amplitude is approximately a constant. Once again investigating equation (34), we see that with a smaller grating period the domains decrease in size, and only a small part of the hyperbolic or trigonometric functions is relevant. As this interval of definition becomes smaller the oscillation amplitude of the eigenfunction has to become smaller, because only then there is the possibility of matching the boundary conditions. This is shown in Fig. 4b for four different ratios between wavelength

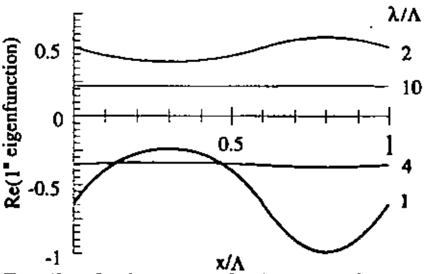

Fig. 4b. Real part of the eigenfunction connected to the eigenvalue in Fig. 4a. for four different grating periods.

and period. As expected, for large reduced wavelengths λ/Λ the eigenfunction becomes a constant and the incoming plane wave couples the same way to this mode as it does for a thin film.

Gratings in the scalar regime

In contrast to zero order gratings, gratings with a period much larger than the wavelength of light ($\Lambda >> \lambda$) have many propagating modes. The properties of such gratings can be described with scalar theory. A detailed description of the transition to a scalar theory in general within the theory of diffraction is given in [21]. There are some publications discussing the limits of scalar diffraction theory for diffraction gratings [22, 23] but little is said about the physical background.

In Fig. 5 we plotted the first hundred eigenvalues of a dielectric lamellar grating as described above for a reduced wavelength of $\lambda/\Lambda = 0.025$. As we said before, the eigenvalues have an upper bound. Therefore, all positive eigenvalues, connected to propagating modes, are in the interval $[0, k_0^2\varepsilon^B_{max}]$. In this case $\varepsilon^B_{\max}$ is equal to the dielectric constant in the second domain.

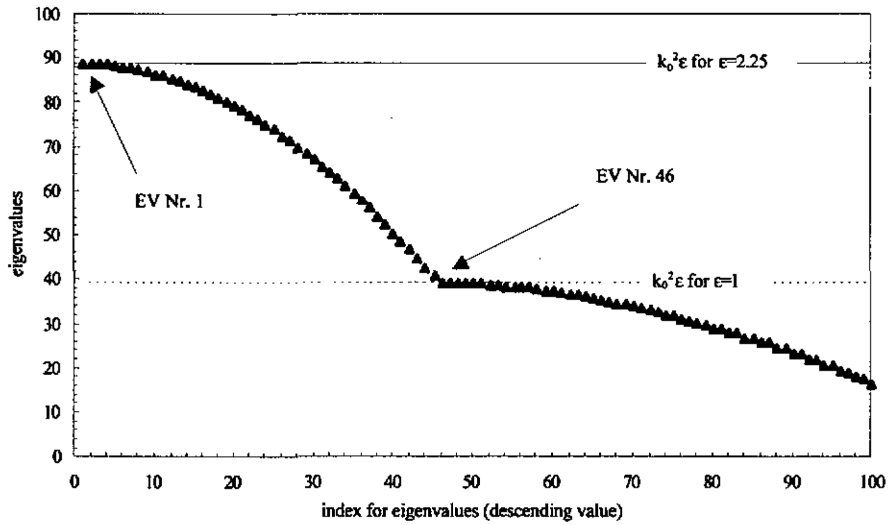

Fig. 5. Eigenvalues for a grating in the scalar regime (λ/Λ= 0.025). Horizontal tangents correspond to wavenumbers in the bulk materials of the two domains respectivly.

The eigenvalues, listed in descending order, start with a horizontal tangent from the upper bound and show a discontinuity in the "derivative" at a value, which is equal to the wavenumber in the first domain. A horizontal tangent appears from this discontinuity again. It is important to realize that both horizontal tangents are at positions equal to the wavenumbers of a plane wave propagating in a bulk dielectric material, equal to the dielectrics in the corresponding domains.

In Fig. 6 and Fig. 7 shown are the real parts of the amplitudes of eigenfunctions of two eigenvalues. Note that for eigenvalue Nr. 1 the eigenfunction in the first domain is a hyperbolic function for a large argument and therefore almost zero in the whole domain with low refractive index. In contrast the amplitude of the trigonometric function in the second domain is very large.

This is very different for the eigenfunction connected to the eigenvalue Nr. 46: Here the eigenfunction can be described with trigonometric functions in both domains. However the amplitudes in both domains differ extremely, as can be seen from Fig. 7. As a consequence an incoming plane wave will mainly couple to the eigenfunction denoted by Nr. 46 in the first domain. In the second domain the same plane wave will mainly couple to the eigenfunction by Nr. 1, with the corresponding largest eigenvalue.

Note that there is a high number of eigenvalues with approximately the same values as Nr.1 and Nr.46, the eigenfunctions of which behave as described above. In the case of large grating periods we conclude that in each domain coupling to those eigenfunctions is most efficient, the eigenvalues of which are equal to the wavenumber in the bulk material of the corresponding domain. Propagation in y-direction behaves as expected from scalar theory or even geometrical optics.

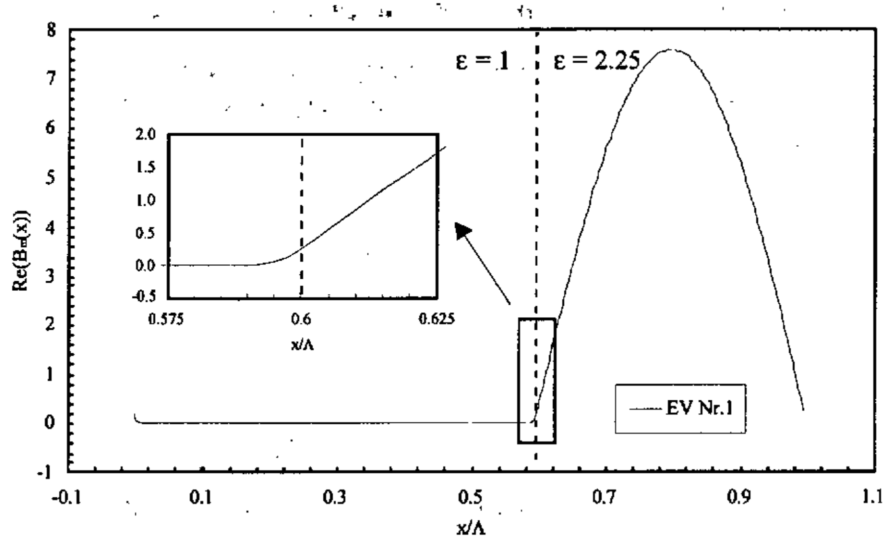

Fig. 6. Eigenfunction connected ta the largest eigenvalue of the grating of Fig. 5. The amplitude in the domain with low refractive index is a hyperbolic function with large argument and therefore almost everywhere in that domain close to zero. In contrast the amplitude in the domain with high index is a trigonometric functian with small argument. This leads to a large amplitude in this domain. Note that the eigenfunction at the domain boundaries are continuous and differentiable, according to the boundary conditions.

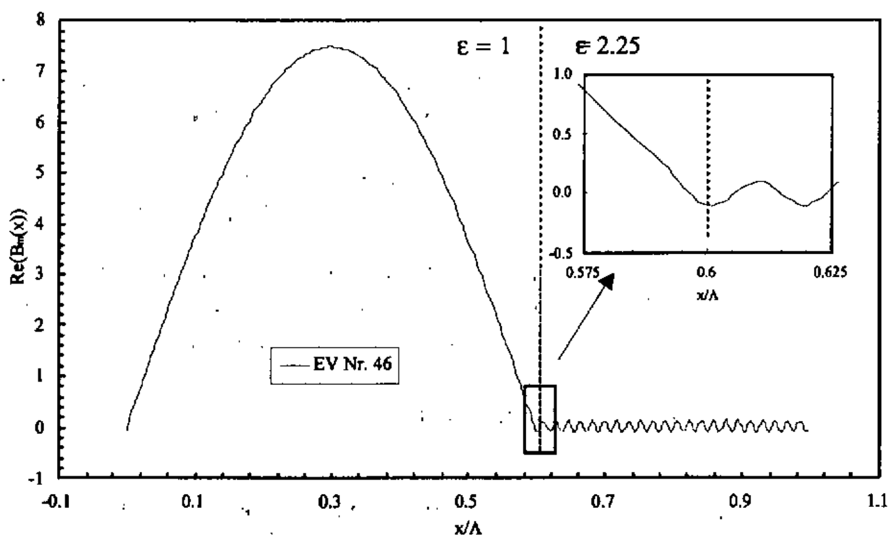

Fig. 7. Eigenfunction connected to the eigenvalue Nr. 46 af the grating of Fig. 5. In both domains the amplitudes are trigonometric functions. However, in the low index domain the argument is small, whereas in the high index domain the argument leads to a strong oscillation. Again the boundary conditions at the domain interfaces are fulfilled, leading to a large amplitude in the low index domain.

2.4. Solution of the diffraction problem for lamellar stacks

Once the eigenfunctions in each lamellar grating layer are calculated, we know that the electromagnetic fields in each layer can be expressed as a sum over these eigenfunctions.

For example in layer B we have

$$\mathcal{B}(x,y) = \sum_{m=1}^{\infty}\left(b^{+}_{m}\exp[i\sqrt{\mu^{B}_{m}}\,(y-y_{A\to B})]\right)B_{m}(x) + \sum_{m=1}^{\infty}\left(b^{-}_{m}\exp[-i\sqrt{\mu^{B}_{m}}\,(y-y_{B\to C})]\right)B_{m}(x)\,, \tag{38}$$

where $y_{A\to B}$ denotes the interface between layer A and layer B.

The coefficients b^{+}_{m}, b^{-}_{m} are still unknown constants. To calculate them we use the boundary conditions applied at the layer interfaces.

We will proceed in the following steps:

- matching the fields between two neighbouring layers leads to two sets of linear equations for each inner layer (not adjacent to a homogeneous halfspace).
- matching the fields between the two outer layers and their adjacent inner layers gives us one set of linear equations for both outer layers.
- matching the fields between the two outer layers and the homogeneous halfspaces leads to one set of linear equations for both outer layers.

The matching is performed by using orthogonality relations and Fourier expansions of the eigenfunctions. Special care has to be taken, how those relations and expansions are established in order to retain good convergence properties.

matching the fields between two neighbouring inner layers

At the interface of these layers we use the boundary conditions to match the fields. We only calculated a limited number of eigenfunctions and therefore have to truncate the infinite sum in (38). The number of eigenfunctions taken into account can be chosen independently in every layer. Let N^{B}_{EV} be the truncation order in layer B and N^C_{EV} the truncation order in layer C. Then the boundary conditions lead to

$$\begin{aligned}&\sum_{m=1}^{N_{EV}^B}\left(b^+_m \exp(i\sqrt{\mu^B_m}\,h_B)+b^-_m\right)B_m(x)\\&\qquad=\sum_{m=1}^{N_{EV}^C}\left(c^+_m + c^-_m \exp(i\sqrt{\mu^C_m}\,h_C)\right)C_m(x),\end{aligned}\tag{39}$$

and

$$\begin{aligned}&\sum_{m=1}^{N_{EV}^B}\sqrt{\mu^B_m}\left(b^+_m \exp(i\sqrt{\mu^B_m}\,h_B)-b^-_m\right)B_m(x)\\&\qquad=\sum_{m=1}^{N_{EV}^C}\sqrt{\mu^C_m}\left(c^+_m - c^-_m \exp(i\sqrt{\mu^C_m}\,h_C)\right)\left(\frac{\varepsilon^B(x)}{\varepsilon^C(x)}\right)^{\delta_{pol\,H}}C_m(x),\end{aligned}\tag{40}$$

where h_B is the thickness of layer B and h_C the thickness of layer C.

We now need to project the electromagnetic field at the interface along the eigenfunction $B_m(x)$ with the help of orthogonality relations. Botten et al. [5] proceed by defining an inner product according to

$$\langle f|g\rangle=\int_0^{\Lambda}\frac{1}{\varepsilon(x)^{\delta_{pol\,H}}}f^*(x)g(x)dx.\tag{41}$$

The eigenvalue problem (28) may be rewritten in the form

$$L\,B(x)=\mu^B B(x),\tag{42}$$

where the differential operator L is given by

$$L=\partial_x^2+\frac{\delta_{pol\,H}}{\varepsilon^B(x)}\partial_x\varepsilon^B(x)\partial_x+k_0^2\varepsilon^B(x).\tag{43}$$

They show in their paper that the adjoint operator with respect to the scalar-product (41) is given by

$$L^{+} = \partial_x^2 + \frac{\delta_{pol\,H}}{\bar{\varepsilon}^B(x)} \partial_x \bar{\varepsilon}^B(x) \partial_x + k^2 \bar{\varepsilon}^B(x), \tag{44}$$

(where the bars denote complex conjugation, according to the notation of Botten). The eigenfunctions $B_m^{adj}(x)$ of the adjoint eigenvalue problem with respect to this scalar-product fulfil the relations

$$\left\langle B_n^{adj} \middle| B_m \right\rangle = \delta_{nm}. \tag{45}$$

The approach as described above is very elegant, because with this definition of the scalar product (41), the differential operator of the eigenvalue problem is self-adjoint in the case of dielectric materials for both polarizations.

We could follow this approach as well, but in contrast to Botten, we only have approximations of the exact eigenfunctions

$$\lim_{M \to \infty} B_m(x, M) = B_m(x), \tag{46}$$

where M is the order of the approximation. It is not obvious that the approximations $B_m(x,M)$ and the adjoint functions fulfil (45) exactly. (However, note that the convergence of the approximations to the exact eigenfunctions is exponential. The scalar-product is a bilinear-form and the deviation from orthogonality will therefore decrease at least exponentially).

Exact orthogonality, even with these approximations can be reached, if we define the inner product according to

$$\langle f | g \rangle := \int_0^{\Lambda} f^*(x) g(x) dx. \tag{47}$$

In order to construct functions fulfilling the orthonormality relations

$$\tilde{B}_n(x,M): \qquad \int_0^{\Lambda} \tilde{B}_n^*(x,M) B_m(x,M) dx = \delta_{nm}, \tag{48}$$

with our eigenfunction approximations $B_m(x,M)$, we use of the properties of the orthogonal polynomial expansion. Here M denotes the approximation order. Our approximations of the eigenfunctions are given by polynomial expansions on two or more intervals of definition, according to the number of domains. Two coefficients in each domain are not linear independent and can be eliminated, using the boundary conditions. All other coefficients are equal to the components of the eigenvectors we calculated. The corresponding eigenvalues are not degenerated. Therefore the coefficient matrix of the eigenvectors can be inverted. The components of the resulting vectors in return can be used as the coefficients of a polynomial expansion, leading to a set of functions, which is orthogonal to our eigenfunction approximations. In the following we will call these functions 'orthogonal set'.

Please note, that the resulting functions of the orthogonal set are discontinuous. This is a consequence of the fact, that the components of the original eigenvectors, used as coefficients of the polynomial expansion, lead to discontinuous functions. The last two coefficients (eliminated in the eigenvalue problem) are responsible for the correct matching of the functions at the boundaries of the domains. Matching the functions of the orthogonal set in the same way with only two additional coefficients could result in the loss of orthogonality.

With the inversion as described above, orthogonality is exactly fulfilled, even in the case of approximated eigenfunctions. However preliminary calculations show that, in view of convergence, the scalar-product defined by Botten et al is advantageous. Further investigations are necessary to draw final conclusions.

Multiplying equation (39) with a function of the orthogonal set and integrating over the grating period then leads to

$$\begin{aligned}&\sum_{m=1}^{N_{EV}^{B}}\left(b^{+}_{m}\exp(i\sqrt{\mu^{B}_{m}}\,h_{B})+b^{-}_{m}\right)\delta_{nm}\\&\quad=\sum_{m=1}^{N_{EV}^{C}}\left(c^{+}_{m}+c^{-}_{m}\exp(i\sqrt{\mu^{C}_{m}}\,h_{C})\right)\int_{0}^{\Lambda}\tilde{B}_{n}^{*}(x)\,C_{m}(x)dx\,.\end{aligned} \tag{49}$$

For simplicity reasons we dropped the second argument M in $B_m(x,M)$, which denotes the approximation order.

For grating structures where all grating layers have the same vertical interfaces as boundaries of their domains, the polynomials are expanded on the same intervals of definition. Calculation of the integral on the right side of equation (49) then reduces to a summation over the coefficients of the expansions. For all other grating stacks it remains the possibility to calculate the integrals analytically.

We follow a different approach which uses the fact, that the Fourier coefficients are known for many sets of orthogonal polynomials (we need for example Bessel-functions in the case of Legendre or Chebyshev polynomials). Therefore we expand the x-dependent functions in Fourier series

$$\tilde{B}_n(x) = \sum_{p=-\infty}^{\infty} \tilde{b}_{n,p}\, \phi_p(x) \quad ; \quad C_m(x) = \sum_{p=-\infty}^{\infty} c_{m,p}\, \phi_p(x) \tag{50}$$

with

$$\phi_p(x) = (1/\sqrt{\Lambda})\exp(i\alpha_p x), \tag{51}$$

where

$$\alpha_p = \left[\frac{(2p)}{\Lambda}\right] p + k_0 \sin\Theta. \tag{52}$$

Using the orthogonality relation and the Fourier expansion, equation (49) reduces to

$$\begin{aligned} &b^+_n \exp(i\sqrt{\mu^B_n}\, h_B) + b^-_n \\ &\quad = \sum_{m=1}^{N^C_{EV}} \left(c^+_m + c^-_m \exp(i\sqrt{\mu^C_m}\, h_C)\right) \sum_{p=-\infty}^{\infty} \tilde{b}^*_{n,p}\, c_{m,p}\,. \end{aligned} \tag{53}$$

The same procedure applied to the second boundary condition at the interface of the grating layer leads to integrals of the form

$$\int_0^{\Lambda} \tilde{B}^*_n(x) \left(\frac{\varepsilon^B(x)}{\varepsilon^C(x)}\right)^{\delta_{pol\,H}} C_m(x)\, dx, \tag{54}$$

which we can calculate again with the help of Fourier expansions. We use the expansions

$$\tilde{B}_n^*(x)\varepsilon^B(x) = \sum_{p=-\infty}^{\infty} \tilde{b}_{n,p}^{\varepsilon *}\phi_p^*(x) \qquad \frac{C_m(x)}{\varepsilon^C(x)} = \sum_{p=-\infty}^{\infty} c_{m,p}^{\varepsilon}\phi_p(x), \tag{55}$$

where the number of discontinuities corresponds for both terms to the number of interfaces in the corresponding layers. The convergence of the Fourier series is again connected to the question whether the functions and their derivatives are continuous or not. In case of discontinuity the Gibbs phenomenon is responsible for poor (algebraic) convergence properties. Therefore unfortunately both series will show poor convergence properties.

Note that at this point the Gibbs phenomenon is inherently connected to the diffraction problem and cannot be avoided. As we already saw, the eigenfunctions inside one domain are infinitely many times differentiable. We try to expand these functions with the eigenfunctions of the adjacent layers. But these eigenfunctions are at the interfaces of the domains discontinuous in their first or second derivatives and a Gibbs phenomenon results.

The second boundary condition leads us to

$$\begin{aligned} & b^+_n \exp(i\sqrt{\mu^B_n}\, h_B) - b^-_n \\ & = \sum_{m=1}^{N_{EV}^C} \sqrt{\frac{\mu_m^C}{\mu_n^B}} \left(c^+_m - c^-_m \exp(i\sqrt{\mu^C_m}\, h_C)\right) \sum_{p=-\infty}^{\infty} \tilde{b}_{n,p}^{\varepsilon *}\, c_{m,p}^{\varepsilon}. \end{aligned} \tag{56}$$

The difference of equation (53) and equation (56) leads to a set of equations for the b^-_m, which can be written as a vector equation with the structure

$$\mathbf{b}^- = \mathbf{M}_+^{BC}\,\mathbf{c}^+ + \mathbf{M}_-^{BC}\,\mathbf{c}^-. \tag{57}$$

We find the set of equations for the b^+_n similar to the one derived for the b^-_m by investigating the interface between layer A and layer B.

The resulting set of equations has the structure

$$\mathbf{b}^+ = \mathbf{M}_+^{BA}\,\mathbf{a}^+ + \mathbf{M}_-^{BA}\,\mathbf{a}^-. \tag{58}$$

Note that for the b^+ and b^- we eliminated the exponential factor, which normally leads to numerical stability problems [10].

matching the fields of the outer layer to the homogeneous halfspace of transmittance

Special care has to be taken at the interfaces forming the boundary of the grating region. Let C be the layer adjacent to the half space where light is transmitted. The Rayleigh expansion can be used to describe the electromagnetic field

$$\mathcal{T}(x,y)=\sum_{p=-\infty}^{\infty} T_p \exp[i\tau_p(y-y_{U\to out})]\phi_p(x), \tag{59}$$

where
$$\tau_p=\sqrt{\varepsilon_{out}k_0^2-\alpha_p^2}\,. \tag{60}$$

For complex τ_p we choose the imaginary part to be positive, whereas for real τ_p the positive square root is used.

Therefore at the interface $y_{C\to out}$ we can write the boundary conditions as

$$\sum_{m=1}^{N_{EV}^C}\left(c^+_m \exp(i\sqrt{\mu^C_m}\,h_C)+c^-_m\right)C_m(x)=\sum_{p=-\infty}^{\infty} T_p\phi_p(x) \tag{61}$$

and

$$\sum_{m=1}^{N_{EV}^C}\sqrt{\mu^C_m}\left(c^+_m \exp(i\sqrt{\mu^C_m}\,h_C)-c^-_m\right)\frac{C_m(x)}{\varepsilon^C(x)^{\delta_{pol\,H}}} =\frac{1}{\varepsilon_{out}{}^{\delta_{pol\,H}}}\sum_{p=-\infty}^{\infty}\tau_p\,T_p\phi_p(x)\,. \tag{62}$$

Note that we introduced the truncation which is necessary because of the finite number of calculated eigenfunctions.

At this point we need the Fourier expansions

$$C_m(x)=\sum_{p=-\infty}^{\infty}c_{m,p}\,\phi_p(x)\quad ;\quad \tilde{C}^*_m(x)\frac{\varepsilon^C(x)}{\varepsilon_{out}}=\sum_{p=-\infty}^{\infty}\tilde{c}^{\varepsilon *}_{n,p}\,\phi^*_p(x)\,. \tag{63}$$

Multiplying equation (61) with $\phi^*_p(x)$ and integrating leads to an equation for the T_p which can be inserted in (62). If we use the orthogonality relations for the $C_m(x)$ we find the equation

$$\sqrt{\mu_n^C}\left(c^+_n \exp(i\sqrt{\mu^C_n}\, h_C) - c^-_n\right) = \sum_{p=-\infty}^{\infty} \tau_p \sum_{m=1}^{N_{EV}^C}\left(c^+_m \exp(i\sqrt{\mu^c_m}\, h_U) + c^-_m\right) \tilde{c}^{\varepsilon *}_{n,p} c_{m,p}\,, \tag{64}$$

which, after sorting the coefficients, can be written as a vector equation with the form

$$\mathbf{M}_+^{out}\left(N_{EV}^C \times N_{EV}^C\right)\mathbf{c}^+ + \mathbf{M}_-^{out}\left(N_{EV}^C \times N_{EV}^C\right)\mathbf{c}^- = 0. \tag{65}$$

matching the fields of the outer layer to the homogeneous halfspace of reflectance

In the half space of incidence and reflectance, the Rayleigh expansion leads to

$$\mathcal{R}(x,y) = \exp[i\chi_0(y - y_{inc\to A})]\phi_p(x) + \sum_{p=-\infty}^{\infty}\left\{R_p \exp[-i\chi_p(y - y_{inc\to A})]\right\}\phi_p(x)\,, \tag{66}$$

where

$$\chi_p = \sqrt{\varepsilon_{inc} k_0^2 - \alpha_p^2}\,. \tag{67}$$

Here the first term corresponds to the incident plane wave and the terms with the R_p represent the reflected orders. For complex χ_p we choose the imaginary part to be positive, and for real χ_p the positive square root is used.

If A is the layer adjacent to this half space, then again the boundary conditions give

$$\sum_{m=1}^{N_{EV}^A}\left(a^+_m + a^-_m \exp(i\sqrt{\mu^A_m}\, h_a)\right) A_m(x) = \sum_{p=-\infty}^{\infty}\left(\delta_{0p} + R_p\right)\phi_p(x) \tag{68}$$

and

$$\sum_{m=1}^{N_{EV}^A}\sqrt{\mu_m^A}\left(a^+_m - a^-_m \exp(i\sqrt{\mu^A_m}\, h_A)\right) A_m(x) = \frac{\varepsilon^A(x)^{\delta_{pol\,H}}}{\varepsilon_{inc}{}^{\delta_{pol\,H}}}\sum_{p=-\infty}\chi_p\left(\delta_{p0} - R_p\right)\phi_p(x)\,. \tag{69}$$

We now multiply equation (68) with $\phi^*_p(x)$, integrate over one period, and insert the resulting formula for R_p in eq. (69). As before, with the help of Fourier expansions and orthogonality relations for the eigenfunctions in layer A, we derive a set equations for the a^+_m and a^-_m, which can be written as vector equation

$$\mathbf{M}_+^{in}\ \mathbf{a}^+ + \mathbf{M}_-^{in}\ \mathbf{a}^- = 2\chi_0 \tilde{\mathbf{a}}_0^{\varepsilon^*}. \tag{70}$$

With the other vector equations

$$\mathbf{a}^- = \mathbf{M}_+^{AB}\ \mathbf{b}^+ + \mathbf{M}_-^{AB}\ \mathbf{b}^-, \tag{57}$$

$$\mathbf{b}^+ = \mathbf{M}_+^{BA}\ \mathbf{a}^+ + \mathbf{M}_-^{BA}\ \mathbf{a}^-, \tag{58}$$

$$\mathbf{b}^- = \mathbf{M}_+^{BC}\ \mathbf{c}^+ + \mathbf{M}_-^{BC}\ \mathbf{c}^-, \tag{57}$$

$$\mathbf{c}^+ = \mathbf{M}_+^{CB}\ \mathbf{b}^+ + \mathbf{M}_-^{CB}\ \mathbf{b}^-, \tag{58}$$

$$\mathbf{M}_+^{out}\ \mathbf{c}^+ + \mathbf{M}_-^{out}\ \mathbf{c}^- = 0, \tag{65}$$

we have six different sets of linear equations determining the whole diffraction problem. Truncating the number of eigenvalues used in any layer will lead to the same number of equations as there are unknowns in this layer. The whole system of linear equations will have the same structure as given in [10] equation (60), including the stability properties.

Note that up to now we have not introduced any truncation for the Fourier expansions. With the method as described above, truncating the number of Fourier components can be chosen independent of the number of eigenvalues used.

The method of orthogonal polynomial expansion leads to exponential convergence of the eigenfunctions inside the grating layers. With this method discontinuities of the dielectric function are better taken into account than is the case with Fourier expansions. In addition the method allows the choice of the local accuracy for the approximation in an efficient way. If we choose the number of the Fourier components N_f equal to the number of eigenfunctions we could loose parts of these advantages. Further investigations are necessary to find out how this affects the convergence properties of the efficiency calculations.

After solving this system of linear equations, the amplitudes of the transmitted and reflected orders can be calculated with the help of the explicit equations for T_p

and R_p. The efficiencies $\eta_p{}^R$ and $\eta_p{}^T$ of the propagating diffraction orders can be obtained by

$$\eta_p^R = \mathrm{Re}\left\{\frac{\chi_p}{\chi_0}\right\}\left|R_p\right|^2 \quad and \quad \eta_p^T = \mathrm{Re}\left\{\frac{\tau_p}{\chi_0}\left(\frac{\varepsilon_R}{\varepsilon_T}\right)^{\delta_{pol\,H}}\right\}\left|T_p\right|^2. \tag{66}$$

We therefore have a stable and efficient tool to solve diffraction problems with multidomain and multilevel grating stacks. However until now nothing is said about design methods. In the following chapter we show how thin film methods, based on approximations can be used to design optical devices. The final test will always be performed with the rigorous method as described above.

3. Grating design based on thin film methods

The calculation of diffraction efficiencies for gratings with a grating period comparable to the wavelength of light is challenging and connected with considerable numerical effort, as we saw in the last chapter. The use of statistical methods for optimizing broadband applications, where many wavelengths have to be taken into account, such as broadband antireflection (AR-) surfaces and broadband high reflecting mirrors, is therefore limited.

However, dielectric subwavelength gratings with a grating period well below the wavelength of light, can be modelled by effective medium theory. Here the surface grating is approximated by a thin film stack of artificial dielectric media. The effective index in each film depends on the grating material, the duty-cycle, the wavelength of light and the polarization. The wavelength-dependence of the effective index is only important if the wavelength approaches the grating period.

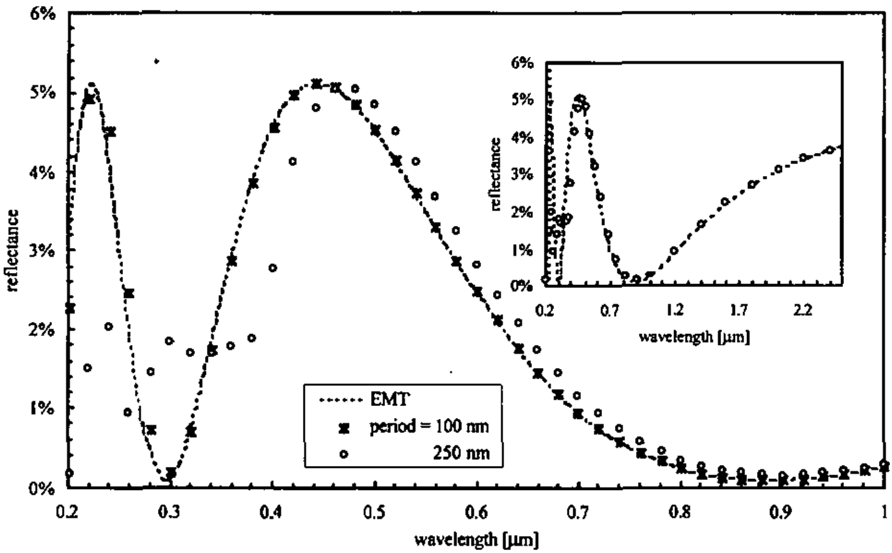

Fig. 8. Reflectance of a 170 nm deep surface grating in polycarbonate ($n = 1.52$, duty cycle $f = 0.45$, E-polarization) for two different grating periods. Also shown is the reflectance of the corresponding 170 nm thick effective thin film with index $n = 1.297$.

In Fig. 8 we plotted the reflectance as a function of wavelength (E-polarization) for a lamellar grating in polycarbonate ($n = 1.586$) with a depth of $h = 170$ nm and a duty-cycle of $f = 0.45$ for two grating periods ($\Lambda = 100$ nm and $\Lambda = 250$ nm) as well as the reflectance of the corresponding thin film layer ($n = 1.297$). As can be seen in the long-wavelength range, effective medium theory (EMT) opens the possibility to use thin film design techniques for subwavelength gratings.

However, even in the long-wavelength range, care has to be taken when EMT is applied on multilayer stacks: we do not know how non-propagating modes affect the coupling between the layers and cause deviations from thin film approximations. It is therefore necessary to check effective index designs with rigorous calculations.

Our first example is based on simulated thermal annealing (STA). It is a very efficient thin film design technique which was developed at the Paul Scherrer Institute [24]. We apply this method in the first section of this chapter in combination with effective medium theory to optimize the profile of a broadband antireflection submicron grating.

Our second example makes use of the well know properties of thin film quarterwave multilayer stacks. They are often used to realize very efficient high reflection coatings. The zone of high-reflectance, or stop band, depends on the refraction index ratio of the two materials used. A new approach to increase this ratio for GaAs and AlAs is based on the thermal oxidation of AlAs [25]. We show that submicron gratings are suitable to improve the properties of the resulting Bragg-mirrors.

3.1. Profile-optimization of high-frequency gratings by simulated thermal annealing

One of the important applications of subwavelength gratings is the broadband antireflection surface. In thin film technology graded index designs [26-31] as well as quarter-wave transformer designs [32-34] are well known approaches, leading to interfaces with very low Fresnel reflection losses. In both cases the lack of stable materials meeting the refractive index requirement for the substrate-air interface have been a problem.

The problem can be overcome with the help of subwavelength gratings. This was shown theoretically [35-38] as well as experimentally [39-41]. New fabrication techniques, such as e-beam writing, start to allow to control to a certain degree the profile shape of even such small grating structures. However, these written prototypes will be expensive. They have a chance to become application relevant if replication techniques can be applied to mass produce such devices. In view of mass production the aspect ratio and with it the actual depth of the grating structure is a limiting factor. Extensive work has therefore been done to find the optimum profile shape [42, 43].

In Ref. [43] the authors compare continuously tapered gratings, designed with use of the optimal Klopfenstein tapering technique [34] and discrete stair-step gratings, designed with use of Chebychev synthesis technique [32, 33].

In order to have the possibility to compare our optimizations, we stick to the specifications given in Ref. [43]. Therefore, the substrate material has an index of refraction of n = 3 and the medium of incidence is air. We have normal incident light. The interval of interest for the light covers all wavelengths from 3 μm to 12 μm. The reflection threshold is set to 0.25%. Following Ref. [43], we define as optimum design, the design with the minimum depth which provides reflectance below a specified threshold level for a specified wavelength range.

First we optimize a multilayer thin film stack with decreasing index of refraction as a function of distance to the substrate. Optimization is performed by simulated thermal annealing. Then we translate the result into a one-dimensional submicron grating, using effective medium theory. Based on rigorous diffraction calculations we compare the resulting reflectance with the reflectance of the thin film approach.

Thin film optimization by simulated thermal annealing (STA)

We follow the method described in Ref. [24] to optimize the thin film stack which has to be translated into a subwavelength grating. At the beginning we have to choose the number of thin film layers we want to use to approximate the grating. In order to have convergence of the optimization process within a reasonable time scale, we limit the number to 23 layers. We define for each layer an index of refraction. This corresponds to certain duty-cycle of the grating. We choose an equally separated index distribution as a function of layer number. The refractive index of the substrate is n = 3. The index of the j^{th} layer is set to

$$n_j = 3 - \frac{1}{12} j \qquad for \quad j \in \{1,2,...,23\}. \tag{67}$$

Optimization of the grating profile can then be performed by optimizing the layer thickness of the corresponding effective thin film stack. During each optimization step the thickness of two randomly chosen layers is changed, using a Monte Carlo step. A quality function is used to compare the actual reflection spectrum with the required filter specifications. STA allows the controlled search for extrema of this quality function even if these extrema are separated by barriers. This is possible because of the thermal fluctuations which were implemented. They allow the system to cross energy-barriers of height proportional to temperature. During the optimization process the temperature is decreased slowly and the system relaxes to an advantageous combination of layer thicknesses.

If the cooling of the system is performed too fast, it often happens that the system is caught in a metastable state. It is difficult to determine, how fast a system should be cooled. Therefore, several realizations are calculated parallel at the same temperature. The heights of all of these realizations are chosen independently. The temperature is then decreased in such a way, that almost all realizations have approximately the same quality, i.e. the ensemble is in thermal equilibrium.

Calculating several realizations has another advantage. Most realizations relax to a broad minimum of the quality function, which is connected to rather broad tolerances with respect to errors in the heights.

It is one important advantage of STA that no good guess is needed for the starting values of the layer thicknesses. Even if we start with a layer thickness of zero, there will be a random distribution of heights after some Monte Carlo steps if the starting temperature is chosen high enough.

In the quality function we implemented the condition that the whole stack thickness should not be above five microns. The result of our thin film optimization is shown in the inlay of Fig. 9a. We plotted the index of refraction as a function of distance to the substrate. There are no layers of zero thickness. This signifies that a continuous design is preferred to a discrete design, which is in contrast to [43]. Fig. 9a shows the resulting reflectance spectrum of the thin film stack (continuos line). Note that the reflectance is below 0.25% over the whole wavelength interval.

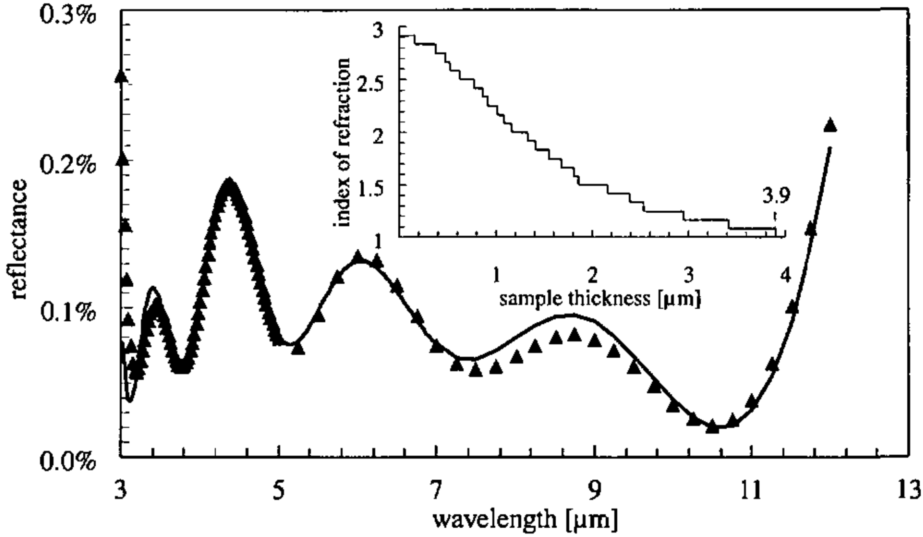

Fig. 9a. Reflectance as a function of wavelength for a 23-layer thin film stack (continuous line). The inlay shows the index as a function of distance from substrate. Also shown (triangles) is the reflectance of the corresponding submicron grating.

The optimum grating profile

On the basis of effective medium theory it is straight forward to transform the thin-film stack into the optimum subwavelength grating structure with a grating period of $\Lambda = 0.5\ \mu m$. We choose to transfer the stack into a one dimensional grating structure. Therefore, it will only be antireflective for one polarization. There is no difficulty in using two dimensional gratings, but at the moment, with our rigorous programs, we are restricted to one dimensional gratings.

The Fig 9b shows the resulting profile shape. The triangles in Fig. 9a show the reflectance of such a grating structure as a function of wavelength. The grating depth (3.89 μm) is well below the Klopfenstein design (5.78 μm). The depth is 1.06 times above the Chebychev design (3.66 μm), but the reflectance is below the threshold level of 0.25% over most of the required range (excluding $\lambda = 3\ \mu m$).

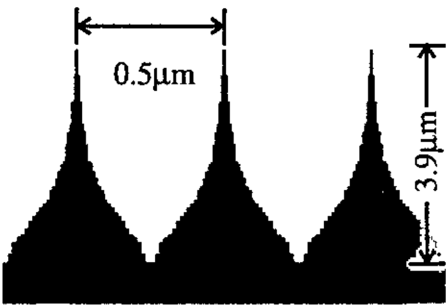

Fig. 9b. Optimized grating profile. The thin stack of Fig. 9a is translated to a submicron grating, using effecitve medium theory.

Differences between the reflection spectrum (belonging to the grating) and the spectrum of the thin film stack in the short wavelength range result from higher order λ/Λ-terms in the effective index, causing dispersion effects. Fig. 10 shows the calculated reflection spectrum for the same grating profile, but different grating periods. In Ref. [43] a grating period of 0.75 µm was used. For this period Fig. 10 shows that we are always below 0.6% reflectivity. For wavelengths above 3.1 µm we are always clearly below the threshold of 0.25%.

Down to 3 µm the reflectance does not reach 0.6%, but is above the threshold. The inlay of Fig. 10 shows the effective index as a function of wavelength for different duty-cycles. The grating period was again 0.5 µm. In order to correct for this effect STA includes the possibility to take dispersion into account, which we did not in this example.

To conclude, simulated thermal annealing permits to optimize thin film stacks for different requirements. Reflection thresholds and smallest possible grating depth can be implemented in the quality function. For the broadband AR-optimization the resulting subwavelength grating approximates a continuous grating structure with a grating depth well below the depth of a Klopfenstein design. The depth is slightly above the depth of the Chebychev design, but the reflectance is below the required threshold over almost the complete optimization interval.

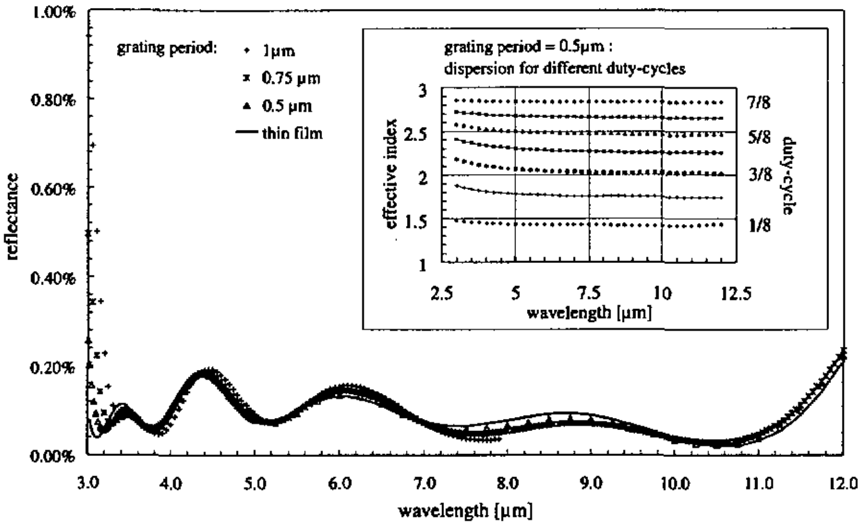

Fig. 10. Influence of the grating period on the reflection spectrum. Spectra for three different grating periods and for thin film stack are shown. The inlay shows the dispersion of a 0.5 µm lamellar grating for different duty-cycles.

Only in the short wavelength range below 3.1 μm the wavelength dependence of the effective index causes differences to the thin film stack. This problem could be overcome by taking dispersion into account during the optimization process. Typically the optimization with simulated thermal annealing terminates in a broad extremum of the quality function. Therefore we expect the design to be rather tolerant with respect to fabrication errors.

3.2. Quarter-wave stacks with increased index ratios

Bragg reflectors are widely used in thin-film optics. They consist of several periods of high- and low-index quarterwave stacks. For a certain stop band they exhibit 100% reflectivity if only the number of layers is chosen to be high enough. However often the stop-band is not broad enough and other design methods have to be used to extend the reflection performance.

Let g be defined as λ_0/λ, where λ_0 is the design-wavelength, i.e. for this wavelength the layers have quarter-wave optical thickness. λ is a wavelength which is element of the interval of interest.

The halfwidth of the reflectance-zone, expressed in Δg, can then be determined by [2]

$$\Delta g = \frac{2}{\pi}\sin^{-1}\left(\frac{n_H - n_L}{n_H + n_L}\right). \tag{68}$$

where n_H is the high refractive index and n_L stands for the material with the low refractive index. Increasing the ratio n_H/n_L leads to an increased stop band.

In Ref. [25] a wide-bandwidth distributed Bragg reflector, using AlAs oxide/GaAs multilayers, was demonstrated. The high/low index ratio is increased by performing a thermal oxidation step, which changes the index of AlAs from 2.91 to approximately 1.5-1.56. The experimental performance of that mirror is in good agreement with the theoretical predicted reflectance spectrum.

One disadvantage of that approach is the limited area of the mirror: Only fields of up to 50 μm could be realized, because the oxidation process has to be performed after growing the mirror. Grooves are necessary to give the oxide the possibility to diffuse inside the layers. Zero order gratings, etched in a stack of thin film layers open as well the way for the diffusion, but in contrast to the larger grooves, they do not limit the mirror size.

If we etch submicron gratings in this stack with a groove width of 0.25 times the grating period, the index of GaAs is decreased from 3.5 to an effective index of 3.1. The corresponding quarterwave-thickness is then 61 nm (for $\lambda_0 = 0.76\,\mu m$ design wavelength). After the thermal oxidation the effective index of the native oxide AlAs grating is approximately 1.42, leading to a quarterwave thickness of 133 nm for the same design wavelength. The resulting index ratio is as high as 2.2 and according to equation (68) this exhibits a halfwidth of $\Delta g = 0.242$ (which was 0.02 for the normal AlAs with n = 2.91). For a design wavelength of $\lambda_0 = 0.76\,\mu m$ the mirror's stop band then ranges from 0.610 μm to 0.990 μm.

Fig. 11 shows the rigorous calculated reflectance of the 15 layer system as a function of the wavelength for E-polarized light. Between 0.63 μm and 0.95 μm the reflectance is above 99.5%. Shown as well is the phase of the reflected light. As long as no higher diffraction orders are propagating, the phase has the wavelength dependence as expected from a thin film Bragg stack. Such a device is well suited for short light pulse applications, where minimum group delay dispersion over a broad wavelength range is required.

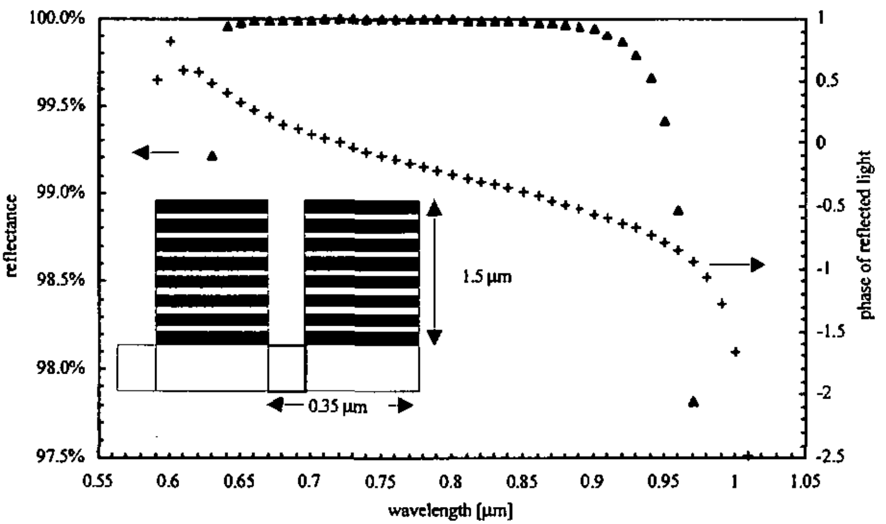

Fig. 11. Calculated reflectance and phase of a multilayer grating. The assumed refraction indices correspond to materials such as GaAs n = 3.5 and oxidized AlAs (n = 1.53). The thin film stack is grown before the thermal oxidation of AlAs. The grating grooves allow the oxide to diffuse fast to all parts of the AlAs layers.

The grating period is chosen to be 0.35 µm in order to avoid higher diffraction orders for wavelengths larger than 500 nm. The stack includes 15 grating layers. The whole grating stack is therefore approximately 1.5 µm deep. We did not fabricate such grating structures. However, colleagues at PSI have already etched grating structures in GaAs with a period of 390 nm and a depth of 1 µm and the etching process could have proceeded further. Therefore, there is no principle experimental problem to etch the necessary grooves.

4. Fabrication and characterization of submicron surface gratings

4.1. Grating fabrication

Recording interference fringes in photographic media by exposing with a standing wave is a well known and often used method to realize diffraction gratings. Much effort has been put into developing different holographic fabrication procedures, including new types of resist, exposure set-ups and developers [44-48]. With this method, grating periods down to 100 nm can be realized [49]. The holographic fabrication is a parallel method which allows the exposure of large areas (one square meter and more) in a short time. Therefore until now this is the most important method to fabricate submicron grating structures.

One of the disadvantages of the holographic exposure is the limited flexibility. It is difficult to realize specified duty-cycles and without additional effort it is not possible to fabricate multidomain gratings or nonperiodic microstructures. This problem can be overcome by using serial methods, i.e. direct writing techniques such as laser lithography [50, 51] and e-beam writing [52-54]. Laser lithography systems are typically able to expose the largest areas and no vacuum is required for the exposure. These systems are therefore more flexible and less expensive compared to the others. However the achievable lateral resolution is typically above $0.5\,\mu m$ (linewidth) and the realization of submicron grating structures, superimposed on devices with diffractive optical elements, is only possible in combination with holography.

With e-beam writing systems structures below 50 nm can be written. This is only true as long as the required structures are not too deep and the proximity effect does not destroy the resolution. It is the consequence of scattered electrons in the resist layer and at the resist substrate interface. There are some possibilities to reduce this effect [55]. The typical scan field size of such systems is below one millimeter. For larger areas stitching errors are a severe problem.

A newer approach is the use of atomic beams [56]. With beams of neutral atoms one does not have to correct for coulomb forces and for some atomic systems basic optical elements such as lenses and mirrors [57] using light forces are

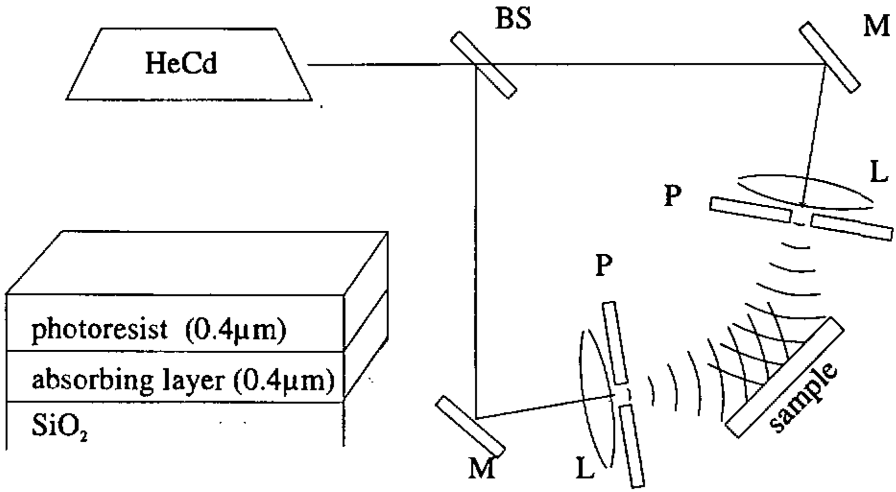

Fig. 12. The element (BS) splits the light of a HeCd-laser (λ = 442 nm) in two beoms. After being reflected at the mirrors (M), they are transformed to approximotely sphericol waves before they are brought to interference. The tronsformation is performed by lenses (L, 40x, NA = 0.65) and pinholes (P, 5 µm). The somple to be exposed is a quarz substrate covered with an absorbing layer and a photoresist layer. The absorbing layer decreases interference effects from the rear side of the sample.

realized. However, such atomic beam machines require considerable technical effort and it is not clear, whether this approach becomes important for lithography.

At the Paul Scherrer Institute the fabrication of diffraction gratings using interferometric exposure has a long tradition and is therefore well developed and documented [12]. The set-up consists of a HeCd-laser light source ($\lambda = 442$ nm) the light of which is split in two beams which are brought to interference under a certain angle θ. This angle defines the period Λ of the standing wave and with it the period of the resulting grating according to

$$\Lambda = \frac{\lambda}{2n\sin(\theta)}. \tag{69}$$

where n is the index of refraction of the medium in which the angle of interference is measured. Changing this medium can be used to realize smaller grating periods [49]. Besides the required mirrors there are microscopic objectives (40x, NA = 0.65) in the optical paths of the two laser beams. For spectral filtering purposes they focus the beams on 5 µm pinholes. As a result of the optical setup, we have approximately spherical waves at the locus (or volume) of interference, where we fix the sample to be exposed. Fig. 12 shows schematically the situation. Only plane waves interfering would lead to an interference pattern with straight lines and a constant grating period. Due to the spherical waves the period is slightly chirped. For our applications it was not necessary to correct for that. However we have to take this effect into account when we compare our measurements with rigorous calculations.

With this set-up we expose a photoresist layer which is spin-coated onto an absorption film covered quartz substrate. The absorbing film between the substrate and the photoresist-layer lowers the risk of disturbing interference effects of light reflected from the interfaces of the device. After exposing and development the resulting gratings have sinusoidal profile in the photoresist. The next process step is to etch the grating grooves down to the substrate. In order to mask the upper parts of the gratings we evaporate a thin metallic layer (6 nm Cr) under an angle of 12°. The angle in combination with the sinusoidal profile defines the Cr-mask and with it the duty-cycle of the grating. One has to be sure that no resist remains in the grating grooves after the O_2 plasma-etch process. Therefore we over-etch the device for a couple of minutes. This and the following fabrication steps are illustrated in Fig. 13.

The following reactive ion etching (RIE) process, used to transcript lamellar gratings in quartz, is performed on the in house commercial RIE-system. For etching of SiO_2 we use CF_4 in combination with a fraction of O_2. The O_2 concentration controls the selectivity, which is the etch ratio between resist and substrate [58]. With our thick layers of resist and absorbing film (in total > 600 nm) this was not very critical. It is difficult to stop the etching process at a specified grating depth. Monitoring the etch rate with a planar sample is not very accurate, because the etch rate for submicron structures differs from the one, measured from structures of larger scale.

The next step is to fabricate a nickel shim by electroplating. This shim is used to replicate the submicron structures by hot embossing. Typically the quartz master is not affected by the electroplating procedure and can be used to fabricate several first generation metal shims. This is in contrast to electroplating directly from the resist where sometimes the thin film is destroyed during the separation process of shim and master.

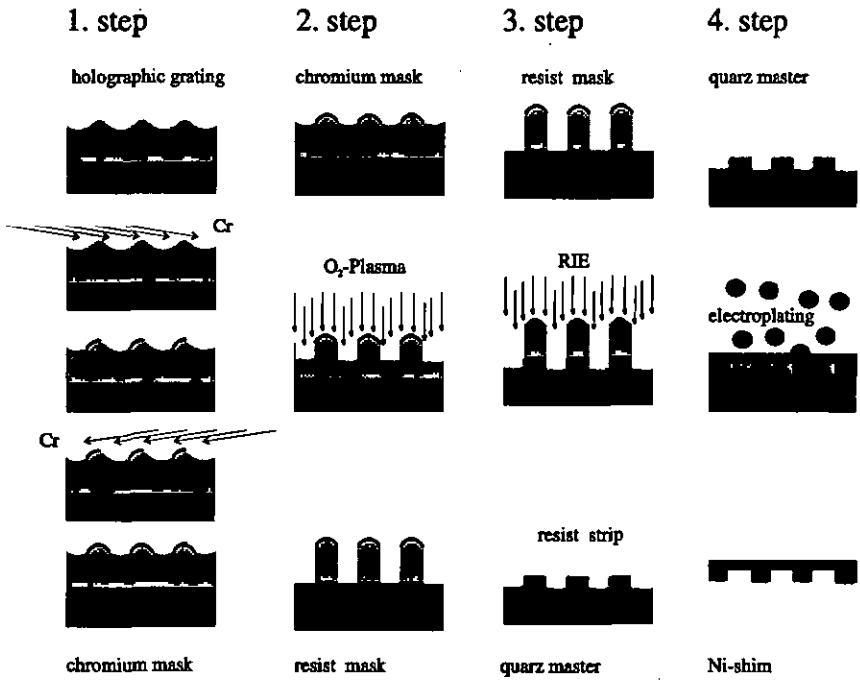

Fig. 13. Illustrated are the four basic steps from the holographic grating to a Ni-shim for hot embossing. It is difficult to realize the correct duty-cycle which is defined by the chromium mask. Another difficulty is the etch depth of the RIE-process, because the etch rate for such small structures differs from the rate of larger structures.

4.2. Experimental methods for polycarbonate-grating profile determination

Once the Ni-master is produced, a hot embossing procedure is straight forward. We will not describe it in detail but focus more on the characterization of such gratings embossed in polycarbonate. There are different methods to determine the profile of such structures. It is possible to scan profiles of microstructures with the atomic force microscope. However, the aspect-ratio of our structures is too high for this method. Another possibility to investigate the profile are SEM micrographs, but for this a well defined edge is needed. Quartz, glass and polymethylmethacrylate (PMMA)-devices are easily investigated. These materials have the advantage that they can be broken with a well defined edge.

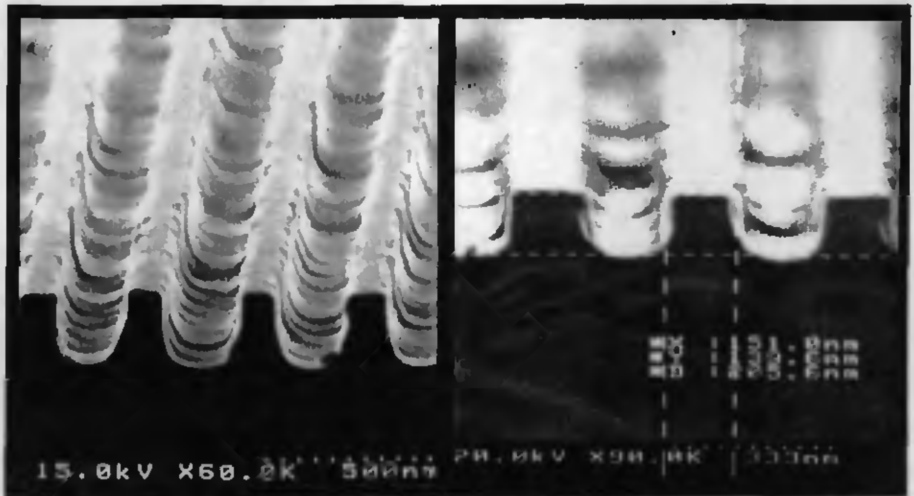

Fig. 14. Two different gratings are investigated. The SEM micrographs show the quarz masters used for electroplating Ni-shims. A well defined edge is realized, when quarz is broken. However note that it is not always possible to extrapolate to the embossed replicas.

Fig. 14 shows the micrographs of the two quartz masters we used for electroplating Ni-shims. Due to the elastic properties of polycarbonate it is not possible to break it with a well defined edge and even cooling down to 70 K (liquid Nitrogen) does not help. It is possible to define the edge already during the exposure process, but in many cases it is important to check the actual profile of the device without changing the master.

One could as well trust the embossing process and use PMMA or even the original quartz master to determine the profile. However, little is known about the rheology of those materials on the scale of such small structures and it is not obvious that it is possible to extrapolate from one polymer-system to another, or from the glass master to the embossed grating. We therefore investigate possibilities to define an edge in the embossed polycarbonate-device, without changing the shim. The methods are shown in Fig. 15 together with the results.

Responsible for these mechanical properties of polycarbonate are the long polymer chains, forming an elastic network. Our first approach therefore focused on breaking these chains in a defined way. This was done by cutting the polycarbonate-foil before the embossing procedure. For the replication both parts where again put together. After embossing, the sample can be broken and the edge can be investigated by SEM. There is a drawback of this procedure: The

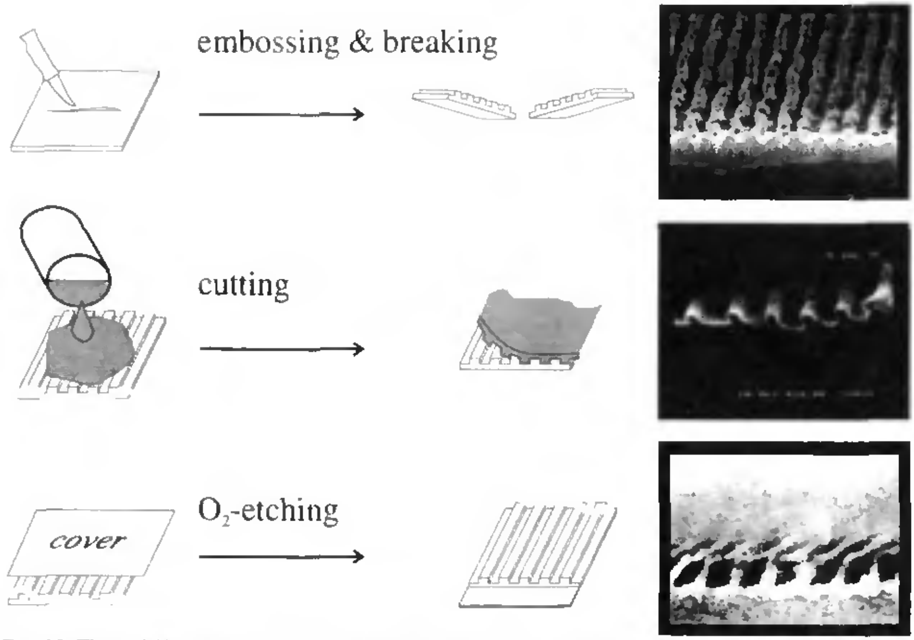

Fig. 15. Three different methods to prepare an edge of a polycarbonate-surface grating. 1) The foil is cut before the hot embossing procedure. After embossing it (often) is possible to break the sample. 2) The grating structure is already embossed. The sample is coated with a material to protect the gratings during the cutting. After cutting, the separating the protection and the sample leads to the profile. 3) The sample is partly covered with a mask which protects the grating from being etched. O_2-plasma etching leads to the profile shown.

profile at the edge and the structure which can be seen in the background of the micrograph show major differences. In addition the discontinuity is reproduced on the nickel shim.

It is not possible to cut the profile after the gratings have been embossed: they are pressed down and deformed. We try to avoid this by covering the embossed gratings with a different material with approximately the same elasticity. For the protection we use a material which in house is normally used to protect or clean nickel shims [59]. The fluid is spread over the element and after drying, the sample is cut before separating device and protection material. The separation can be performed without any problem. As Fig. 15 shows, cutting this system leads to an acceptable edge. However there are still deformations of the profile.

The third approach leaves the profile unchanged. Approximately half of the device is covered with a polymer mask before the system is coated with a thin metallic film. Then the plastic mask is removed and the device is exposed for 20 min to an space, which has to be scanned with rigorous theory, is confined. The first step is to determine experimentally the dispersion of polycarbonate. There are elaborate techniques of measuring the index of refraction such as for example ellipsometry [62]. We prefer to measure the transmitted spectrum as a function of wavelength of a plane polycarbonate-foil and calculate the index of refraction according to

$$n = \frac{1+\sqrt{1-T_0}}{1-\sqrt{1-T_0}}, \tag{70}$$

with

$$T_0 = \left(\frac{2}{T_{gem}} - 1\right)^{-1}. \tag{71}$$

where T_{gem} is measured absolute transmittance through the polycarbonate-foil.

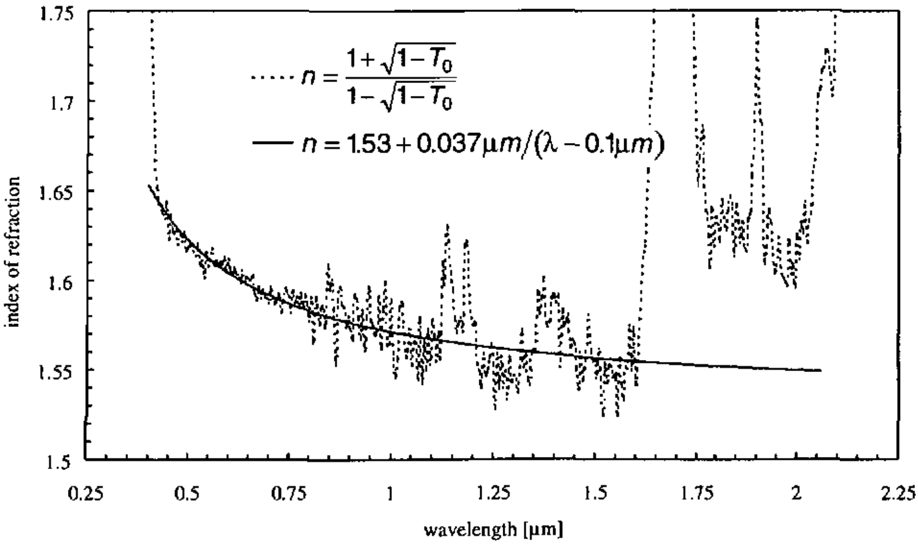

Fig. 16. Index of refraction of polycarbonate as calculated from transmission measurements (broken line). Only in the wavelength interval from 400 nm to 1.1 μm, absorption is not important. We fitt the index in this wavelength range (continuous line) according to the formula given in the legend.

O_2-plasma. The part not covered with the metal is etched and here the grating disappears, whereas the protected part is not affected, which can be seen in Fig. 15. Further work has to be done to define the edge which did not come out too clear of that process, as can be seen from the SEM.

4.3. Grating profile: A comparison between theoretical and experimental transmission-characteristics

A different way to determine the profile of such grating structures is to compare the measured optical properties to the theoretical results of different profile shapes [60, 61]. This means one has to scan the parameter space of grating profiles and periods. To determine the grating period is rather simple, if the wavelength range, where reflectivities or transmission characteristics are measured, includes the wavelength where the first diffraction order just starts to be evanescent. Very often this results in a discontinuity in the first derivative of the measured spectrum. The grating period can then be calculated with the help of the grating formula.

Challenging is the grating profile. There are different possibilities to proceed. As experimental parameter one could measure the zero-order transmission or reflection, at normal incidence or at different angles of incidence. Also one could measure the first diffracted order as a function of wavelength or of angle of incidence. However our goal was to find an easy to perform approach which allows, without much experimental effort, to determine the grating profile.

During the holographic fabrication of sinusoidal gratings in photoresist, the first reflected order is controlled to decide whether the development process should be continued or stopped. The measurement is simple and gives a rough idea of how deep the gratings are. For more quantitative conclusion we think it is better to use the zero order of transmission or reflectance of such a device.

Exact reflectance measurements are difficult to perform: Both, grating surface and rear side of the foil can have low quality flatness, influencing the reflected signal in a unknown way. In addition, measurement of low reflectivities presume either a complicated set-up, or a well specified reference is needed (for relative measurements).

In contrast the absolute measurement of the zero order transmittance is an easy to perform method. If we choose the wavelength scan range to be broad enough, effective medium theory gives a qualitative picture and the theoretical parameter

Fig. 16 shows the resulting calculated index of refraction as a function of wavelength for 0.4 μm to 2.1 μm and the fit we used for our rigorous calculations. Note that absorption below $\lambda = 400$ nm is important. In our calculations we do not take absorption into account. We therefore restrict our calculations to the interval from 0.4 μm to 1.2 μm.

Measurement of the transmission through foils with the embossed gratings is performed the same way. The measured signal can then be compared with calculated spectra. In Fig. 17 we plotted the calculated transmission as a function of wavelength (thin, continuous lines) for lamellar gratings. Shown for four different duty-cycle are the results for four different heights. Shown as well is the measured transmittance as a function of wavelength for our first example (thick continuous line). As can be seen clearly, it is not possible to fit the measured signal to theoretical results for lamellar gratings. The graph with the duty-cycle $f = 0.35$ shows in addition the calculation results for the grating profile shown in the inlay of Fig. 18.

This agreement is shown for a broader wavelength range in Fig. 18. Down to 540 nm the measured signal (continous line) is well reproduced (broken line). However, below this wavelength the measured transmittance is significantly higher than the theoretical values indicate. Here higher orders of transmission start to couple. They are totally internal reflected at the rear side and impinge again onto the grating structure. Part of the light is then coupled back and contributes to the measured transmission. Taking this effect into account (crosses in Fig. 18) leads to slightly too high values. From our calculations we know that most of the light which coupled in the first order, is totally internally reflected at the grating as well. It will as long undergo internal reflections, until it couples to a different order. For this light surface roughness of the grating structure is more likely to lead to straylight, decreasing the transmission.

The original quartz master is shown in Fig. 14 in the left micrograph. Note that the nickel shim is a negative replica of that. The embossed structure corresponds to the SEM micrograph. The embossed grating can be seen in the second SEM of Fig. 15.

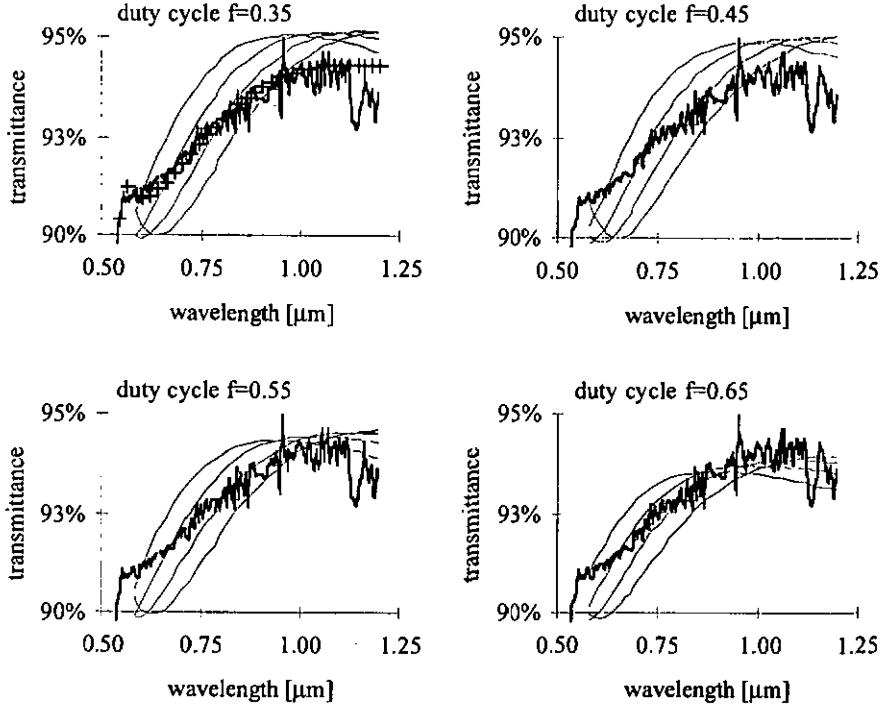

Fig. 17. The measured transmission signal cannot be fitted to the calculated transmittance of a lamellar grating structure. This is shown for four different duty-cycles and different grating depths (continuous thin lines). The continuous thick lines indicate the measured signal. This is to compare with the results from the grating profile as assumed in Fig.18 (crosses in the graph with duty-cycle $f = 0.35$).

We investigate a second example: a grating with 140 nm depth. The original quartz master has almost rectangular profile shape as shown in the right micrograph of Fig. 14. For this grating as well, theoretical calculations and experimental measurements could be brought to good agreement as can be seen in Fig. 19. The assumed profile is shown in the inlay of the figure. The embossed structure is shown in the first SEM of Fig. 15.

We conclude that measurement of the zero order transmittance in combination with rigorous calculations is a straight forward and easy to perform method to determine the profile of one-dimensional submicron surface gratings in transparent substrates.

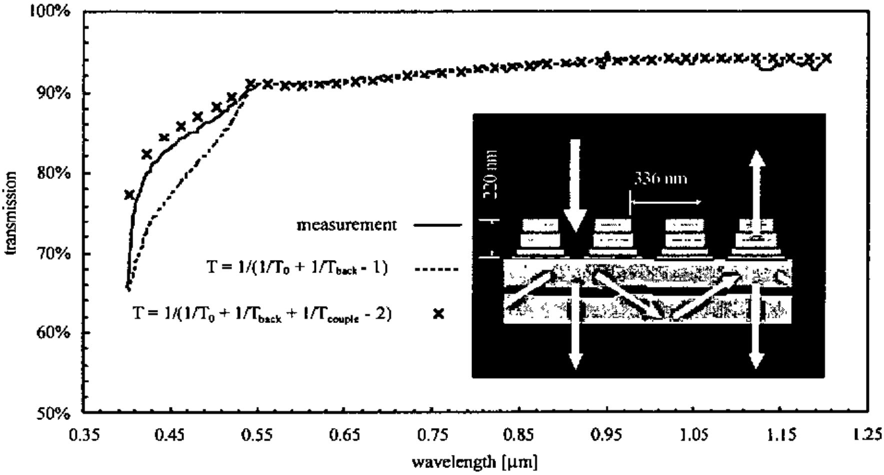

Fig. 18. Measured (E-polarization) transmittance as a function of wavelength (continuous line) and calculated values for the grating shown in the inlay. There is good agreement between theory and experiment for wavelengths above 540 nm. Below 540 nm higher orders of transmission start to couple. They are totally internally reflected at the rear side and impinge again onto the grating structure. Crosses indicate the resulting transmission if this effect is taken into account (to compare with the broken line).

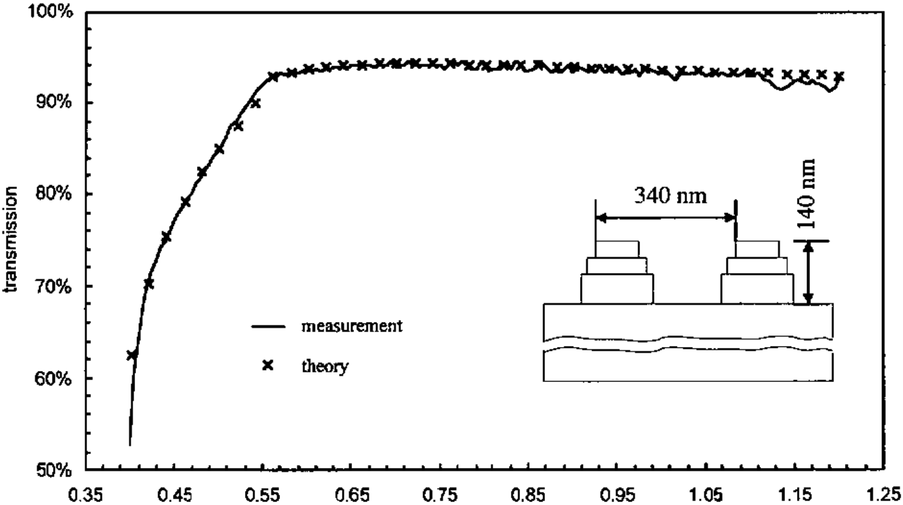

Fig. 19. Measured (E-polarization) transmittance as a function of wavelength (continuous line) and calculated transmission for the grating shown in the inlay. Note that even for the wavelength region where higher transmission orders propagate, there is good agreement between theory and experiment. The inlay shows schematically the grating structure.

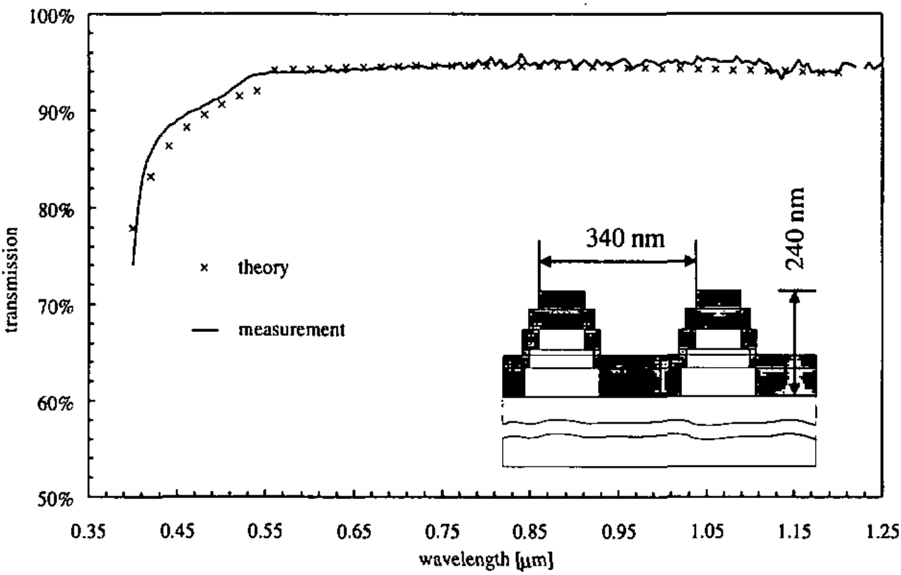

Fig. 20. Measured (E-polarization) transmittance as a function of wavelength (continuous line) and calculated transmission for a MgF_2-coated grating. Especially in the low wavelength range there are differences between theory and experiment: the coating geometry is difficult to simulate. In addition little is known about the optical properties of MgF_2 for such a coating. We therefore assume a constant index of refraction of 1.38 for MgF_2.

4.4. Coated grating structures

Very different is the situation for coated grating structures. Very little is known about the coating geometry and the refractive index of a coating. MgF_2 for example changes its refractive index during several days after evaporation [2] due to humidity. In addition the influence of the grating structure on the optical properties of the coating material is an open question. The theoretical description of such devices is therefore difficult.

We coated the grating shown in the first SEM of Fig. 15 with 100 nm MgF_2 and measured the zero order transmission spectrum. For the calculations we assume an index of refraction of 1.38. The calculations are performed taking dispersion of the polycarbonate foil into account. The left inlay of Fig. 15 shows the structure used for the approximation. As expected the theoretical description of such a device is not as convincing as for the uncoated structures.

In this chapter we investigated the characterization of surface grating structures. There is an additional interesting result: The transmission measurements confirme the antireflection (AR)-properties of submicron grating structures as expected from chapter 2. Comparing Fig. 19 and Fig. 20 shows that the broad AR-properties are even improved by coating the surface grating with MgF_2. In the following chapter we investigate these properties in more detail. In addition other possible application of such structured thin film systems are investigated.

5. Applications based on thin film-grating combinations

It is an important part of this work to search for new possibilities with structured thin films or thin film coated gratings. This includes the investigation of various designs for new applications as well as the experimental possibility to fabricate such devices. Although we did not fabricate all of the devices, we discuss in this work the realistic possibility of fabricating the structures was always a stringent requirement.

We investigate

- a broadband antireflection structure for solar energy applications.
- an asymmetric coated grating for applications such as light trapping and light coupling.
- antireflection structures on optical elements such as blazed gratings.
- polarizing submicron gratings for narrow band polarizers.
- high- and low-pass edge filters.

5.1. Broadband antireflection structure

We have seen in chapter 3 and chapter 4, that surface grating structures are well suited as broadband antireflection surfaces. Good AR-coatings have been realized on glass substrates, based on thin film technology for spectra, as broad as the visible range. However, for spectra in the range of the solar spectrum (from 400 nm to 2100 nm) few convincing solutions are known. In addition stable antireflection coatings on plastic materials are still a difficult task and only few commercial products are available [63, 64].

Submicron grating structures with special profile shapes as discussed in chapter 3 are difficult to fabricate. Possibly special etching techniques could be used to approximate the profiles as required. Replication-techniques should then lead to acceptable costs for the devices. However, the typical gratings are rather deep and it is therefore not trivial to replicate them. In addition the surface of polycarbonate itself can be easily scratched and a coating with a harder material would be an advantage.

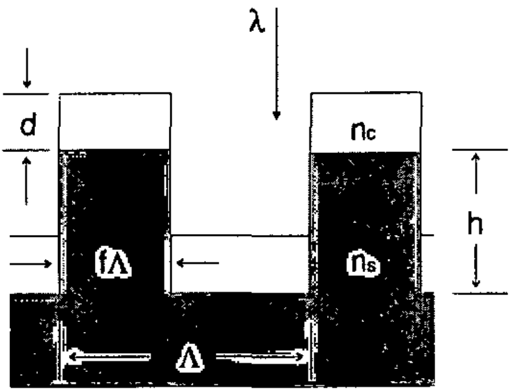

Fig. 21. Geometry of the coated grating structure. The surface grating, with period Λ, duty-cycle f and grating depth h, is embossed in the substrate with index n_s. It is covered with a dielectric thin film of thickness d. The refractive index of the coating material is smaller than the index of the substrate.

Magnesium fluoride (MgF_2) is one of the few dielectric materials with a refractive index (n = 1.38) clearly below the index of glass and with good mechanical properties. It is therefore the most important coating material for antireflection coatings. Our investigations focus on the possibility of using this dielectric material and its advantages in combination with surface gratings. In particular, we present calculations and experiments with MgF_2-coated grating structures for solar energy applications.

Our approach can be motivated from the point of few of effective medium theory: As we know, a lamellar high frequency grating can be described on the basis of effective medium theory. It approximates a one layer (two level) thin film system. Coating this grating with a dielectric thin film leads to a three layer (four level) thin film stack. The outermost layer has obviously an effective index between MgF_2 and air, suitable to act as the missing stable material with very low refractive index. The device is schematically shown in Fig. 21.

Our theoretical investigations are based on grating structures with a period of 250 nm. For a grating in polycarbonate with this period we are in the regime, where rigorous diffraction theory has to be used for scanning the grating parameter space. The remaining grating parameters are the duty-cycle (f), grating-depth (h) and coating-thickness (d). The results of our calculations are discussed in detail in paper II. For the parameters f = 0.45, h = 170 nm and d = 100 nm the average reflectivity, weighted with the solar spectrum, is below 0.6 % for a wavelength range from 300 nm to 2100 nm. As discussed in the paper for the critical experimental parameters such as duty cycle, grating depth, and coating thickness, the calculated tolerances are fairly large to deviations from the optimal values.

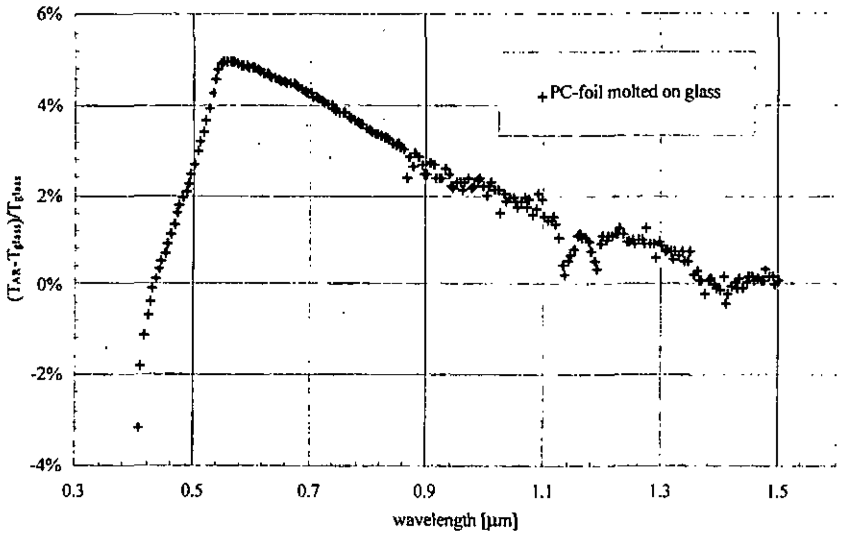

Fig. 22. Transmission through a polycarbonate-glass device. The outer surface of the foil consists of a MgF_2-coated grating structure, forming an antireflection surface. It was fabricated before the foil was molten on the glass. Transmission (T_{AR}) through the molten compound is obviously higher than through the untreated bare glass reference (T_{glass}). We conclude that the grating survives even heating to the glass temperature of polycarbonate.

Paper III describes the fabrication and characterization of such a device. However for fabrication reasons we use a period of 340 nm. The depth of the grating is 140 nm and the MgF_2 layer has a thickness of 100 nm. Weighted with the solar energy spectrum the measured reflectivity is below 0.6 %. For solar energy applications different angles of incidence of the sun light during a day have to be taken into account. Transmission measurements are presented for polycarbonate-foils with antireflection-structures on both sides. These measurements show, that the daily average photon loss per air-plastic interface can be reduced by at least 3 % compared to the untreated surface.

Discussed in paper IV are stability properties of such devices. MgF_2 coated gratings in polycarbonate turn out to be more resistant to heat compared to bare gratings. Even melting the substrate cannot destroy the coated grating structure. This is shown in Fig. 22, where we put a polycarbonate-foil on a glass substrate and heat the system until the polycarbonate-foil melts on the glass and forms a compact device. As the figure shows, the transmission is increased compared to the bare glass surface, indicating that the AR structure survived the heating.

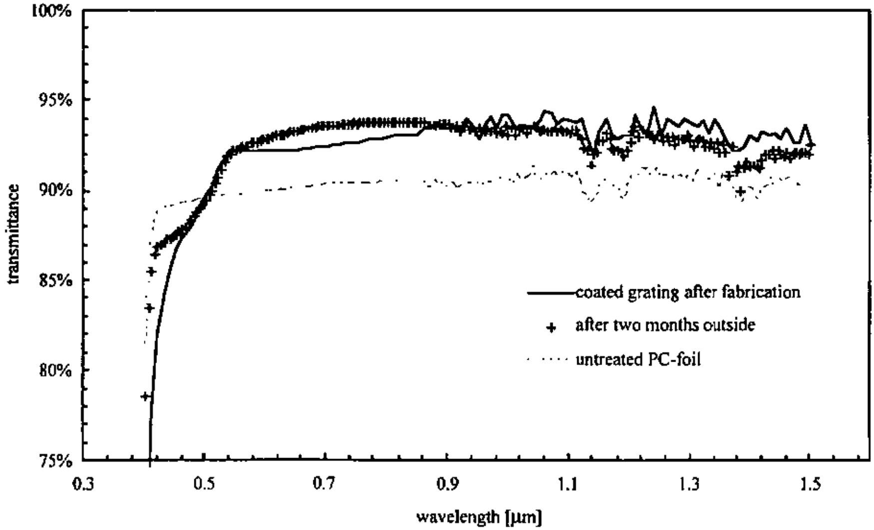

Fig. 23. E-polarization transmission characteristics of the broadband AR-structure before and after the device was exposed for two months to rough weather conditions. The grating depth decreased during that time, but the main antireflection characteristics are retained.

A scotch-tape test shows, that the MgF_2 coating adheres better to PC-surfaces, if it is structured. As a consequence these devices are rather stable when exposed to normal weather conditions. Fig. 23 shows the transmission characteristics of the BAR structure before and after the device was exposed for two months to 'Swiss winter conditions'. Transmission measurements indicate, that the grating depth decreased during that time, but the main antireflection-characteristics are retained.

It is important to see how the AR performance of coated grating structures compares to other approaches for broadband antireflection. The triangles in Fig. 24 show the measured transmittance as a function of wavelength for a eight layer thin film coating on polycarbonate. The backside of the device is not antireflection treated. Note that this device is optimized for the visible range. The transmission of the coated gratings is slightly below the thin film device up to 700 nm. For solar applications the thin film device is not suitable at all. The figure shows as well the transmission performance of a moth-eye structure. The structures are realized on both sides of the element. For the rear side we therefore assume an additional decrease of transmission (corresponding to an untreated polycarbonate surface).

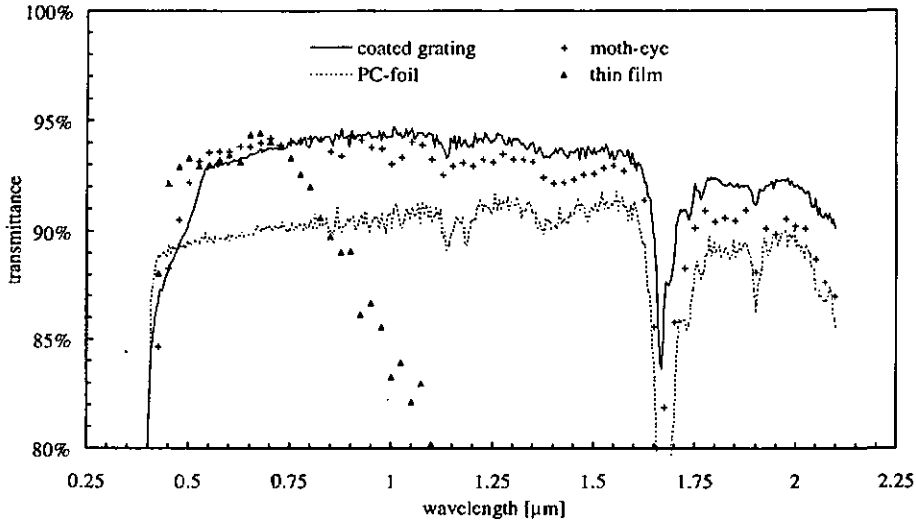

Fig. 24. Transmittance (unpolarized light) for different antireflection surfaces on plastic materials. Just one side is AR-treated. The triangles indicate the measured transmittance of a conventional thin film stack. Note that this stack was optimized only for the visible range. The measurements on moth-eye structures where performed with foils having structures on both sides. The crosses indicate the decreased transmission values if one of the surface is simulated to be untreated. This is to compare with the performance of the coated grating structure (continuous line). We take the untreated polycarbonate foil as reference, which is shown by the broken line.

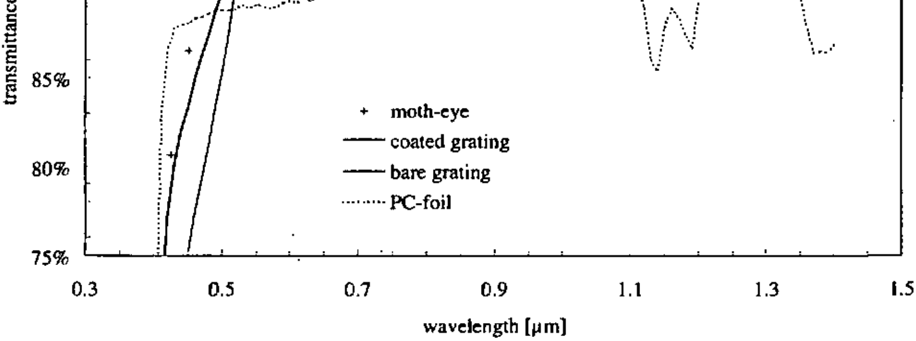

Fig. 25. Transmittance (unpolarized light) for different antireflection surfaces on plastic materials. Both sides of the foil are AR-treated. Obviously for the parts of the visible range the moth-eye structure shows better performance. However the coated grating structure was optimized to cover the whole range of the solar spectrum and in the long wavelength range the moth-eye is not deep enough. Note the sharp edge at 530 nm for the coated grating structure. Here higher orders of transmission start to couple.

Again, up to 700 nm the moth-eye transmission performance is above the coated grating, but then up to 2100 nm our structure clearly wins. The transmission through devices where both sides are AR-treated, is shown in Fig. 25. Note that the coated grating device was optimized for the solar spectrum and not especially for the visible range. A change in the coating thickness could possibly improve the performance in the visible range significantly.

5.2. Asymmetric coated gratings

In paper II the theoretical and experimental possibility to improve light trapping in a solar cell is presented. The idea of R. Morf was to optimize submicron grating structures on the rear side of a thin silicon cell in order to couple the long wavelength part of the solar spectrum into higher orders of reflection. His calculations showed that the use of gratings, approximating a sawtooth-profile, is of advantage, because disturbing symmetry effects, leading to an effective outcoupling, are avoided.

Directional evaporation of dielectric materials opens the possibility to evaporate at angles not perpendicular to the grating surfaces and therefore to realize asymmetric grating structures without much experimental effort. This could be used for improved light trapping and for grating couplers.

We coated in polycarbonate embossed gratings with MgF_2 at an angle of around 85°. In order to have a stronger effect, we fabricated on both sides of the sample such asymmetric structures according to the inlays of Fig. 26 and Fig. 7. Shown in both figures is the measured transmittance as a function of the wavelength of light. Fig. 27 is the result of a measurement after turning the grating by 180° around an axis normal to the surface.

Simulation of such a device is difficult. In addition to the difficulties described in chapter 4 (strong influence of the unknown coating geometry and unknown MgF_2 dispersion), higher orders of reflection appear also at the backside of the structure which themselves impinge again on the grating at the frontside. This leads to a high number of propagating orders inside the device, which are able to couple back again to the transmission order.

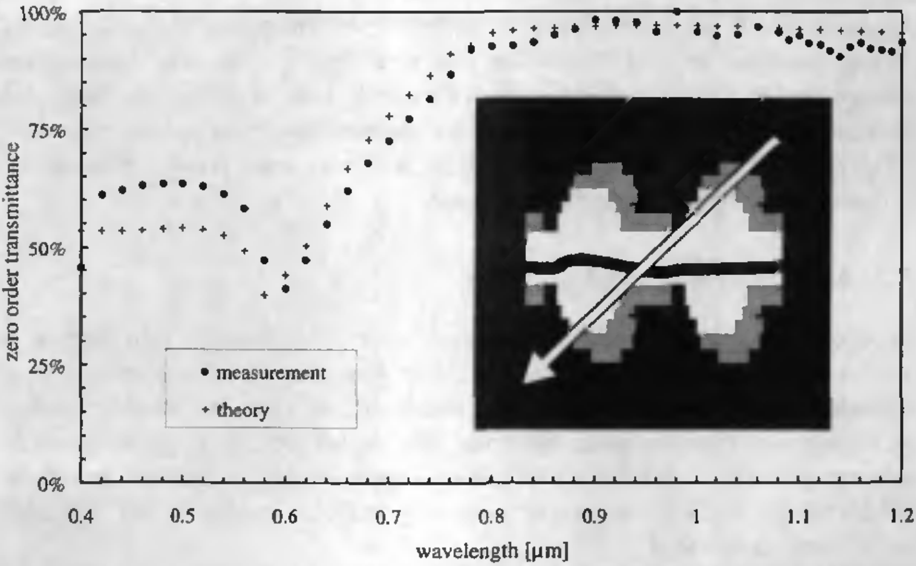

Fig. 26. Transmission at oblique incidence (angle = 45°) for a coated grating structure as schematically shown in the inlay. Theory and experiment do not agree completely but show roughly the same tendency. The difficulties are probably due to the unknown exact grating geometry and its influence on the index of refraction of the coating material. Note the resonant coupling at the wavelength of 600 nm.

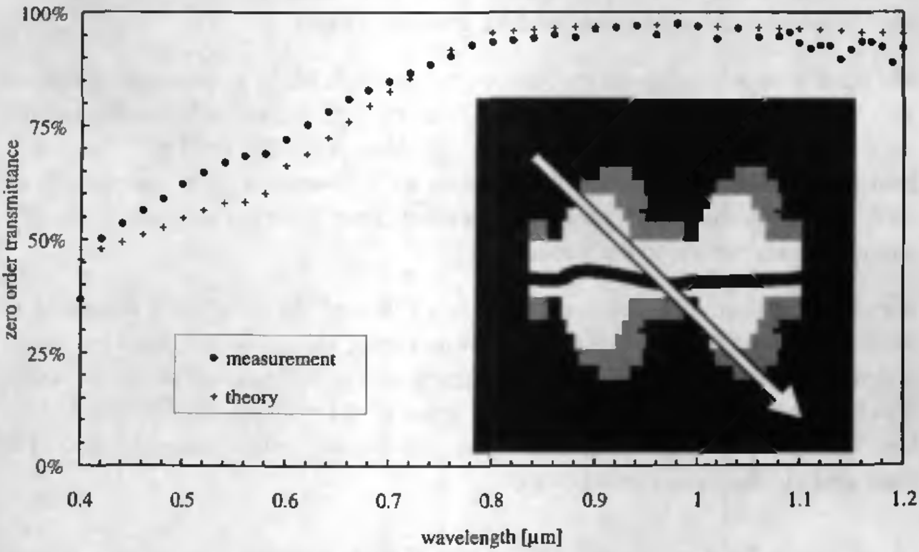

Fig. 27. Same situation as in Fig. 26, but the angle of incidence is now changed to -45°. Note that the resonant coupling at 600 nm almost disappeared. This asymmetry-effect is introduced by the tilted coating procedure.

The crosses in both figures indicate the results of our calculations. Note that there is a good agreement in the area where no higher diffraction orders are propagating. In the short wavelength range (below 600 nm) the qualitative structure of the measured transmission is roughly followed. Note that is was not possible to simulate the measured signals with the lamellar structures as shown in paper IV.

Our coating material was MgF_2 in order to stick to one dielectric material throughout the whole work, but the asymmetric effect is expected to be more effective for coating materials with high indices of refraction.

5.3. Submicron gratings on the surface of optical elements

Many of the transmission elements based on refraction are antireflection coated with a more or less broad effective range, depending on the application. An increasing number of elements (refractive as well as diffractive) is realized with plastic materials. As already discussed before, stable coatings for such materials are not easy to produce. It is therefore an interesting question, whether the earlier discussed moth-eye structures or coated grating structures can be superimposed on such devices (experimental challenge) and how their performance is affected (theoretical question). Once a shim is produced with such superimposed structures, replication techniques could lead to cheap antireflection "coated" devices. If the AR-performance is not effective enough the device can be thin film coated with an improved mechanical stability due to the submicron structures.

We investigate AR-structures on blazed gratings. For the theoretical calculations we assume a grating period of 6 μm and a substrate index of refraction of $n = 1.54$. The goal is to maximize the first order transmission efficiency for a wavelength of $\lambda = 633$ nm (light of a He-Ne laser). We calculated the diffraction efficiencies for this system as a function of depth of the blazed grating. The spheres in Fig. 28 indicate the calculated first order transmission efficiency. The optimum depth for a blazed grating without AR-grating is at 1.16 μm. As expected, the first order diffraction efficiency is increased and the maximum is displaced to a deeper grating depth.

Effective medium theory predicts an optimum AR-submicron grating depth of 140 nm for a duty cycle of $f = 0.5$ for lamellar gratings (E-polarization case). In our calculations we increase the submicron grating depth proportional to the depth of the blazed grating. The proportionality factor is chosen in such a way, that the

AR-grating depth is 140 nm for the optimum depth of the blazed grating. Fig. 29 shows how the reflectance spectra of both devices compare. Note that for the system without AR-structures the sum over all reflected orders is close to 5% for any of the investigated wavelengths. In addition Fig. 29 shows how the different reflected orders, contributing to the sum.

Our calculations are performed with a 20 grating layer discretization. We used 22 layers in the case of the AR superimposed grating, where we assumed lamellar structures. Please note that the experimental AR-structures will be moth-eye structures. Due to their profile they simulate rather a graded index layer than a thin film layer with constant (effective) index of refraction.

Fabrication of AR-superimposed blazed gratings with a period of 16 µm is possible using e-beam writing. In a first exposure step the blazed gratings are written and developed, but not to the final depth. It follows the second exposure which is dedicated to the moth eye structures. After this, a second developing step should lead to the desired superimposed structures.

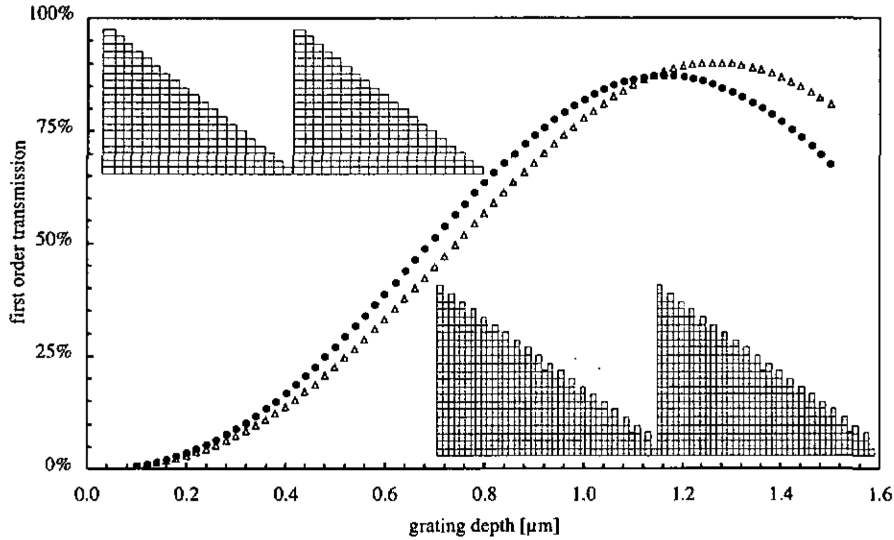

Fig. 28. Calculated first order transmission efficiency for a blazed grating with antireflection structures superimposed (triangles), as a function of grating depth. Dots show the efficiency for a blazed grating without AR-structures. With the AR-structures the maximum efficiency is increased from 87% to 90%.

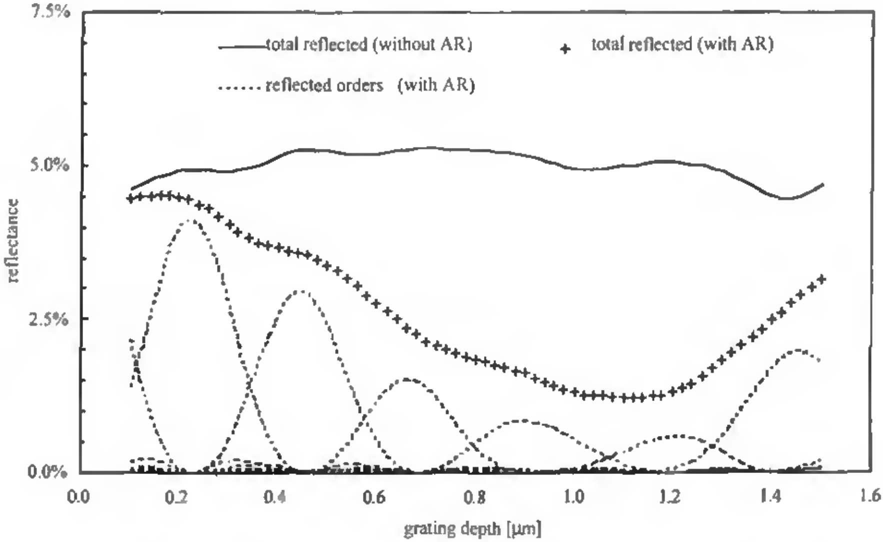

Fig. 29 Calculated reflectance as a function of grating depth for a blazed grating with and without AR-structures superimposed. The total of the reflected light for the grating without AR-structures sums up to approximately 5%. For the blazed grating with the superimposed AR-structures this value is decreased to 1.2% for the height of maximum first order transmission efficiency.

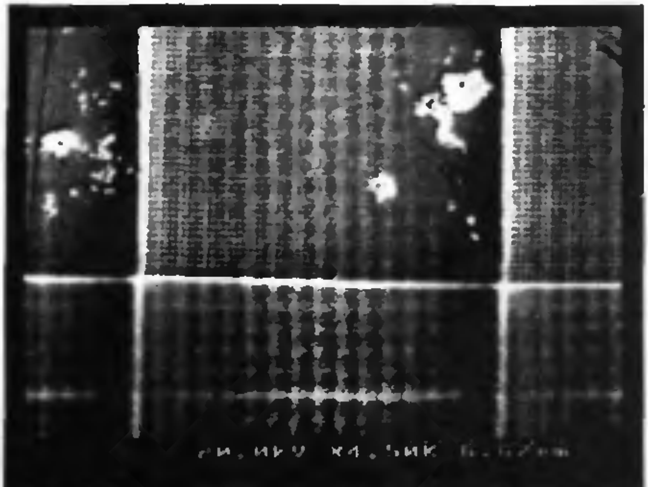

Fig. 30. SEM-micrograph of a blazed grating with 16 μm period. The thick white vertical lines mark one period. The upper part of the picture shows the region, where the device was in addition e-beam exposed with a 300 nm periodic pattern, leading to a AR-superimposed structure. Note that in deeper regions of the blaze structure the AR-structures disappear.

Fig. 30 shows in an SEM the result of such a procedure for a 16 μm blazed grating. The micrograph is divided in six sections: two rows and three columns. The columns have a width of 16 μm and represent the blazed grating. Going from left to right in each column means to go down the blaze. The horizontal line separates the region where we exposed dots with a period of

300 nm (upper part) from the region where we only exposed the blazed grating (lower part). In the lower part of the picture there are some periodic patterns which are probably due to the e-beam writing procedure. In the upper part there are some additional periodic pattems of smaller scale which are quite clear on the left side of every column and seem to faint away, if one goes to the right inside the column. Those smaller structures have a periodicity of 300 nm. They are the superimposed AR structures.

This device was fabricated to demonstrate the possibility of two exposures. Unfortunately we overdid the developing and reached the underlying quartz substrate. Therefore we do not expect a very high efficiency for the coupling.

5.4. Polarizing gratings

In the case of high-frequency one-dimensional gratings, the effective thin film has birefringent properties as can be seen from Fig. 31. Shown is the effective index as a function of the duty cycle for a one-dimensional lamellar grating layer with n = 2.4 in the first domain and n = 1.38 in the second domain (out of two).

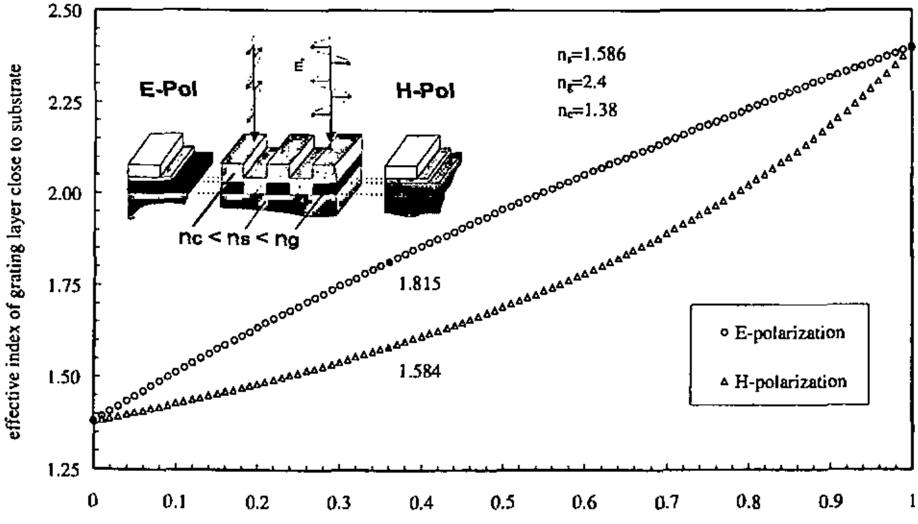

Fig. 31. The effective index is always between the indices of the contributing materials. For one-dimensional gratings the index will differ for the two polarizations. If the grating consists of a combination of materials with refraction indices above and below the index of the substrate, there is a duty-cycle for which the effective index for one polarization is equal to the substrate index. Changing the grating depth does then not affect the transmission properties for this polarization. In analogy to λ/2-layers (= absentee layers) in thin film optics, we call such gratings 'absentee-gratings'.

For the H-polarization the effective index is $n_H = 1.584$ in the interesting grating layer for a duty-cycle of $f = 0.36$. This is very close to the index of the substrate and H-polarized light, impinging on the grating, will experience almost no difference to the substrate. In thin film optics $\lambda/2$-layers are called absentee layers, because their existence has no effect on the reflection or transmission properties of a thin film stack. In analogy to this, we call such a grating-substrate combination as shown in Fig. 31, one-dimensional absentee-grating.

There are two important properties of such a grating layer:

- one-dimensional absentee gratings are absent only for one polarization.
- changing the thickness of the polarizing absentee grating does not change the optical properties for one polarization as far as they can be described by effective medium theory.

Note that the MgF_2-coating according to Fig. 31 acts as a two layer antireflection coating.

For the same duty-cycle ($f = 0.36$) we have a value of $n_E = 1.815$ for the E-polarization, as can be seen in Fig. 31.We can choose the layer thickness to have maximum possible reflectivity for this index, which does not change anything for H-polarized light. The result is a dielectric polarizer.

Unfortunately, due to the small difference between n_E and the index of the substrate, the reflection effect is very limited. As a consequence the polarization contrast ratio (PCR), which is defined as the quotient of the transmittance of the polarizations (T_H/T_E) is rather poor. There is the possibility to build quarter-wave stacks in analogy to the stack as described in chapter 3. Another possibility is to increase the grating period and approach the rigorous regime, where modes, known as leaky modes [65] become important. Our rigorous diffraction calculations show, that PCR of 15000 can be (theoretically) realized for a narrow band. This is illustrated in Fig. 32. Plotted on the first axis is the transmission of the H-polarisation as a function of wavelength. Note that the transmittance is close to 100% as soon as we are leaving the resonant regime. On the second logarithmic axis we plotted the inverse PCR.

This narrow-band polarizer combines aspects of the narrow-band optical filters, as proposed in [66], with properties of the polarization components as discussed in [65] and AR-effective thin film layers.

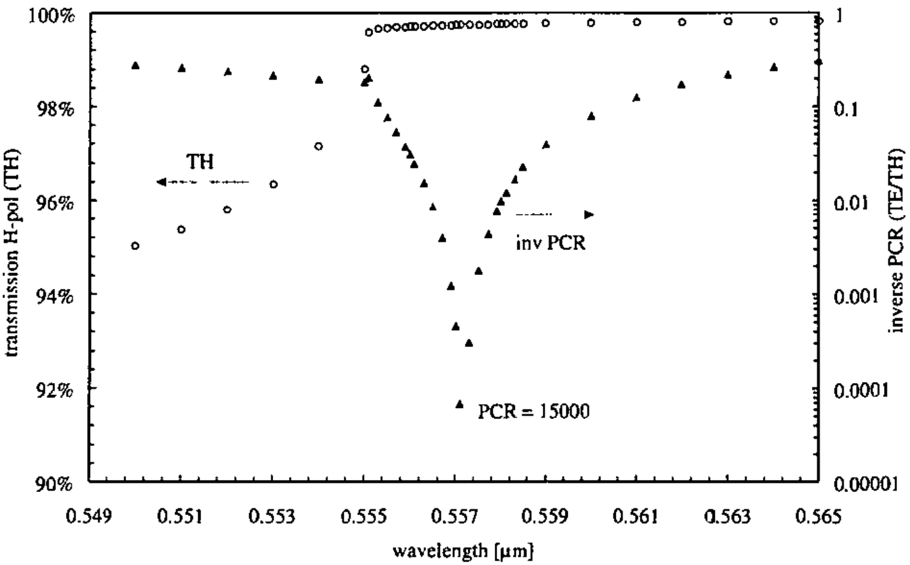

Fig. 32. The index difference for the two polarizations in Fig. 31 is too weak to be useful for a polarizer. However in the resonant regime leaky modes start to couple and the polarizing effect is very strong. The grating period is fixed to 350 nm and the duty-cycle, according to Fig. 31 is f = 0.36. The calculations show the transmission of H-polarized light (right axis). Note that above 0.555 nm the transmission is above 99%, due to the AR-effect of the MgF_2 coating. The logarithmic axis shows the inverse polarization contrast ratio (inv. PCR). Note that the PCR peaks to 15000 in rigorous theory.

Such devices can be important for applications where a polarisation selective, high reflecting mirror is needed. In Vertical Cavity Surface Emitting Lasers (VCSELs) it is still a problem to control the polarization of the emitted light. In theory it is possible to realize an absentee layer with GaAs on AlAs (typically used in this technology) in combination with SiO_2.

5.5. High and low pass filters

Low- or high-pass filters with very sharp edges in the visible range are a challenge in thin film optics. In most cases they are based on Bragg stacks with quarter wave thin film layers, which provide stop bands with a reflectance equal to 100% (see chapter 3). The problem are the ripples which appear in the pass band and which are in most cases not acceptable for the high -or low-pass filter. The broken line in Fig. 33 shows the calculated reflectance as a function of wavelength for such a Bragg stack.

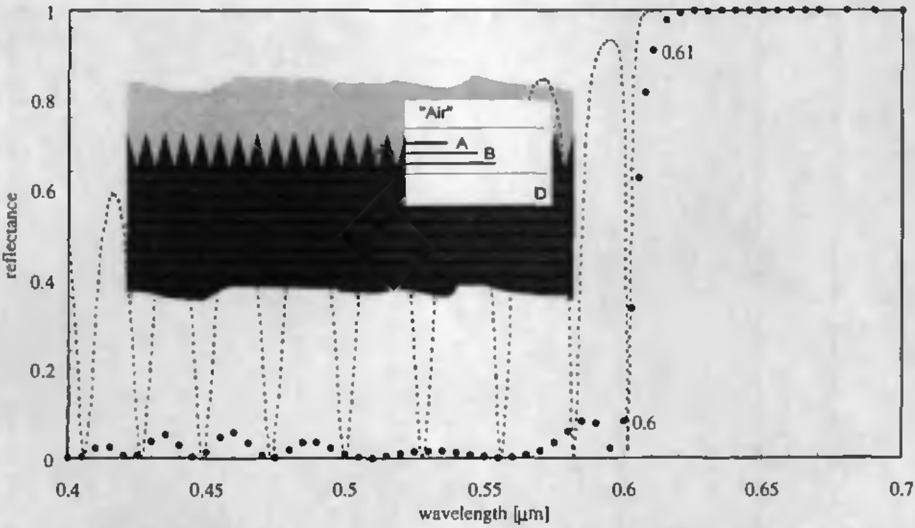

Fig. 33. Reflectance as a function of wavelength for a quarter-wave stack. The broken line shows the reflectance of a conventional Bragg-stack. Note the strong oscillations in the pass-band due to the fact that the 'Herpin-layer' is not matched to cover and substrate. This is avoided with AR-structures etched in the layers. The dots show rigorous calculations for a 23-layer system with AR-structures on both sides.

The reason why these ripples appear is not very difficult to understand: due to the special properties of the transfer matrix of a quarter-wave stack such a device can be described by replacing the stack by one single thick dielectric layer and the corresponding Herpin index [2]. In the region of the stop band this index becomes imaginary and as a consequence the reflectance equals 100%. In the pass band region the index is real. However approaching the stop band region the absolute value of the Herpin index increases to infinity. This is represented by the thick white line in Fig. 34. Therefore, for some wavelengths the 'Herpin layer' is an odd multiple quarter wave (maximum reflectivity) and for some wavelengths it is a multiple half wave layer. If one approaches the stop band, these oscillations will become even worse, due to the increasing or decreasing Herpin index. Note that as consequence a higher number of quarter wave layers, forming the Herpin-layer, leads to a higher oscillation frequency.

The ripples can be partly suppressed by matching the quarter wave stack to the outer space. This can be done using refinement methods (as for example simulated thermal annealing, described in chapter 2) or analytical approaches as described in [2].

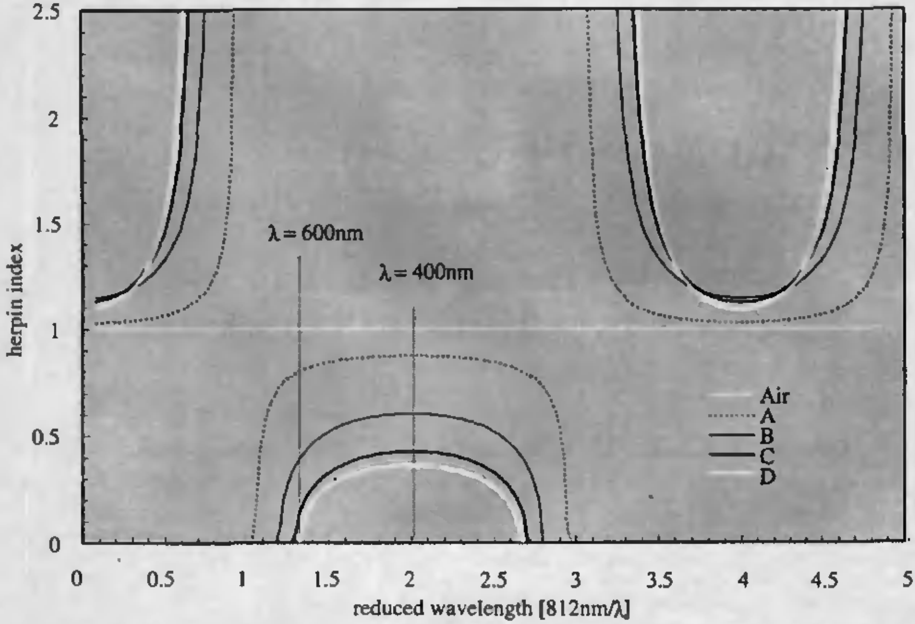

Fig. 34. Herpin index as a function of reduced wavelength for the four different levels in the quarter-wave grating structure according to Fig. 33. For any wavelength element of the pass band interval there is a smooth refration index transition from the 'Herpin layer' to the surrounding medium. This can be seen following the lines for the wavelength 600 nm and 400 nm.

According to this reference, a graded index film would be the optimum to match the system. However even in the case of a graded index film, because of the dispersion of the Herpin index, the matching can only be perfect for one (or two) wavelengths in the pass band region.

With the help of tapered profile surface grating this problem can be avoided. The design is shown in the inlay of Fig. 33. We investigated the Herpin index for three different levels denoted by A, B, and C coming from the 'air' halfspace and ending in the quarter wave 'bulk' D. The index is plotted in Fig. 34. We see that for the wavelength $\lambda = 400$ nm and $\lambda = 600$ nm and all wavelengths in between, the transition from the quarter wave stack to the air is smooth and probably does not give rise to any strong reflections. This is confirmed by the rigorous calculations. The results are plotted in Fig. 33. As can be seen, the ripples are almost suppressed. Note, that for such a high frequency pass filter the grating period has to be small enough in order not to have any diffraction orders coupled for wavelengths in the pass band.

6. Summary

In this work we have developed methods to investigate theoretically and experimentally the properties of thin-film coated submicron gratings and microstructured thin films.

Rigorous diffraction theory, based on the expansion of eigenfunctions in orthogonal polynomials, was developed to calculate arbitrary one-dimensional multidomain submicron gratings. Aspects of convergence where investigated and the transition from the rigorous regime to the limits of larger grating periods (scalar theory) as well as smaller grating periods (effective medium theory) were discussed.

We showed that thin film design methods, such as simulated thermal annealing and quarterwave-stacks together with effective medium theory can be applied for the optimization of microstructured thin films. Rigorous calculations are necessary at least to confirm the (theoretical) correct performance of the devices.

One part of our work focused on the question how theory and experimental measurements of efficiencies compare. We restricted ourselves to the measurement of the zero order transmission. We were able to describe uncoated grating structures, embossed in polycarbonate in a correct way. It was not possible to fit the measured transmittance with the calculated values of lamellar gratings. A more complete comparison of theoretical and experimental values requires the determination of the exact profile of the surface grating structure. As a consequence this can be used to determine the grating profile based on measurements of the zero order transmission. Different methods to prepare a well defined edge for SEM investigations of gratings embossed in polycarbonate, where developed.

The theoretical description of MgF_2 coated grating structures was not convincing, due to the unknown coating geometry and its effect on the index of refraction of the coating material. However, the special optical properties we measured, such as broadband antireflection and asymmetry-effects for tilted coatings could be reproduced qualitatively in theory. Because of the desirable mechanical properties of such MgF_2 coated submicron structures, they are an interesting approach for applications, such as solar energy devices and grating couplers.

The following table lists the devices we investigated and their important properties:

device	performance	design	investigations	application
broadband AR-structures	3 µm-12 µm R < 0.25%	surface grating, optimal profile depth: 3.9 µm	theoretical, optimized with STA	only of theoretical interest
broadband AR-structures	0.4 µm-1.2-µm R < 1%	MgF_2-coated surface grating depth: 0.27 µm	theoretical, experimental	solar devices, AR-coatings on plastics
AR-structured blazed grating	reduced Fresnel loss, increased efficiency from 87% to 90%	blazed grating, AR-structures superimposed total depth: 1.26 µm	theoretical (performance), experimental (fabrication)	surface of many optical elements
asymmetric gratings	differences in transmission of up to 30% for tilted angles with opposite sign	embossed grating with tilted coating depth: 0.24 µm	theoretical, experimental	light trapping, grating coupler
mirrors with increased reflectance zone	630 nm-950 nm R > 99.5%, smooth phase	15 layer quarter-wave stack with grating grooves depth: 1.5 µm	theoretical	mirrors for short laser pulses
absentee gratings	polarization contrast ratio up to 15000	structured thin film on substrate and additional coating depth: 0.23 µm	theoretical	narrow band polarizer
edge filters	sharp edge, R= 100% stop band, R < 10% pass band	quarter-wave stack with etched AR-structures depth: 0.7 µm	theoretical	high- and low-passfilters for the visible region

Most interesting for applications in near future are designs with rather shallow surface structures and additional thin film coatings. Structuring of the plastic or even glass substrates can then be realized by embossing. The following coating steps are easily performed.

The fabrication of micostructured thin films on a large scale is more difficult. Processes of evaporating a thin film stack on a substrate are well established, but the following etch steps for the submicron grating are not jet well developed. However, there is a rapid development of these techniques and we expect them to become as established as today is the evaporation of thin films. Especially the deep grating structures, as was the case in theory, are still a challenge.

To our opinion, microstructured thin films exhibit a large potential for various applications, and we think that they become as important in the field of optics, as their unstructured equivalents.

Acknowledgments

Starting my Ph.D.-work at the Paul Scherrer Institute in July of 1993, I found a very complicated structure (cf. Fig. 35), which was already optimized. The figure shows its approximation with 54 layers, each layer consisting of approximately 100 domains. In addition shown is the increasing efficiency for the wavelength range from 1993 nm to almost 1997 nm.

There are several important properties of this structure:

- Most important for the performance were the outermost parts of the structure. I did not know, whom to thank first. Once again, periodic grating structures, as was often the case in my work, provided a solution.

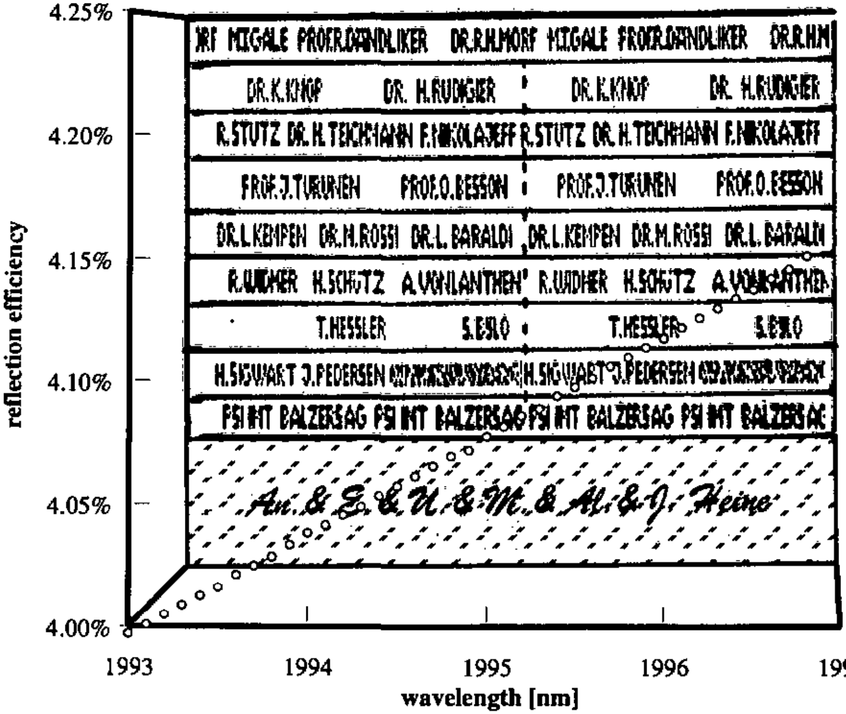

Fig. 35. The structure I entered when I jained the optics group at PSI in Zürich. Note that this is just an approximation and I am sure that there are still same important names missing, such as Dr. R. Kunz, Dr. J. Söchtig, Dr. H. Sigg, ...

- Very important as well was the 'layer' closest to the substrate. I wish to thank the support of the Balzers AG, the Paul Scherrer Institute, and the Institute of Microtechnology.

- In addition I want thank the Diffractive Optics Group at the Chalmers University of Technology in Sweden. I had the possibility to join this sympathetic group for two weeks. We fabricated a lot of tea and the e-beam written AR-superimposed blazed gratings. This is, to my opinion, one of the highlights of this work.

- My family and my friends were the basis of my work. They form the 'substrate', providing stability and confidence in all the complicated and strange design strategies for my live.

In such a device, every layer and its constructive contribution is important and could not be removed without affecting the resulting efficiency in a serious way. During my time as a Ph.D.-student I found many people, friends supporting me. There were always open ears for my problems and time for discussions, even when they themselves were living in a difficult period of time.

Thank You

REFERENCES

[1] J.C. Maxwell, "*A Treatise on Electricity and Magnetism*", First edition published in 1873. The third edition, originally published by Clarendon Press in 1891, was republished in unabridged form in 1854 (New York: Dover).

[2] H.A. Macleod, "*Thin-Film optical Filters*", 2nd ed. (Macmillan, New York, 1986).

[3] R. Petit, ed., *Electromagnetic Theory of Gratings* **22** (Topics in current Physics, Springer-Verlag, Berlin, 1980).

[4] K. Knop, "Rigorous diffraction theory for transmission phase gratings with deep rectangular grooves", *J. Opt. Soc. Am.* **68,** 1206-1210, (1978).

[5] L. C. Botten, M. S. Craig, R. C. McPhedran, J. L. Adams and J. R. Andrewartha, "The dielectric lamellar grating", *Opt. Act.* **28,** 413-428, (1981).

[6] L. C. Botten, M. S. Craig, R. C. McPhedran, J. L. Adams and J. R. Andrewartha, "The finitely conducting lamellar diffraction grating", *Opt. Act.* **28,** 1087-1102, (1981).

[7] L.C. Botten and R.C. McPhedran, "Highly conducting lamellar gratings", *Opt. Act.* **28,** 1103-1106, (1981).

[8] M.G. Moharam and T.K. Gaylord, "Rigorous coupled-wave analysis of grating diffraction - E-mode polarization and losses", *J. Opt. Soc. Am.* **73,** 451-455, (1983).

[9] Lifeng Li and Charles W. Haggans, "Convergence of coupled-wave method for metallic lamellar diffraction gratings", *J. Opt. Soc. Am.* **10,** 1184-1189, (1993).

[10] R.H. Morf, "Exponentially convergent and numerically efficient solution of Maxwell's equations for lamellar gratings", *J. Opt. Soc. Am. A.* **12,** 1043-1056, (1995).

[11] M.G. Moharam, DA. Pommet, and E.B. Grann, and T.K. Gaylord, "Stable implementation of the rigorous coupled-wave analysis for surface-relief gratings: enhanced transmittance matrix approach", *J. Opt. Soc. Am. A.* **12,** 1077-1086, (1995).

[12] H.W. Lehmann and M.T. Gale, "Submikrongitter: Massgeschneiderte Beugung des Lichts,", *Technische Rundschau,* **81**, 46-53, (1989).

[13] H.P. Herzig, ed., Micro-Optics: Elements, Systems, and Applications (Taylor & Francis, London, 1997), (ISBN: 0 7484 0481 3 HB).

[14] D. Hofstetter,"*Monolithically Integrated Interferometer for Optical Displacement Measurement*", Dissertation, University of Neuchâtel, (1996).

[15] J.D. Jackson, *Classical Electrodynamics,* 2nd ed., (John Wiley & Sons, NewYork, 1975).

[16] T. Possner and R. Göring, "Transmission phase gratings by ion-exchange in optical glasses", *in 10th Topical Meeting, GRIN'92,* Santiago di Compostela, Spain (1992).

[17] R.P Salimo. J. Saarinen, J. Tueunen, A. Tervonen, "Graded-Index Diffractive Elements by Thermal Ion-Exchange in Glass" *Appl. Phys. Let.* **66**, 917-919, (1995).

[18] D. Gottlieb and S.A. Orszag, *Electromagnetic Numerical Analysis of Spectral Methods: Theory and Applications*, (Society of Industrial and Applied Mathematics, Philadelphia, Pa. 1989).

[19] Dale C. Flanders, "Submicrometer periodicity gratings as artificial anisotropic dielectrics", *Appl. Phys. Lett.* **42**, 492-494, (1983).

[20] Eric B. Grann, M. G. Moharam, and Drew A. Pommet, "Artificial uniaxial and biaxial dielectrics with use of two-dimensional subwavelength binary gratings", *J. Opt. Soc. Am. A.* **11**, 2695-2703, (1994).

[21] M. Born and E. Wolf, *Principles of Optics*, 6th edition, (Pergamon, Oxford, 1989).

[22] D.A. Pommet, M.G. Moharam, and E.B. Grann, "Limits of scalar diffraction theory for diffractive phase elements", *J. Opt. Soc. Am. A* **11**, 1827-1834, (1994).

[23] D.A. Gremaux and N.C. Gallagher, "Limits of scalar diffraction theory for conducting gratings,", *Appl. Opt.* **32**, 1948-1953, (1993).

[24] R.H. Morf and R. E. Kunz, "Dielectric filter optimization by simulated thermal annealing", *Thin Film Technologies III,* Proc. SPIE **1019**, 211-217, (1988).

[25] M.H. MacDougal, H. Zhao, P.Daniel Dapkus, M. Ziari and W. H. Steier, "Wide bandwidth distributed Bragg reflectors using oxide/GaAs multilayers", *Electron. Lett.* **30**, 1147-1148, (1994).

[26] R. E. Collins, *Foundations for Microwave Engineering* (Mc-Graw Hill, New York, 1966), Chap. 5, pp. 221-254.

[27] W.H. Southwell, "Gradient-index antireflection coatings,", *Opt. Lett.* **8**, 584-586, (1983).

[28] W.H. Lowdermilk and D. Milam, "Graded-index antireflection surfaces for high-power laser applications", *Appl. Phys. Lett.* **36**, 891-893, (1980).

[29] Michael Jay Minot, "Single-layer, gradient refractive index antireflection films effective from 0.35 to 2.5 μm", *J. Opt. Soc. Am.* **66**, 515-519, (1976).

[30] M.J. Minot, "The angular reflectance of single-layer gradient refractive-index films", *J. Opt. Soc. Am.* **67**, 1046-1050, (1977).

[31] R. Jacobson, "Inhomogeneous and coevaporated homogeneous films for optical applications" in *Physics of Thin Films,* G. Haas, M. Francombe, and R. Hoffman, eds. (Academic, New York, 1975) Vol. 8, p.51.

[32] H.J. Riblet, "General synthesis of quarter-wave impedance transformers,", IRE Trans. on Microwave Theory Techniques **MTT-5**, *36-43.* (1990).

[33] Leo Young, "Synthesis of multiple antireflection films over a prescribed band", *J. Opt. Soc. Am.* **57**, 967-974, (1961).

[34] R. W. Klopfenstein, "A transmission line taper of improved design," Proc. IRE **44**, 31-35, (1956).

[35] D. Raguin and G.M. Morris, "Analysis of antireflection-structured surfaces with continuous one dimensional surface profiles", *Appl. Opt.* **32**, 2582-2598, (1993).

[36] D. Raguin and G. M. Morris, "Antireflection structured surfaces for the infrared spectral region", *Appl. Opt.* **32**, 1154-1167, (1993).

[37] E. N. Glytsis and T. K. Gaylord, "High-spatial frequency binary and multilevel stairstep gratings: polarisation-selective mirrors and broadband antireflection surfaces," *Appl. Opt.* **32**, 4459-4470, (1992).

[38] T. K. Gaylord, W. E. Baird, and M. G. Moharam, "Zero-reflectivity high spatial-frequency rectangular-groove dielectric surface-relief gratings", *Appl. Opt.* **25**, 4562-4567, (1986).

[39] R. C. Enger and S. K. Case, "Optical elements with ultrahigh spatial-frequency surface corrugations", *Appl. Opt.* **22**, 3220-3228, (1983).

[40] R. C. Enger and S. K. Case, "High-frequency holographic transmission gratings in photoresist", *J. Opt. Soc. Am.* **73**, 1113-1118, (1983).

[41] S.J. Wilson and M.C. Hutley, "The optical properties of 'moth eye' antireflection surfaces", *Opt. Act.* **29**, 993-1009, (1982).

[42] E.B. Grann, M.G. Moharam, and D.A. Pommet, "Optimal design for antireflection tapered two-dimensional subwavelength grating structures", *J. Opt. Soc. Am. A.* **12**, 333-339, (1995).

[43] E.B. Grann and M.G. Moharam, "Comparison between continuous and discrete subwavelength grating structures for antireflection surfaces", *J. Opt. Soc. Am.* **13**, 988-992, (1996).

[44] Yu. N. Denisyuk, *Sov. Phys.-Doklady,* **7**, 543, (1962).

[45] N.K. Sheridon, "Production of blazed holograms", *Appl. Phys. Lett.* **12**, 316-318, (1968).

[46] W.T. Tsang and S. Wang, "Simultaneous exposure and development technique for making gratings on positive photoresist", *Appl. Phys. Lett.* **24**, 196-199, (1974).

[47] M. J. Beesely and J. G. Castledine, "The use of photoresist as a holographic medium,", *Appl. Opt.* **9**, 2720-2724, (1970).

[48] P. Ehbets, H.P. Herzig, P. Nussbaum, P. Blattner, and R. Dändliker, "Interferometric fabrication of modulated submicometer gratings in photoresist," *Appl. Opt.* **34**, 2540-2547, (1995).

[49] C.V. Shank and R.V. Schmidt, "Optical technique for producing 0.1-μm periodic surface structures", *Appl. Phys. Lett.* **23**, 154-155, (1973).

[50] M.T. Gale and K. Knop, "The fabrication of fine lens arrays by laser beam writing", Proc. SPIE **398**, 347-353, (1983).

[51] M.T. Gale, M. Rossi, H. Schütz, P. Ehbets, H.P. Herzig, and D. Prongué, "Continuous-relief diffractive optical elements for two-dimensional array generation", *Appl. Opt.* **32,** 2526-2533, (1993).

[52] T. Fujita, H. Nishihara amd J. Koyama, "Blazed gratings and Fresnel lenses fabricated by electron-beam lithography", *Opt. Lett.,* **7,** 578-580, (1982)

[53] D. Zaleta, W. Daschner, M. Larsson, B.C. Cress, J. Fan, K.S. Urquhart and S.H. Lee, "Diffractive optics fabricated by electron-beam direct write methods," Proc. SPIE **CR49**, San Diego, 117-137 (1993).

[54] J.M. Stauffer, Y. Oppliger, P. Regnault, L. Baraldi, and M.T. Gale, "Electron beam writing of continuous resist profiles for optical applications", J. Vac. Sci Technol. B **10**, 2526-2529 (1992).

[55] M. Ekberg, F. Nikolajeff, M. Larsson, and S. Hård, "Proximity-compensated blazed transmission grating manufacture by direct-writing electron-beam lithography", Appl. Opt. **33,** (1994).

[56] U. Drodowsky, M. Drewsen, T. Pfau, S. Nowak, and J. Mlynek, "Atom lithography using light forces," Microelectronic Engineering **30**, 383-386, (1996).

[57] W. Seifert, C.S. Adams, V.I. Balikin, C. Heine, Yu. Ovchinnikov, and J. Mlynek, "Reflection of metastable argon atoms from an evanescent wave," *Phys. Rev. A* **49**, 3814-3823 (1994).

[58] L. Kempen,"*Integrated Optical Sensor Modules*", Dissertation, University of Neuchâtel, (1996).

[59] Aquapell 3350-015 farblos, "Hochflexibler, physikalisch trocknender Abziehlack auf der Basis wasserverdünnbarer Dispersionsharze." Dr. Renger, Automobil- und Industielacke,

[60] C.J. Raymond, M.R. Murmane, S.S.H. Naqvi, and J.R. McNeil, "Metrology of subwavelength Photoresist Gratings Using Optical Scatterometry," *J. Vac. Sci. Technol B* **13**, 1484-1495, (1995).

[61] P. Blattner, H.P. Herzig, S.S.H. Naqvi, "Scanning Spot Metrology for Testing of Photolithographic Masks," *Opt. Eng.* **34**, 2425-2427, (1995).

[62] R.M.A. Azzam and N.M.Bashara, *Ellipsometry and Polarized Light*, North Holland, (1987).

[63] E.A. Bernheim, "Coatings for plastic and glass", Proc. SPIE **2622**, 151-156, (1995).

[64] JL. Bala, "Automated Optical Assembly", Proc. SPIE **2622**, 157-164, (1995).

[65] D.H. Raguin, S. Norton, and M. Morris, "Subwavelength structured surfaces and their applications,", *Critical Reviews of Optical Science and Technology* **CR49**, 234-261, (1993).

[66] R. Magnusson and S.S. Wang, "New principle for optical filters", *Appl. Phys. Lett.* **61**, 1022-1024, (1992).

ABSTRACTS OF PUBLICATIONS I-IV

Paper I

Legendre- and Chebychev polynomial expaosions, optimized for rigorous calculations of stacks of lamellar gratings

Claus Heine and Rudolf Morf

We investigate the modal expansion based on high order polynomial expansions. It is used for the calculation of the Helmholtz equation of lamellar one-dimensional gratings. It is related to the method of finite elements. We compare the methods by investigating their convergence properties. A criterion is developed for an optimal distribution of the local resolution to approximate the eigenfunctions in a grating layer. We found the use of Chebychev polynomials advantageous for the solution of the eigenvalue problem for metallic gratings

Paper II

Submicrometer gratings for solar energy applications

Claus Heine and Rudolf H. Morf

Diffractive optical structures for increasing the efficiency of crystalline silicon solar cells are discussed. As a consequence of the indirect band gap, light absorption becomes very ineffective near the band edge. This can be remedied by use of optimized diffraction gratings that lead to light trapping. We present blazed grating that increase the optically effective cell thickness by approximately a factor of 5. In addition we present a wideband antireflection structure for glass that consists of a diffraction grating with a dielectric overcoat, which leads to an average reflection of less than 0.6% in the wavelength range between 300 and 2100 nm.

Paper III

Coated submicron gratings for broadband antireflection in solar energy applications

Claus Heine, Rudolf H. Morf, and Michael T. Gale

Experiments demonstrating the broadband antireflection performance of MgF_2-coated surface-relief gratings in polymer foil are discussed. The measured mean reflectance was as low as 0.6 % for the wavelength range of 400 to 1500 nm. As a consequence, the transmission losses at the glass surface of a solar energy device can be reduced from about 7.5 % to 3.1 %, averaged over the day. The coated gratings are more stable against heat than bare surface gratings and the MgF_2 coating also exhibits better adhesion to the structured surface than it does to the plane surface.

Paper IV

Claus Heine, Rudolf H. Morf, and Michael T. Gale

Submicron gratings with dielectric overcoat: performance and stability

Measurements on broadband antireflection structures show that the combination of dielectric overcoating with grating microstructures leads to improved stability. Various types of designs are presented.

Paper I

to be submitted to JOSA A

Legendre- and Chebyshev polynomial expansions optimized for rigorous calculations of stacks of lamellar gratings

Claus Heine and Rudolf Morf

We investigate the modal expansion based on high order polynomial expansions. The method is used fro the calculation of the solutions od the Helmholtz equation of lamellar one-dimensional gratings. It is related to the method of finite elements. We compare the methods by investigating their convergence properties. A criterion is developed for an optimal distribution of the local resolution to approximate the eigenfunctions in a grating layer. We found the use of Chebychev polynomials advantageous for the solution of the eigenvalue problem for metallic gratings.

1. Introduction

New possibilities in microtechnology, such as laser and electron-beam writing allow to fabricate devices with feature sizes in the order of the wavelength of light. These can be grating structures with periods of several microns and more. It opens the way to applications using diffractive optical elements based on binary gratings [1] such as "artificial blazed gratings" [2] or Damman gratings [3]. In addition, more and more, continuous relief components become important for applications such as microlens arrays [4, 5, 6] and fan-out elements [7]. The writing techniques are quite time consuming (several hours and even days are typical). However electroplating and embossing techniques open the way to mass production and can help to keep the fabrication costs per device acceptably low.

Calculation of diffraction efficiencies of such devices has been the subject of extensive research for many years [8, 9]. Calculations of efficiencies of gratings with large grating periods and small feature sizes require efficient design methods. Several methods have been developed to calculate rigorously the efficiencies of dielectric as well as metallic lamellar gratings [10-13]. Often stacks of lamellar gratings are used to approximate one-dimensional gratings with arbitrary geometry. It is only recently that some important numerical problems [14] have been solved, such as poor convergence properties for the TM-polarization case as well as numerical instabilities for very deep gratings [15, 16].

The method using high order orthogonal polynomial expansion as developed and described in [15] exhibits exponential convergence of the solutions inside one lamellar layer. Following this approach one has to divide the lamellar grating layer into rectangular areas (domains) with locally constant optical properties. The solutions of Maxwell's equations inside the domains are approximated by an expansion in terms of orthogonal polynomials. The choice of the maximum order of the polynomial expansion inside each domain is one of the factors which determine the computational effort for the solution of the diffraction problem. Therefore it is worth investigating how this effort can be minimized without sacrificing accuracy.

The method used is related to the method of finite elements and it will be instructive to compare their convergence properties. We develop a criterion for the optimal distribution of the expansion orders over the grating layer.

One section of this work is devoted to metallic gratings. As already mentioned in [15] sets of orthogonal polynomials different from the previously studied Legendre polynomials exhibit better approximation properties.

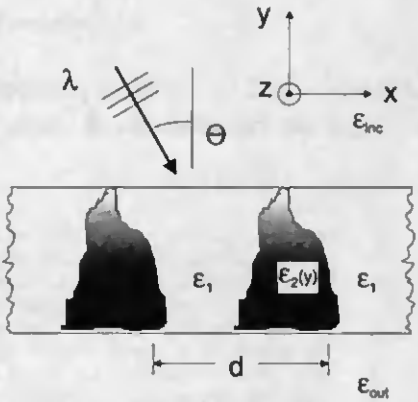

Fig. 1. Geometry of the diffraction problem.

2. The diffraction problem

We consider a plane wave with vacuum wavelength λ_0 incident at an angle Θ on a one-dimensional grating structure with grating period d. We restrict ourselves to nonconical diffraction. This situation is illustrated in Fig. 1. We approximate an arbitrary grating profile by a stack of lamellar gratings as shown in Fig. 2. Our goal is to calculate the diffraction efficiencies of the different transmitted and reflected orders. The strategy is to find the solutions of Maxwell's equations inside each layer and to match the layers fulfilling the boundary conditions. To take for example layer B the solutions inside will have the form

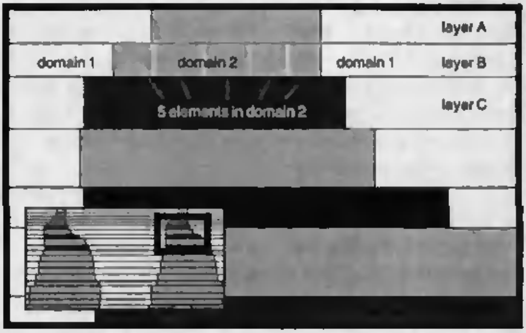

Fig. 2. Approximation of an arbitrary one dimensional grating structure by a stack of lamellar gratings.

$$\mathcal{B}(x,y) = \sum_{m=1}^{\infty} \left(b^+_m \exp[i \sqrt{\mu^B_m}\, (y - y_{A\to B})] + b^-_m \exp[-i \sqrt{\mu^B_m}\, (y - y_{B\to C})] \right) B_m(x)\,, \quad (1)$$

where $y_{A\to B}$ denotes the position of the interface between layer A and layer B and b^+_m, b^-_m are unknown constants to be determined. The x-dependent functions $B_m(x)$ as well as the values μ^b_m which are in general complex are determined by solving the eigenvalue problem

$$\frac{d^2}{dx^2} B(x) + k_0^2 \, \varepsilon_B(x) = \mu^B \, B(x) , \tag{2}$$

where the wavenumber k_0 is defined by $k_0 = (2\pi)/\lambda_0$. The dielectric constanty is specified in layer B by $\varepsilon_B(x)$.

3. Solution of the eigenvalue problem

We proceed as described in [15] and divide each grating layer in two or more domains D inside which the dielectric constant does not vary spatially (it still is a function of wavelength of light). We are allowed to subdivide each domain into subintervals by introducing additional (vertical) interfaces. These subintervals could form the geometrical framework for a finite element approximation and therefore we call them elements. The number of domains in the grating layer B is given by N_D. The number of elements $N_E(D)$ in Domain D will be equal to N if we introduce N-1 additional interfaces in this domain.The situation is illustrated in Fig. 2 for layer B. We now approximate the eigenfunctions $B_m(x)$ in each element given by $[x_{D,E-1}, x_{D,E}]$ with an expansion of orthogonal polynomials P_l:

$$B_m(x) = \sum_{D=1}^{N_D} \sum_{E=1}^{N_E(D)} \sum_{l=0}^{M_{D,E}+1} b_{m,l}^{D,E} \, P_l(\xi(x)) . \tag{3}$$

where $M_{D,E}+1$ is the order of the approximation in element E of Domain D and $P_l(\xi)$ is the set of orthogonal polynomials used in this element E. Note that in each element two coefficients of the expansion can be eliminated, using the boundary conditions. Therfore $M_{D,E}$ is the number of free parameters in each element. Typically we use Legendre polynomials, but as we will see later, it can be of advantage to use Chebyshev polynomials. The orthogonal set is defined on the interval [-1,+1]. The transformation from the interval $[x_{D,E-1}, x_{D,E}]$ to this interval is performed by the linear function $\xi(x)$. The approximation constants $b_{m,l}^{D,E}$ are to be calculated from the eigenvalue problem.

In principle, there are now two possibilities to increase the accuracy of the calculation: i)One could increase the number of elements in the domains and keep the order of the expansion fixed. This is the well known method of finite elements. As an example we calculate the eigenvalues of a dielectric lamellar grating with two domains. We choose a normalized grating period of $d/\lambda_0 = 5$. In the first domain D_1 we assume an index of refraction of n = 1. In the second domain D_2 we choose an index of $n_2 = 1.5$. The size of D_1 was 1.5 times the size of D_2. Fig.†3 shows the calculated error of the 10^{th} largest eigenvalue as a function of the order of approximation in the second domain. This is the sum of the orders over the elements in the domain. The lines connect calculated errors for the same degree of polynomial expansion in each element but with an increasing number of elements. Different lines indicate different polynomial orders used for the finite element approximation. For this simple grating, the exact eigenvalue is found with the help of the transcendental equation derived by Botten et al [10].

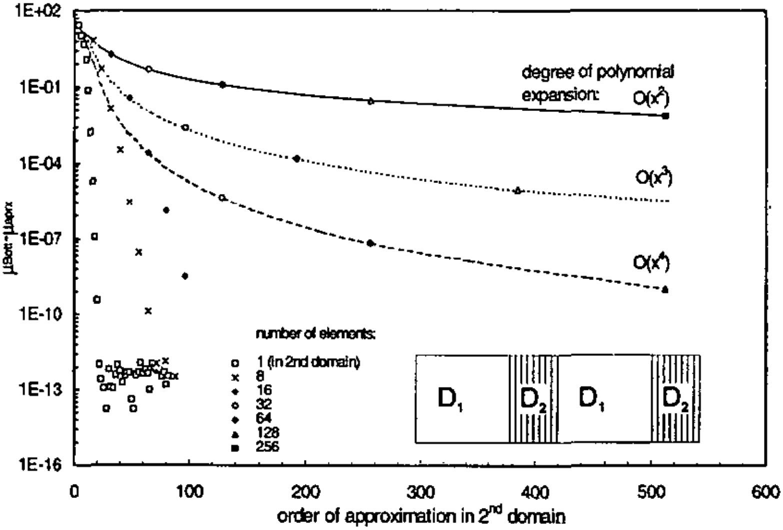

Fig. 3. Plotted is the error of an eigenvalue as a function of the order of approximation in the second domain (out of two) of a dielectric lamellar grating layer. The second domain is divided in an increasing number of elements. The lines connect calculated errors for the same degree of polynomial expansion in each element. Different lines indicate different polynomial orders used for the finite element approximation. Each symbol is related to a fixed number of elements but an increasing order of the polynomial expansion inside the elements.

ii) A different approach is to keep the number of elements constant and to increase the order of the polynomial expansion inside every element. The calculated error for the same eigenvalue as in the example above is also shown in Fig.†3. The symbols represent calculated eigenvalue-errors for the same number of elements but an increasing order of the polynomial expansion in each element. It can be seen that both the method of finite elements and the method of high order polynomial expansion are closely related to each other. The error decreases according to a powerlaw for the method of finite elements. In contrast, for the high order polynomial expansion we have an exponential decrease of the error . We conclude that it is favorable to keep the number of elements in one domain as low as possible. In Fig†3 we see that (computer precision limited) maximum accuracy is reached quite fast (for the case of just one element) and that further expansion only leads to more computational effort without improving the result. In the following section we establish a criterion to distribute the approximation orders over the two or more domains present in the grating layer.

4. Criterion for the distribution of expansion orders

In [15] already a reasonable criterion has been proposed:

$$M_{D,E} = p\sqrt{|\varepsilon_D|}\,\Delta x_{D,E}, \tag{4}$$

where $\Delta x_{D,E}$ is the size of the actual element and p is a constant. Increasing the accuracy of calculation is performed by increasing the parameter p. The factor $\Delta x_{D,E}$ takes into account the mapping of the element to the interval [-1,+1]. The square root of the dielectric constant is related to the difference of the optical density and its influence on the eigenfunctions.

In order to get a deeper insight and to improve the criterion we have to take a look at the eigenfunctions. For simplicity reasons we restrict ourselves to the case of normal incidence and to purely dielectric gratings. Suppose we already solved the eigenvalue problem given by equation (2). Then the solutions $B_m(x)$ fulfill:

$$\frac{d^2}{dx^2}B_m(x) + \left(k_0^2\varepsilon(x) - \mu^B_m\right)B_m(x) = 0. \tag{5}$$

For known eigenvalues μ^B_m, inside each element E_D in Domain D the solutions can be written as:

$$B_m(x) = B_{m,co}(E_D)\cos\left(\sqrt{k_0^2\varepsilon_D - \mu^B_m}\,x\right) + B_{m,si}(E_D)\sin\left(\sqrt{k_0^2\varepsilon_D - \mu^B_m}\,x\right). \tag{6}$$

$B_{m,co}(E_D)$ and $B_{m,si}(E_D)$ are constants which are used to match the boundary conditions between two elements.

A criterion for the convergence is given in [17]. It says that the order $M_{D,E}$ for which exponential convergence sets in is related to the number of zeros $N^{D,E}_{zeros}$ of the approximated function in the element. This relation is given by:

$$M_{D,E} \cong \pi N^{D,E}_{zeros}. \tag{7}$$

We know from equation (6) that for the corresponding eigenfunction the number of zeros in the element will be:

$$N^{D,E}_{m,zeros} = \frac{\sqrt{k_0^2\varepsilon_D - \mu^B_m}}{\pi}\,\Delta x_{D,E} \tag{8}$$

In the case of an eigenvalue connected to an evanescent mode ($\mu^B_m < 0$) the argument under the square root in equation (6) will always be positive. Therefore exponential convergence for eigenvalue μ^B_m should set in if:

$$M_{D,E} > \pi N^{D,E}_{zeros} = \sqrt{k_0^2\varepsilon_D - \mu^B_m}\,\Delta x_{D,E}. \tag{9}$$

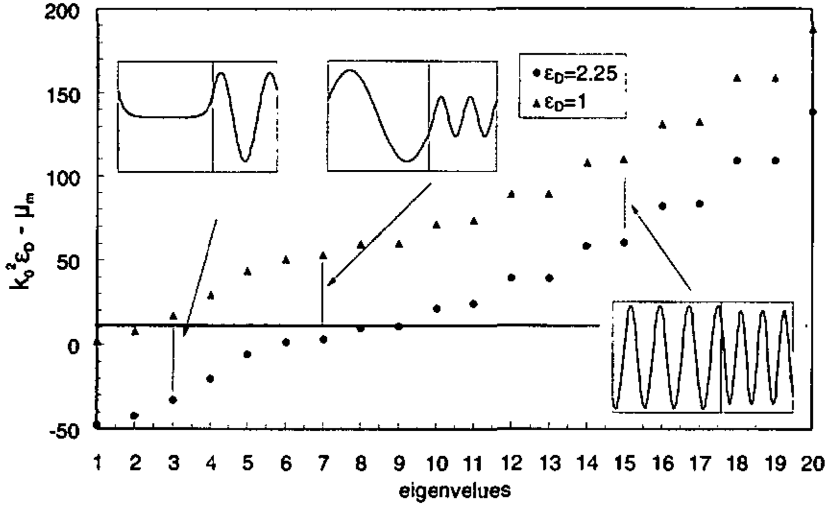

Fig. 4. In each domain of a dielectric grating the eigenfunctions are either sinusoidal or hyperbolic functions depending on the sign of the square of the 'wavenumber' ($k_0^2\varepsilon_D$-μ_m) in the domain. Shown are three different eigenfunctions for a dielectric grating layer with two domains. Note that for very small eigenvalues (μ_m << 0) the eigenfunctions approximate the homogeneous case as explained in the text. We plotted in addition the 'wavenumbers' in the order of decreasing eigenvalues. Dotts belong to the domain with ε_D = 2.25, triangles belong to ε_D =1.

Some of the propagating eigenmodes are related to hyperbolic solutions for $B_m(x)$ in domains with small dielectric constant (if $\mu^B_m > k_0^2\varepsilon_D$ as shown in Fig. 4 for the 3rd largest eigenvalue). They have their zeros distributed in the complex plane and we have to modify our criterion. The problem can be reduced to the question how an exponential function on a limited interval of definition can be approximated by a polynomial expansion. As outlined in the appendix the expansion order has to be at least

$$M_{D,E} = \frac{\sqrt{k_0^2\varepsilon_{B,max} - k_0^2\varepsilon_D}}{2}\Delta x_{D,E} \qquad , \qquad (10)$$

where $\varepsilon_{B,max}$ is the maximum value of the dielectric constant in the actual layer.

We plotted the eigenfunctions for three different eigenvalues in Fig. 4. The argument under the square root in equation (6) which is something like the square of the 'wavenumber' in the domain, leads either to a trigonometric or hyperbolic characteristic in a domain. In Fig. 4 also shown is this argument as a function of the eigenvalues.

The decay of the evanescent modes in a diffraction problem will correspond to the square roots of the negative eigenvalues. In order decide how to distribute the expansion orders in each element we therefore proceed in the following way: First we decide which fastest decay we want to take into account. This is connected to a lower bound μ_{min} for the eigenvalues. In each element we calculate for a value μ which is below that lower bound the $M_{D,E}$ according to equation (9) and compare it to the $M_{D,E}$ resulting from equation (10), the maximum of which will be our expansion order in the element. Please note that for eigenvalues close to the lower bound μ_{min} exponential convergence only starts to set in and is not finished if the parameter μ is chosen too close to μ_{min}.

In order to test this criterion we calculated the first order transmission efficiency of a subwavelength diffractive optical element nominally the same as described in [18]. It is an "artificial blazed" grating structure consisting of 20 domains in one grating period. Shown in Fig. 5 is the calculated first order transmission as a function of the order of the approximation M(p), where p is the parameter determining the approximation order ($p^2 = \mu$) We used three different methods to distribute the expansion orders over the domains

$$\begin{aligned} &\text{i)} \quad M_D(p) = p\sqrt{|\varepsilon^D|}\,\Delta x_D \\ &\text{ii)} \quad M_D(p) = p\,\Delta x_D \\ &\text{iii)} \quad M_D(p) = \sqrt{k_0 \cdot |\varepsilon^D| + p^2}\,\Delta x_D \end{aligned} \tag{12}$$

The order of the approximation is then given by:

$$M(p) = \sum_D^{N_D} M_D(p) \quad . \tag{13}$$

Hereby is (i) representing the original criterion of [15], ii) is a criterion that leads to homogeneous resolution over the whole grating period and iii) corresponds to the method as developed above. The calculation accuracy is increased by increasing the parameter p. In view of calculation accuracy the method described above (iii) clearly wins.

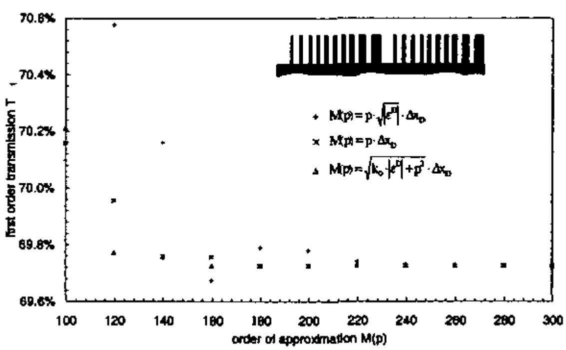

Fig. 5. First order transmission efficiency of an artificial blazed grating structure (example from [18]) as a function of approximation order. Two periods of the structure are shown in the inlay. Three different methods were used to choose the degree of the polynomials in the domains. The order of approximation results from summation of these degrees over all domains.

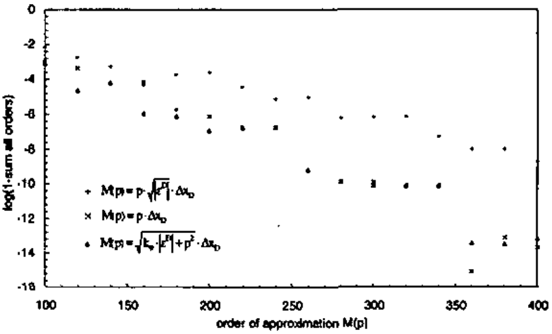

Fig. 6. Deviation from the energy conservation for the diffraction efficiency calculations of Fig. 6. note that for high approximation orders approximation with homogeneous accuracy and approximation according to our criterion asymptotically lead to the same distribution of the polynomial orders inside the domains.

In Fig. 6 we plotted the error in the energy as a function of the order of approximation. Energy conservation alone is not sufficient to signify accurate diffraction efficiency calculations. However the decrease of the error in the energy conservation allows for conclusions concerning the convergence properties of a calculation method. Note that for a very high order of approximation our method approaches asymptotically the method of homogeneous resolution, where no optical properties of the materials used in the grating are taken into account:

$$\lim_{p\to\infty} \sqrt{k_0 \left|\varepsilon^D\right| + p^2}\ \Delta x_D = p\,\Delta x_D \qquad (14)$$

This is due to the fact that for very small eigenvalues ($-\mu_m >> k_0^2\varepsilon_D$) the zeros of the eigenfunctions are approximately equidistant distributed over the whole grating layer and the eigenfunctions correspond more or less to homogeneous solutions in an averaged index dielectric medium. It reflects the aspect, that high frequency gratings can be modeled as artificial index dielectric layers [19-21] using effective medium theory [22, 23].

Metallic gratings

Until now we used Legendre polynomials for the expansion of the. Solving the eigenvalue problem corresponds to the minimization of the integral deviation of the approximation from the exact eigenfunction according to

$$\min \int_{-1}^{1} w(\xi)\left|f(\xi) - \tilde{f}_M(\xi)\right|^2 d\xi \qquad ,$$

where M is the order of the approximation and $w(\xi)$ is the weighting connected to the set of orthogonal polynomials. For Legendre polynomials the weighting is a constant and the accuracy of the approximation is the same over the whole interval of definition. Therefor these polynomials are the best choice for dielectric domains. However in metallic domains the eigenfunctions are exponentially decaying with the distance from the domain boundary. Chebyshev expansion with the strong weighting of the interval boundaries

($w(\xi) = 1/\sqrt{1-\xi^2}$) could lead to better convergence properties as already noted in [15]. In a metallic domain we therefore approximate the eigenfunction according to:

$$B(x) = \sum_{l=0}^{N_D} b_l^D \, T_l \qquad , \qquad (15)$$

were T_l denotes the Chebyshev polynomial of order l. Fig. 7 shows the convergence of the real part of an eigenvalue as a function of the approximation order in the metallic domain. In the dielectric domain we choose a Legendre type expansion with $M = 40$ in order to be sure that the approximation of eigenfunctions in this domain is very accurate. In the metallic domain the eigenfunction is approximated by Legendre polynomials (continuous line) and Chebyshev polynomials (cross symbols). In terms of convergence rate the method with the Chebyshev approximation in the metallic domain clearly wins. A different approach could be to divide the metallic domain in three elements and to keep the expansion order in the second element low, because in this domain the eigenfunctions are expected to be close to zero. The broken line in Fig.†7 shows the decreasing error with increasing order of expansion in the two outer metallic elements. It can be seen that both orthogonal polynomial approximations with just one domain show better convergence. Therefore in the metallic case as well as in the dielectric case additional interfaces should be avoided. It is important that in all cases the expansion in the dielectric domain is a Legendre type expansion.

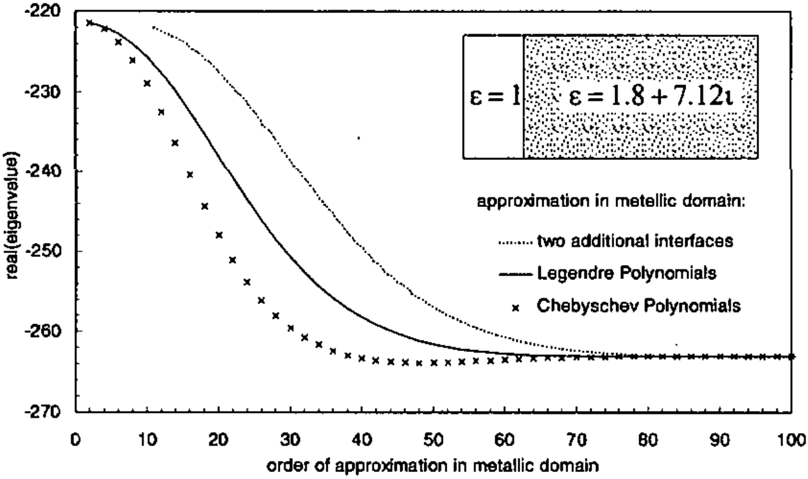

Fig. 7. Convergence of the real part of an eigenvalue for a metallic grating. In the metallic domain Legendre type polynomials (continuous line) and Chebyshev type polynomials (crosses) are used. Shown as well is the convergence if the metallic domain is divided in three elements and the approximation order in the second element is kept low.

Conclusions

In this paper we compare the method of high order polynomial expansion to the method of finite elements. We find that additional interfaces offer no advantage for the convergence rate. We give a criterion how to distribute the polynomial orders over the domains. This is only shown for the case of a dielectric grating and for normally incident light. However, the criterion is easily generalized to the case of oblique incidence. In the case of metallic gratings the complex dielectric constant can lead to a fast decay of the eigenfunctions. It is therefore possible that the criterion has to be modified. For metallic gratings the expansion of the eigenfunctions in Legendre series in the dielectric part and combining this with a Chebyshev type expansion in the metallic part of the grating turns out to be optimum in view of convergence rate.

Appendix

For the approximation of the hyperbolic functions it is not possible to count the zeros in order to find a criterion for the approximation order because these functions do not have most of their zeros on the real axis. The problem can be reduced to the question how an exponential function on a limited interval of definition can be approximated by a polynomial expansion. The exponential function to approximate is defined on an interval of size x_D and we first want to transformation it to the interval [-1,+1]

$$\tilde{x} = (x+1)\frac{x_D}{2} \quad \text{with} \quad x \in [-1,+1] \qquad .$$

The polynomial function used to approximate the exponential function has to include terms which have the potential to be at least as steep as the exponential function, independent of any proportional factors. This steepness is determined by the logarithmic derivation. The exponential function is steepest at the interval boundaries. The logarithmic derivative of the exponential function is a constant

$$\frac{d}{dx}\ln(Ae^{\alpha x}) = \alpha \qquad .$$

The exponential will be approximated by a polynomial function, the highest order term of which can be described as

$$f(x) = x^M$$
$$\frac{d}{dx}\ln(x^M) = \frac{M}{x} \qquad .$$

Therefore we set

$$\frac{M^D}{x} \geq \alpha \qquad ,$$

and at the boundary $x = x_D/2$

$$M^D \geq \frac{\alpha x^D}{2} \qquad ,$$

and with $$\alpha = \sqrt{\mu_m - k_0^2 \varepsilon_D}$$

we have $$M^D \geq \frac{\sqrt{\mu_m - k_0^2 \varepsilon_D}\, x_D}{2}.$$

Note that this result is proportional to the number of zeros of the hyperbolic functions on the imaginary axis.

Acknowledgments

The authors are grateful to M.T. Gale and K. Knop in our laboratories for numerous discussions. C. Heine gratefully acknowledges financial support from Balzers AG.

References

[1] Michael W. Farn, "Binary gratings with increased efficiency", *Appl. Opt.* **31,** 4453-4458, (1992).

[2] W. Stork, N. Streibl, H. Haidner, and P. Kipfer , "Artificial distributed-index media fabricated by zero-order gratings", *Opt. Lett.* **16,** 1921-1923, (1991).

[3] Jari Turunen, J. Michael Miller and Mohammad R. Taghizadeh, "Rigorous diffraction analysis of Damman gratings", *Opt. Commun.* **81,** 337-342, (1991).

[4] EOS Topical Meetings Digest Series **2,** *Microlens arrays,* 1993, ISSN 1167-5357,13.-14. May 1993, NationalPhysical Laboratory, Teddington UK.

[5] Hessler T., Gale M.T., Rossi M. and Kunz R.E. "Fabrication of Microlens Arrays by Direct Writing in Photoresist, *EOS Topical Meetings Digest Series* **5,** (1995) 37-43.

[6] E. Noponen, J. Turunen, A. Vasara, "Electromagnetic theory and design of diffractive-lens arrays,", *J. Opt. Soc. Am. A.,* **10,** 434-443, (1993).

[7] M. Rossi, R.E. Kunz,"Focusing fan-out elements based on phase matched Fresnel lenses", *Opt. Commun..,* **112,** 258-264, (1994).

[8] R. Petit, ed., *Electromagnetic Theory of Gratings,* Vol. 22 of Topics in current Physics (Springer-Verlag, Berlin, 1980).

[9] K. Knop, "Rigorous diffraction theory for transmission phase gratings with deep rectangular grooves", *J. Opt. Soc. Am.* **68**, 1206-1210, (1978).

[10] L. C. Botten, M. S. Craig, R. C. McPhedran, J. L. Adams and J. R. Andrewartha, "The dielectric lamellar grating", *Opt. Act.* **28**, 413-428, (1981).

[11] L. C. Botten, M. S. Craig, R. C. McPhedran, J. L. Adams and J. R. Andrewartha, "The finitely conducting lamellar diffraction grating", *Opt. Act.* **28**, 1087-1102, (1981).

[12] L.C. Botten and R.C. McPhedran, "Highly conducting lamellar gratings", *Opt. Act.* **28**, 1103-1106, (1981).

[13] M.G. Moharam and T.K. Gaylord, "Rigorous coupled-wave analysis of grating diffraction - E-mode polarization and losses", *J. Opt. Soc. Am.* **73**, 451-455, (1983).

[14] Lifeng Li and Charles W. Haggans, "Convergence of coupled-wave method for metallic lamellar diffraction gratings", *J. Opt. Soc. Am.* **10**, 1184-1189, (1993).

[15] R. H. Morf, "Exponentially convergent and numerically efficient solution of Maxwell's equations for lamellar gratings", *J. Opt. Soc. Am. A.* **12**, 1043-1056, (1995).

[16] M.G. Moharam, Drew A. Pommet, and Eric B. Grann, T.K. Gaylord, "Stable implementation of the rigorous coupled-wave analysis for surface-relief gratings: enhanced transmittance matrix approach,", *J. Opt. Soc. Am. A.*, **12**, 1077-1086, (1995).

[17] D. Gottlieb and S.A.Orszag, *Electromagnetic Numerical Analysis af Spectral Methods: Theory and Applications*, (Society of Industrial and Applied Mathematics, Philadelphia, Pa., 1989).

[18] M.E. Warren, R.E. Smith, G.A. Vawter, and J.R. Wendt, "High-efficiency subwavelegth diffractive optical element in GaAs for 975 nm", *Opt. Let.* **20**, 1441-1443, (1995).

[19] Eric B. Grann, M. G. Moharam, and Drew A. Pommet, "Artificial uniaxial and biaxial dielectrics with use of two-dimensional subwavelength binary gratings", *J. Opt. Soc. Am. A.* **11**, 2695-2703, (1994).

[20] E. N. Glytsis and T. K. Gaylord, "High-spatial frequency binary and multilevel stairstep gratings: polarisation-selective mirrors and broardband antireflection surfaces.," *Appl. Opt.* 32, 4459-4470, (1992).

[21] Dale C. Flanders, "Submicrometer periodicity gratings as artificial anisotropic dielectrics", *Appl. Phys. Lett.* **42**, 492-494, (1983).

[22] T. K. Gaylord, W. E. Baird, and M. G. Moharam, "Zero-reflectivity high spatial-frequency rectangular-groove dielectric surface-relief gratings", *Appl. Opt.* **25**, 4562-4567, (1986).

[23] D. L. Brundrett, E. N. Glytsis, and T. K. Gaylord, "Homogeneous layer models for high-spacial-frequency dielectric surface-relief gratings: conical diffraction and antireflection designs", *Appl. Opt.* 33, 2695-2706, (1994).

Paper II

a reprint from Applied Optics

Submicrometer gratings for solar energy applications

Claus Heine and Rudolf H. Morf

Diffractive optical structures for increasing the efficiency of crystalline silicon solar cells are discussed. As a consequence of the indirect band gap, light absorption becomes very ineffective near the band edge. This can be remedied by use of optimized diffraction gratings that lead to light trapping. We present blazed gratings that increase the optically effective cell thickness by approximately a factor of 5. In addition we present a wideband antireflection structure for glass that consists of a diffraction grating with a dielectric overcoat, which leads to an average reflection of less than 0.6% in the wavelength range between 300 and 2100 nm.

1. Introduction

In an economic analysis of photovoltaic (PV) energy production, the efficiency of solar cells plays an extremely important role. Indeed, the actual cost of a cell plays a relatively minor role if cells of different efficiencies are compared. This is basically because fixed costs of module construction, support structures, glass protection covers, wiring, and, last but not least, the needed area tend to dominate the final cost of energy.[1] Most of these scale directly with the required area and are thus, for a given amount of energy, inversely proportional to the cell efficiency.

The efficiency of a solar cell can be divided into the external efficiency, which is defined as the fraction of incident light absorbed in the cell, and the internal efficiency, which measures the fraction of the absorbed photon energy that is available as electric energy at the terminals of the cell. The internal or electronic efficiency depends on a number of loss mechanisms, including recombination processes, series resistance losses in the contact, and losses that are due to the existence of parasitic parallel conductances. These are not the subject of this paper. However, in the following we keep in mind that, for the minimization of bulk recombination processes, the cell thickness must not exceed the diffusion length of minority carriers.[2] This, in turn, is controlled by the quality of the Si material. Particularly, in the case of low-cost polycrystalline Si, the diffusion length is rather small (between 10 and ~200 μm, depending on the process used). On the other hand, as a consequence of the indirect band gap of Si, the absorption of light near the band gap (~1.1 eV) becomes very small, and thus, in such thin cells, that part of the solar spectrum cannot be absorbed completely.

It has long been recognized that the efficiency of Si solar cells can be enhanced by the use of well-designed optical structures. These include antireflection (AR) coatings for minimizing the reflection losses at the front surface as well as structures designed to help trap the light within the cell. The most widely used structure consists of pyramids or inverted pyramids etched into the top and also often into the rear cell surface.[3] This structure depends on the use of single-crystal material with (100) surface orientation and cannot be used with polysilicon. Also, the lateral scale of these pyramids cannot easily be reduced below a few micrometers, and thus their use with very thin cells is limited. Another drawback of such structures is that they lead to an increase of the cell surface and thus to larger surface recombination losses. These structures are based on geometric optics considerations[4–6] and make use of the fact that the critical angle of incidence, Θ_c, beyond which light is totally internally reflected, is very small: $\Theta_c = \arcsin(n_{Si}^{-1}) \approx 16°$. In particular, for a randomly structured reflector at the backside of the cell, the fraction of light within the cone $\Theta < \Theta_c$ is only $(1/n_{Si})^2 \approx 8.6\%$, where n_{Si} denotes the refractive index of Si. However, for a well-designed AR coating, light inside this cone would indeed be lost. In

The authors are with the Paul Scherrer Institute Zurich, CH 8048 Zurich, Switzerland.

Received 1 August 1994; revised manuscript received 30 September 1994.

0003-6935/95/142476-07$06.00/0.

addition there are also dissipation losses if metal reflectors are used, and generally random surfaces tend to enhance the absorption of lossy metals.

In this paper we discuss the application of submicrometer (hereafter referred to submicron) grating structures for increasing the efficiency of solar cells. The modeling and the optimization of the diffractive structures are based on the approach outlined in Ref. 7 and described in detail in Ref. 8.

In *Section 2* we discuss an alternative approach to the light-trapping problem, which is based on fine regular gratings. Our goal is to develop light-trapping devices that do not increase the surface area at which increased recombination losses would outweigh the benefits of increased light absorption. This is done by effective separation of the electronic device structure, in which electron-hole pairs are generated and collected from the optical structures used for enhancing the absorbed light within the electronically active region in the Si. We limit our discussion to one-dimensional gratings, which are, however, optimized for the most effective light trapping of unpolarized light.

In Section 3 we turn our discussion to a new structure designed to minimize reflection losses. Typically, solar cells as well as solar collectors are protected by glass cover sheets, whose surfaces contribute ~4% to reflection losses for each interface between air and glass. For such a wide spectral range as is needed for solar energy applications, traditional AR coatings are not very efficient, basically because of the lack of stable and hard dielectric materials with low enough refractive indices. Instead, we present a broadband AR (BAR) structure, which consists of a surface grating (in glass or a plastic materials with a refractive index similar to that of glass) and a dielectric overcoat. Hereby the AR properties of a zero-order grating for long wavelengths[9–15] are combined with those of dielectric coatings. We present a BAR structure that, in the spectral range of 300–2100 nm reflects less than 0.52% of the incoming solar energy flux. This same BAR structure can be employed to minimize the reflection losses for a glass-covered PV solar cell made from crystalline Si.

2. Submicron Gratings for Light Trapping

In a first attempt, we examined rectangular grating structures, as illustrated in Fig. 1. At the top surface, a 5-nm-thick SiO_2 passivation layer and an AR coating, which consisted of a 50-nm TiO_2 and a 100-nm SiO_2 layer, were assumed. These grating structures are characterized by three geometric structural parameters, i.e., the period Λ of the grating, its depth h, and its duty cycle f, which is defined as the ratio between groove width $f\Lambda$ and period Λ. The grating is coated by a low-loss metal; for this purpose, we selected Ag.

By numerical solution of Maxwell's equations, using the method of Botten *et al.*[16] and its extensions by Herzig *et al.*[7] and Morf,[8] we examined the light-

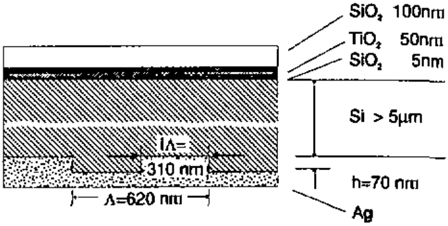

Fig. 1. Rectangular grating optimized for use with thin Si solar cells. Λ is the grating period, f is the duty cycle, and h is the grating depth.

trapping characteristics of such rectangular grating structures in an exhaustive manner. Note that the method of modal expansion is particularly suited for varying grating depth as the eigenmodes of the Helmholtz equation do not depend on the depth parameter. A preliminary account of this work has been published in Ref. 17. The best structure with a rectangular cross section is illustrated in Fig. 1. One can understand its period, $\Lambda = 620$ nm, by observing that, for normal incidence with a wavelength $\lambda = 1100$ nm (which coincides with the band edge of Si), the second-order mode in Si travels parallel to the surface, according to the grating equation,

$$\sin(\Theta_m) = m\lambda/\Lambda n_{Si}.$$

Here the wavelength in vacuum is denoted by λ, m denotes the diffraction order, and Θ stands for the angle relative to the normal. The refractive index $n_{Si} = 3.5$ is the refractive index of Si at $\lambda = 1100$ nm. Thus, in the spectral range, where Si bcomes a very inefficient absorber, the optical path length is greatly enhanced if the incident radiation is effectively coupled into the second diffracted order. This is achieved by the grating parameters $f = 0.5$ and $h = 60$ nm. At this point, we make three interesting observations:

(1) Gratings with smaller period $\Lambda = 310$ nm, which are designed to optimize the coupling of the first-order diffracted wave, do not lead to as effective a light trapping. Also, their sensitivity to aspect ratio variation is substantially greater, such that fabrication tolerances would have to be very tight (within 5%).

(2) These one-dimensional (linear) gratings help to trap light of both polarizations, although they represent a compromise. For polarized light, more effective light trapping is possible.

(3) Symmetric grating structures like these rectangular gratings may not be the most efficient structures for light trapping; this is illustrated in Fig. 2. By symmetry, both right- and left-moving diffracted waves are coupled by the grating with equal magnitude.

As a result, a diffracted wave, after undergoing total reflection at the front surface, will impinge

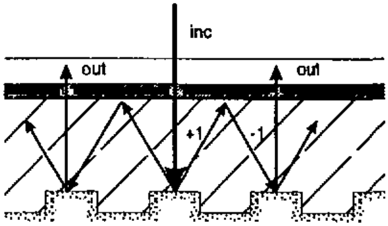

Fig. 2. In a symmetric grating structure $\pm n$th-order modes are excited with equal strength. According to the reciprocity theorem the minus first order (-1) impinging on the grating excites the zero-order outgoing wave (out) in the same way the zero-order incident (inc) couples to the plus first order $(+1)$.

again on the grating, albeit reduced in intensity by the absorption in the Si. In the same way that such a wave is generated by an incoming zero-order wave, according to the reciprocity theorem it will necessarily couple to an outgoing zero-order wave. This therefore limits the performance of the light trapping. This can be avoided by the use of nonsymmetric or blazed grating geometries, as illustrated in Fig. 3. Here we are free to demand that both zero order as well as left-moving reflection orders be suppressed as a result of the precise geometric structure. So, ideally, we are left with right-moving diffracted waves as illustrated in Fig. 3. When such a wave, after total reflection at the front surface, impinges on the grating, there is no *a priori* reason that is has to generate a zero-order outgoing wave such that, at least in principle, perfect light trapping can be achieved, at least for selected wavelengths.

We have examined again, by numerical solution of Maxwell's equations, a large class of blazed grating structures. To simplify the numerical calculations, we choose the staircase type of blazed gratings. The best three-level structure is illustrated in Fig. 4. Its light-trapping qualities are substantially improved over the rectangular grating of Fig. 2, as evidenced in Fig. 5, where the spectrally averaged reflection loss for unpolarized light is shown as a function of the thickness of the Si sheet. Note that for a 40-μm-

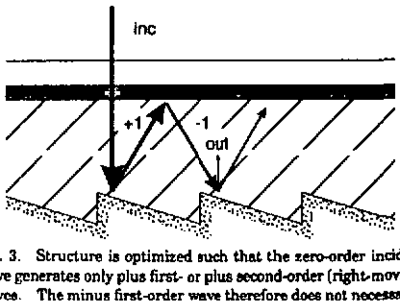

Fig. 3. Structure is optimized such that the zero-order incident wave generates only plus first- or plus second-order (right-moving) waves. The minus first-order wave therefore does not necessarily couple to the zero-order outgoing wave.

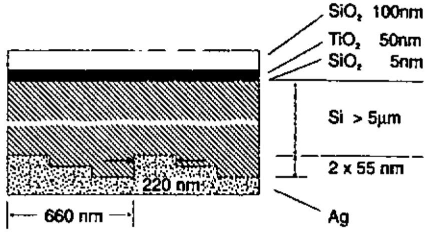

Fig. 4. Optimized staircase approximation to a blazed grating for a thin Si solar cell.

thick cell that incorporates this blazed grating structure, the total reflection loss is just twice the reflection loss of the AR-coated front surface and approximately equivalent to that of a Si cell, with a planar reflector at the back, that is five times thicker. By contrast, the rectangular grating yields an effective optical thickness that is approximately a factor of 3 larger.

To demonstrate these grating effects experimentally, our colleagues at the Paul Scherrer Institute have manufactured blazed grating structures. In Fig. 6(a) we show a scanning electron micrograph of a grating structure in Si, made by ion-beam etching. The manufactured grating structures in Si differ from the calculated structure in two main points: the fabricated sawtooth gratings are not of the staircase type and have an additional SiO_2 layer on the grating, which results during the fabrication process (details of this process will be published elsewhere). We do not know how these differences affect the light trapping. However, the efficiency of a blazed grating structure can be seen from the reflection spectrum for this structure, which is shown in Fig. 6(b).

Here the grating is coated by an Al reflector. The thickness of the Si sheet is 40 μm. This reflection spectrum is compared with that of Si sheets of 60-,

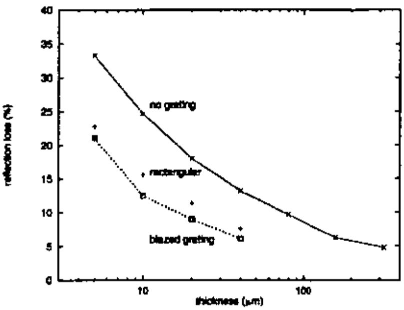

Fig. 5. Reflection loss as a function of Si cell thickness for a cell with a planar reflector (no grating), with a rectangular grating (Fig. 3) and with the staircase grating (blazed grating) of Fig. 4. Note that the reflection loss of the Si surface with a two-layer AR coat is ~2.5%.

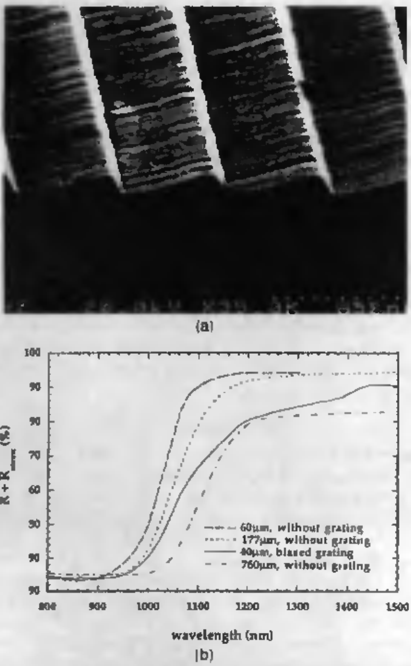

Fig. 6. (a) Scanning electron micrograph picture of a blazed grating in Si with a 660-nm period fabricated by ion-beam etching. (b) Reflection spectrum measured for the grating of (a). The total reflection is the sum of specular reflected (R) and diffuse scattered light (R_{streu}) resulting from surface roughness effects. Note the absence of an AR coating, which leads to a reflection of $\approx 35\%$ for $\lambda \approx 900$ nm. The blazed grating leads to an optically effective thickness that lies between that of a 177-μm and a 760-μm cell with a planar reflector.

177-, and 760-μm thicknesses. As can be seen, the additional light absorption that is due to the blazed grating leads to a marked shift of the reflection edge toward a longer wavelength, and we conclude that the claim of an effective thickness, which should be of the order of five times that of a cell with a planar reflector, is indeed substantiated.

3. Broadband Diffractive Antireflection Structure

In this section we present a BAR structure for solar applications based on a submicron grating and a dielectric overcoat. Figure 7 shows the geometry of the proposed BAR device. The structure is a lamellar surface relief grating embossed in a substrate with a thin dielectric coating deposited on and between the grooves.

The refractive index of the coating is smaller than the index of the substrate. Zero-order gratings are well known to form AR surfaces.[9-15] For a zero-order grating, the period has to be small enough:

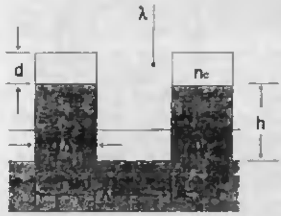

Fig. 7. Geometry of a BAR structure: a lamellar surface relief grating embossed in a substrate with diffraction index n_s. A dielectric coating $n_c < n_s$ is deposited on and between the grating grooves. The period of the grating is Λ, h is the grating groove depth, f is the duty cycle, and d is the thickness of the coating. Calculations were made for normally incident light with wavelength λ between 300 and 2100 nm.

all higher orders of reflection are above cutoff and therefore are evanescent in the interesting wavelength interval between 300 and 2100 nm, outside of which the total solar energy flux amounts to less than 0.3%. This condition can be derived from the grating equation for backward diffraction:

$$\sin \theta_m = \frac{m\lambda}{n_i \Lambda} - \sin \theta_i,$$

where Λ is the grating period, θ_i is the angle of incidence, m is the diffracted order, and θ_m is the corresponding diffraction angle. The refractive index of the medium of incidence is n_i. In our case this medium is air, and therefore, throughout this section, n_i equals 1. The mth backward diffracted order is not propagating if there is no real solution for θ_m, i.e.,

$$|\sin \theta_m| = \left| \frac{m\lambda}{\Lambda} - \sin \theta_i \right| > 1.$$

This is fulfilled for all $m \neq 0$ only if

$$(\lambda/\Lambda) > 1 + \sin \theta_i.$$

If we allow all possible angles of incidence, this means that

$$\Lambda < (\lambda_{\min}/2) = 150 \text{ nm}.$$

This is a small period that is difficult to fabricate in practice. Larger grating periods are easier to fabricate but reflect parts of the flux in higher orders. As a compromise we have chosen 250 nm as the grating period, which can be readily realized with holographic techniques by the use of a visible laser (e.g., a HeCd laser at $\lambda = 442$ nm).

As the grating substrate we take polycarbonate (PC) for our calculations. We assume a constant refraction index of 1.586. It is part of the optimization procedure to determine the optimal grating groove depth and duty cycle.

This grating is now combined with a dielectric coating. This leads to a structure that can be interpreted as a three-level grating.

A. Results of the Rigorous Calculations

We use the numerical method described in Ref. 8 to solve Maxwell's equations to calculate the optimal parameters for BAR. During the optimization, the grating period is kept fixed at 250 nm. The reflection characteristics of the BAR structure are then calculated for various grating depths, duty cycles, and coating thicknesses. For a pure lamellar grating in a PC substrate, the optimum AR performance results for a duty cycle of 0.45 and a grating groove depth of 130 nm. This grating reflects 1.46% of normally incident energy flux of unpolarized light. The optimal BAR composed of an overcoated grating has the same duty cycle but, with $h = 170$ nm, is considerably deeper. If this grating is coated with 100-nm MgF_2, less than 0.52% of the normal incident solar flux between 300 and 2100 nm is reflected from the surface. It is not possible to treat the coating and the grating structure in an independent manner. Nevertheless, as calculations show, the best coating thickness for a BAR turns out to be rather independent of the grating depth and its duty cycle. Figure 8 shows the results of calculations for different values of d.

The best duty cycle turns out to be 0.45 for an optimal grating depth of 170 nm. Those two values cannot be optimized independently.

These results should be compared with those one can get with unstructured dielectric BAR multilayers. With simulated thermal annealing[18] we optimized two different systems: First, we allowed up to eight layers in a system of sequences of MgF_2 ($n = 1.38$) and CaF_2 ($n = 1.25$). The optimization resulted in an AR system consisting of only two layers.

The second system consisted of four coating materials: MgF_2 ($n = 1.38$), cryolite ($n = 1.35$), BaF_2 ($n = 1.3$), and CaF_2 ($n = 1.25$). Simulated thermal annealing eliminated cryolite and BaF_2 by reducing their thicknesses to 0. The optimization of both systems leads to the identical system of two coatings and gives an average reflectivity of 0.95%, which is almost a factor of 2 above the reflectivity of our BAR structure. Although these are real coating materials, their physical and chemical properties cause problems in the realization of such an AR coating. With conventional materials for AR coatings such as SiO_2, Al_2O_3, Ta_2O_5, or TiO_2 together with MgF_2, we were not able to find a solution for which the average reflection can be reduced below 1%.

B. Discussion of the Tolerances

From the theoretical point of view the possibility of combining two different sources of low reflectivity to a BAR device is interesting. The desire to confirm this experimentally and use it for commercial applications makes it necessary to examine the tolerances one needs in view of experimentsl uncertainties.

A grating with a period of 250 nm can be produced accurately by holographic techniques, as described in Ref. 19. The correct duty cycle is more difficult to realize. Figure 9 shows that E polarization and H polarization have their minimum average reflectivity at different duty cycles. This corresponds to the birefringence properties of such high-frequency gratings. Note that for E-polarized light the average reflectivity can be as small as 0.37% for a duty cycle of $f = 0.35$. A minimum average reflectivity of 0.52% for H-polarized light is given for $f = 0.55$. For unpolarized normal incident light both polarizations contribute to an equal amount to the average reflectivity for a given duty cycle. The decrease of reflectivity for one polarization and increase for the other one in the duty cycle interval between the minima almost cancel each other for unpolarized light. Therefore the average reflectivity has a flat minimum as a

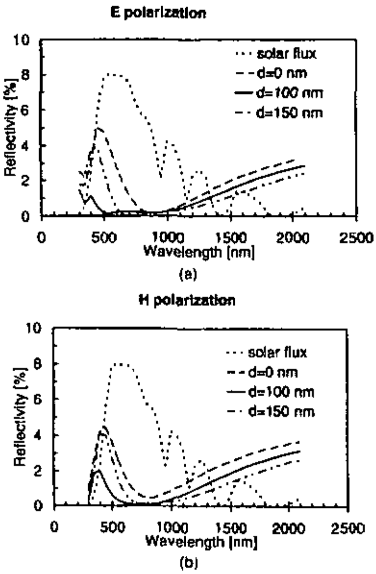

Fig. 8. Effect of a dielectric coating on a lamellar grating for (a) E polarization, (b) H polarization. We also show the incident solar energy flux in arbitrary units as a function of wavelength.

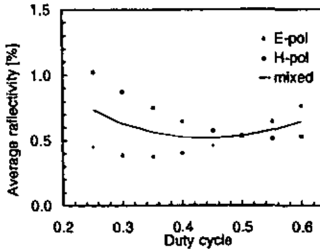

Fig. 9. Average reflectivity of a BAR as a function of the duty cycle for E and H polarizations and unpolarized light. The grating depth is 170 nm, and the coating thickness is 100 nm.

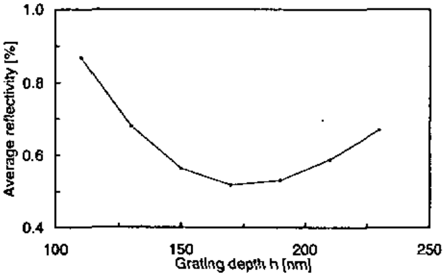

Fig. 10. Average reflectivity of a BAR as a function of the grating depth. The duty cycle is 0.45, and the coating thickness is 100 nm.

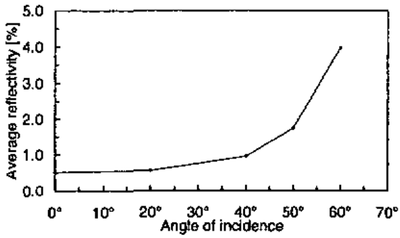

Fig. 12. Average reflectivity as a function of the angle of incidence. The BAR optimized for normal incidence reflects up to ±40° less than 1% of the incoming solar flux.

function of the duty cycle, and thus no very accurate control is needed. We get an average reflectivity below 0.6% for a duty cycle between 0.35 and 0.5. From the experimental point of view this is a reasonable range.

In most cases, depth h of the grating is controlled by an etching technique. Figure 10 shows the average reflectivity as a function of the grating depth. Minimum reflectivity is reached for $h = 170$ nm; within the interval of 150 to 200 nm it is less than 0.6%. Neither the duty cycle nor the grating depth should lead to experimental problems. Electroplating of this structure gives a shim that can be used for embossing the desired grating in PC. By means of this technique, PC grating surfaces can be mass produced very cheaply.

As a last step these PC gratings have to be coated with a dielectric coating by a directional deposition technique such as evaporation. This process can be realized in mass production. The thickness of the coating can be controlled experimentally with relatively high accuracy. Nevertheless Fig. 11 shows that between 90 and 110 nm the average reflectivity is less than 0.56%.

The BAR structure was optimized for normal incidence. In solar converters that use additional optics such as reflectors, part of the incoming flux does not

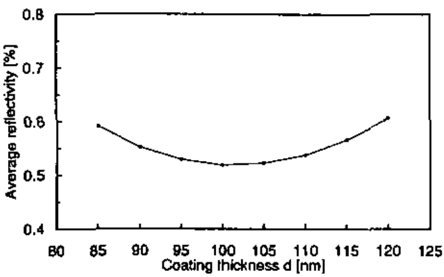

Fig. 11. Average reflectivity of a BAR as a function of coating thickness d. The duty cycle is 0.45, and the grating depth is 170 nm.

fall perpendicularly on the surface. Figure 12 shows the average reflectivity as a function of the angle of incidence. The angular dependence is very weak up to angles of $\Delta\theta_i \approx \pm 40°$, with less than 1% of the incoming flux being specularly reflected. For angles of incidence of $\Delta\theta_i > 10°$, higher-order reflected waves are generated; however, their contributions to the average reflectivity are negligible.

It can be stated that for all critical experimental parameters of a BAR structure, such as duty cycle, grating depth, and coating thickness, the calculations show that tolerances are fairly large to deviations from the optimal values. The use of PC as a substrate opens the way to mass production, which fulfills the low-cost condition for the large areas of photothermal or PV converters. Instead of PC, other embossable substrate materials such as polyvinyl chloride or poly(methyl methacrylate) may be used for BAR structures.

Solar cells of the type described in Section 2 have to be protected with glass. This leads to one or more glass–air interfaces that would benefit from an optimized BAR structure. In the relevant spectral range (380–1200 nm), the integrated loss is 0.32% in this case. Note that for PV use, the appropriate weighting is the spectral photon flux, as the number of electron-hole pairs generated inside the PV cell is not proportional to the incident energy flux but to the number of photons. Reflection loss that is due to the glass–air interface is then reduced by a factor of 10. The total reflection loss of a 10-μm-thick solar cell (see Fig. 8) without a blazed grating protected by glass (two interfaces) amounts to ~30%. Using BAR structures for both glass–air interfaces and a blazed grating for light trapping in Si reduces the reflection loss to ~13%.

To conclude, we have presented two types of submicron diffraction gratings for use in solar energy applications, one a blazed grating designed to improve the optical absorption in thin Si solar cells, the other a BAR structure comprising a surface relief grating combined with a dielectric overcoat.

R. H. Morf has benefited from many stimulating discussions with his late advisor, Guenther Harbeke. The authors are grateful to M. T. Gale and K. Knop in our laboratories and to H. Rudigier of Balzers AG for numerous discussions. The experimental part of the work was done by our colleagues at the Paul Scherrer Institute, Zurich: (in alphabetical order) H. Birbaumer, B. Curtis, H. Kiess, H. Schütz, H. Siegwart, and A. Vonlanthen. Financial support by the Bundesamt für Energiewirtschaft is gratefully acknowledged. C. Heine gratefully acknowledges financial support from Balzers AG.

References

1. D. Strese und J. Schindler, "Kostendegression Photovoltaik: Fectigung multikristalliner Solarzellen und ihr Einsatz im Kraftwerksbereich," Rep. 0328830A (Bundesminister für Forschung und Technik, Bonn, Germany, 1988). A short review can be found in Bild Wiss. (July 1988), p. 36.
2. H. J. Hovel, *Solar Cells*, Vol. II of the Semiconductor and Semimetals Series (Academic, New York, 1975), p. 97.
3. P. Campbell and M. A. Green, "Light trapping properties of pyramidally textured surfaces," J. Appl. Phys. **62**, 243–249 (1987).
4. D. Redfield, "Multiple-pass thin film silicon solar cell," Appl. Phys. Lett. **26**, 647–648 (1974).
5. A. Goetzbergrr, "Optical confinement in thin Si solar cells by diffuse back reflectors," in *Proceedings of the Fifteenth IEEE Photovoltaic Specialists' Conference* (Institute of Electrical and Electronic Engineers, New York, 1981), p. 867.
6. E. Yablonovitch, "Statistical ray optics," J. Opt. Soc. Am. **72**, 899–907 (1982).
7. H. P. Herzig, M. T. Gale, H. W. Lehmann, and R. Morf, "Diffractive components: computer generated elements," in *Perspectives for Parallel Optical Interconnects*, P. H. Lalanne and P. Chavel, eds. (Springer, New York, 1993) Chap. 5, pp. 71–107.
8. R. H. Morf, "Exponentially convergent and numerically efficient solution of Maxwell's equations for lamellar diffraction gratings," J. Opt. Soc. Am. A (to be published).
9. R. C. Enger and S. K. Case, "Optical elements with ultrahigh spatial-frequency surface corrugations," Appl. Opt. **22**, 3220–3228 (1983).
10. D. Raguin and G. M. Morris, "Antireflection structured surfaces for the infrared spectral region," Appl. Opt. **32**, 1154–1167 (1993).
11. D. Raguin and G. M. Morris, "Analysis of antireflection-structured surfaces with continuous one-dimensional surface profiles," Appl. Opt. **32**, 2582–2598 (1993).
12. T. K. Gaylord, W. E. Baird, and M. G. Moharam, "Zero-reflectivity high spatial-frequency rectangular-groove dielectric surface-relief gratings," Appl. Opt. **25**, 4562–4567 (1986).
13. E. N. Glytsis and T. K. Gaylord, "High-spatial frequency binary and multilevel stairstep gratings: polarization-selective mirrors and broadband antireflection surfaces," Appl. Opt. **32**, 4459–4470 (1992).
14. M. E. Motamedi, W. H. Southwell, and W. J. Gunning, "Antireflection surfaces in silicon using binary optics technology," Appl. Opt. **31**, 4371–4376 (1992).
15. D. L. Brundrett, E. N. Glytsis, and T. K. Gaylord, "Homogeneous layer models for high-spatial-frequency dielectric surface-relief gratings: conical diffraction and antireflection designs," Appl. Opt. **33**, 2695–2706 (1994).
16. L. C. Botten, M. S. Craig, R. C. McPhedran, J. L. Adams, and J. R. Andrewartha, "The dielectric lamellar grating," Opt. Acta **28**, 413–428 (1981); "The finitely conducting lamellar diffraction grating," Opt. Acta **28**, 1087–1102 (1981).
17. R. H. Morf and H. Kiess, "Submicron gratings for light trapping in silicon solar cells: a theoretical study," in *Proceedings of the Ninth International Conference on Photovoltaic Solar Energy*, W. Palz, ed. (Commission of the European Communities, Brussels, Belgium, 1989), pp. 313–316.
18. R. Morf and R. E. Kunz, "Dielectric filter optimization by simulated thermal annealing," in *Thin Film Technologies III*, K. H. Guenther, ed., Proc. Soc. Photo-Opt. Instrum. Eng. **1019**, 211–217 (1988).
19. R. E. Kunz, J. Edlinger, B. J. Curtis, M. T. Gale, L. U. Kempen, H. Rudigier, and H. Schütz, "Grating couplers in tapered waveguides for integrated optical sensing," in *Chemical, Biochemical, and Environmental Fiber Sensors V*, R. A. Lieberman, ed., Proc. Soc. Photo-Opt. Instrum. Eng. **2068**, 313–325 (1994).

Paper III

JOURNAL OF MODERN OPTICS, 1996, VOL. 43, NO. 7, 1371–1377

Coated submicron gratings for broadband antireflection in solar energy applications

C. HEINE, R. H. MORF, and M. T. GALE

Paul Scherrer Institut Zürich, Badenerstrasse 569, CH-8048 Zürich, Switzerland

(*Received 7 November 1995*)

Abstract. Experiments demonstrating the broadband antireflection performance of MgF_2-coated surface-relief gratings in polymer foil are discussed. The measured mean reflectance was as low as 0·6% for the wavelength range of 400 to 1500 nm. As a consequence, the transmission losses at the glass surface of a solar energy device can be reduced from about 7·5% to 3·1%, averaged over the day. The coated gratings are more stable against heat than bare surface gratings and the MgF_2 coating also exhibits better adhesion to the structured surface than it does to the plane surface.

1. Introduction

In most solar energy applications, one or more glass protection layers represent the entrance gate for the incoming photons. Reflections at the outer air/glass interface not only reduce the efficiency of the solar device but can also result in a visual brightness which in many applications is not acceptable or even dangerous. It is therefore worthwhile searching for cheap possibilities to minimize these reflections. Efficient and stable antireflection coatings are available for the visible region as well as for the infrared [1]. Problems arise if antireflection is required over a very broad wavelength region, such as in solar energy applications. This is because of the lack of stable thin film materials with a small index of refraction. The approach of achieving artificial low-index materials by structuring the surface periodically on a subwavelength scale is a recent and active field of interest [2–8]. Early investigations on artificial moth-eye structures were carried out by Wilson and Hutley [9]. These structures have excellent antireflection properties, but have to be rather deep for very broad wavelength performance. Recent publications address the question how this depth can be reduced by choosing the proper grating profile shape [10, 11]. Unfortunately little has been published on the fabrication of such gratings.

Recently, we proposed the use of coated subwavelength gratings for such applications in [12]. The gratings have a period of the order of the wavelength of light and an easily fabricated rectangular profile. We are thus not in the regime where the concept of an artificial refractive index holds. We have found that such structures allow excellent broadband antireflection. Detailed calculations, based on the rigorous diffraction theory described in [13], show that these structures also exhibit acceptable tolerances with respect to geometric imperfections.

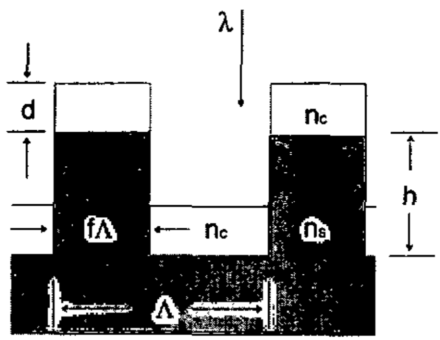

Figure 1. Geometry of a BAR structure: a lamellar surface relief grating (substrate index n_s) and a dielectric coating (index $n_c > n_s$) deposited on and between the grating grooves. The period of the grating is Λ. h is the grating groove depth, f is the duty cycle, and d is the thickness of the coating.

2. Coated grating geometry and fabrication

The structure for solar broadband antireflection (BAR) proposed in [12] is a lamellar surface-relief grating embossed in a substrate with a thin dielectric coating on and between the grooves. Figure 1 shows schematically the geometry of the BAR device. Note that the refractive index of the coating is smaller than the index of the substrate. The adjustable parameters of this device are the grating period Λ, the grating depth h, the duty cycle f and the coating thickness d. We use polycarbonate (PC) as a substrate material ($n = 1{\cdot}59$) into which the gratings can be embossed. In view of mass production and stability aspects, a ratio of the grating ridge to the grating depth (aspect ratio) close to one is favourable. Our calculations show that the duty cycle f has to be close to 0·5 and the optimum grating depth h is about 170 nm. This is independent of the exact grating period. With such a duty cycle and grating depth the grating period of 340 nm leads to the desired aspect ratio 1. Note that with such a grating period, no higher reflected orders appear for normal incident sunlight. For the dielectric coating, we use MgF_2 ($n = 1{\cdot}38$) which is a standard material for antireflection coatings.

The grating fabrication is performed in three steps. First the embossing shim is fabricated. In a second step the grating is embossed into the PC substrate and in a third step the structured surface is coated with MgF_2.

The Ni shim containing a grating with a period of 340 nm can be fabricated by holographic techniques. The two-beam interference pattern from a HeCd laser ($\lambda = 442$ nm) is used to expose a photoresist film on a quartz substrate. With the help of this grating mask, reactive ion etching is used to etch an approximately rectangular profile into the quartz substrate. The appropriate grating depth is more important than the correct profile shape because deviations from the rectangular shape do not deteriorate the antireflection properties. The Ni shim is obtained by electroplating the structured quartz surface in a Ni bath [14]. In solar applications where the PC foil is in direct contact with the light absorbing medium such as the cover sheet of a solar cell or converter, just one side has to have coated gratings. The reflection measurements are carried out on such a structure. In applications where both the front and back side contribute, such as greenhouses, a sandwich

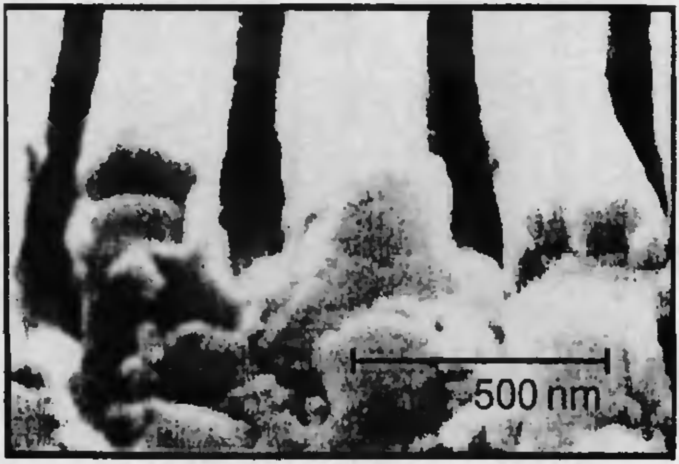

Figure 2. Scanning electron micrograph picture of a grating with a 340 nm period and a 100 nm thick MgF_2 coating. The apparent bad quality of the SEM micrograph is due to the difficulty to obtain a well defined cross-section of polycarbonate.

embossing technique with two shims is used. The transmission measurements were carried out on devices fabricated in this way. The coatings of the gratings with MgF_2 is straightforward. The distance between evaporation source and PC substrate has to be large enough in order not to destroy the grating by heating. The required tolerance of 10% in a coating thickness of 100 nm can easily be met. Figure 2 shows an SEM micrograph of a coated grating on a PC substrate.

3. Reflectivity of coated gratings

We have measured the reflectivity of the structured and/or coated surfaces of PC foils for normal incident light in the wavelength interval of interest from 400 to 1500 nm. The backside of the devices was roughened and blackened to eliminate its influence on the reflection measurements. Figure 3 shows the reflectivity for E-polarized light as a function of the wavelength for four different kinds of surfaces on the PC substrate. The broken line corresponds to the untreated PC surface. The continuous lines are the measured reflectivities of the PC substrate with a MgF_2 coating (thin line), with a bare grating (medium line) and with a coated grating (thick line). The coated grating has, for unpolarized light between 400 and 1000 nm, an absolute reflectance below 1%. Weighted with the solar energy spectrum, the measured mean reflectance was 0·6%.

Note that these fabricated gratings, with a depth of only 140 nm (in constrast to the calculated optimal depth of 170 nm), still show good AR performance. The crosses indicate calculated values of a lamellar bare grating with $\Lambda = 340$ nm period, $h = 140$ nm grating depth and a duty cycle of $f = 0{\cdot}52$. The measured reflectance could not be fitted with h and f as fit parameters. Our fabricated gratings show better antireflection performance than the calculations predict, which indicates that deviations from the rectangular profile as well as dispersion effects of the PC material may need to be treated in a more thorough way.

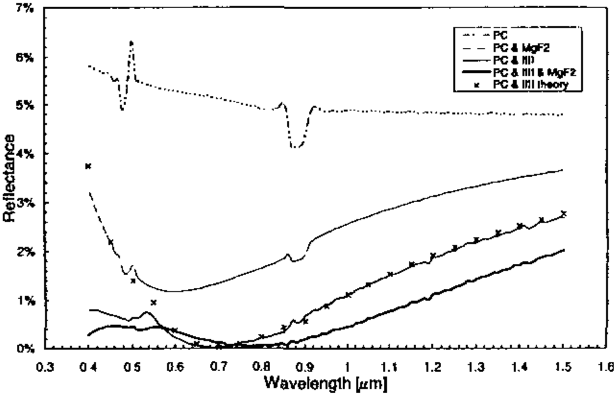

Figure 3. Measured reflectivity for E-polarized light at normal incidence. The broken line corresponds to the untreated PC surface. The continuous lines are the measured reflectivities of the PC substrate with a MgF_2 coating (thin line), with a bare grating (medium line) and with a coated grating (thick line). The crosses indicate calculated values of a bare grating with 140 nm grating depth.

4. Transmission of coating gratings

Efficiency considerations for solar energy applications lead to the question of how much of the incident light is really transmitted to the absorbing medium. Our structure is optimized for normal incidence. The angle at which sunlight is incident on the surface changes during the day. It is therefore interesting to know the transmission performance of the surface structure for obliquely incident light. We have a grating period of 340 nm. This means that for non-conical incidence, higher orders of backward diffraction can appear at rather small angles. In contrast this is not the case if the plane of incidence is parallel to the grating grooves (perpendicular to the grating vector). This can be realized during the whole day if the solar panel is fixed on a paraxial mount with the grating grooves well oriented, schematically shown in figure 4. Note that we have this advantage because of using one-dimensional gratings. Such a mount is not possible for two-dimensional submicrometre surface profiles.

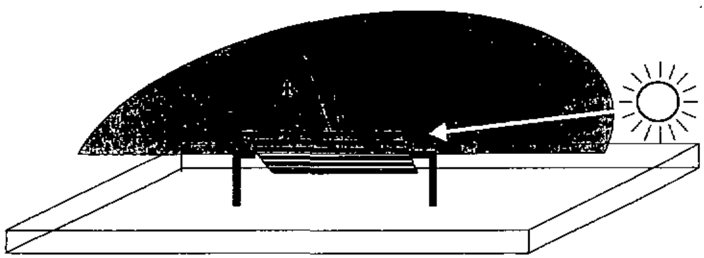

Figure 4. Paraxial mount of a solar panel with the grating vector **K** perpendicular to the plane of incidence. As a result no higher orders of reflection appear during the whole day.

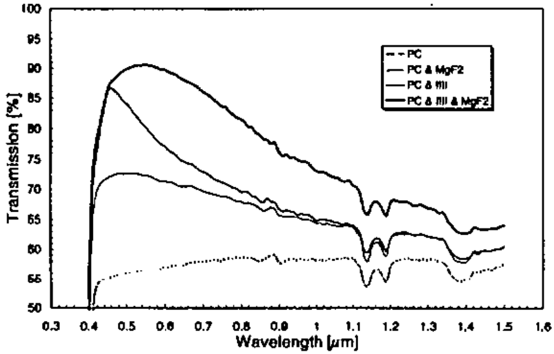

Figure 5. Measured transmission as a function of wavelength of light for E-polarization and an angle of incidence of 70° (grating vector **K** perpendicular to the plane of incidence). The broken line corresponds to the untreated PC surfaces. The continuous lines correspond to the PC substrate with MgF_2 coatings (thin line), with bare gratings (medium line) and with coated gratings (thick line) on both sides.

Figure 5 shows the transmission as a function of wavelength of light for E-polarization and an angle of incidence of 70° (plane of incidence perpendicular to the grating vector). The transmission of the untreated PC foil is represented by the broken line. The continuous lines correspond to the transmission when both sides are MgF_2-coated (thin line) or gratings are embossed (medium line) and coated (thick line). Note that for the wavelength $\lambda = 580$ nm, which corresponds to the energy maximum of the solar spectrum, the transmission is increased by more than 30% compared to the untreated PC foil. Figure 6 shows the measured percentage of lost photons of the sunlight as a function of angle of incidence for

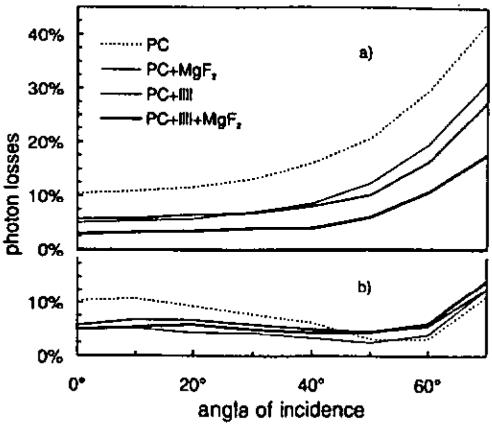

Figure 6. Measured percentage of lost photons of the sunlight as a function of angle of incidence (*a*) for E-polarization and (*b*) for H-polarization. The grating vector **K** was perpendicular to the plane of incidence. Note that up to 40° the angular dependence is weak.

both polarizations. Averaged over the day for an untreated PC foil, about 14% of the photons are lost due to reflection losses. Those losses are reduced to 6% with coated gratings on both sides. Calculated back to one interface the loss of 7·5% with a plane PC is reduced to 3·1% with a coated grating.

5. Stability considerations

The reduction of reflection with coated gratings works very well under clean laboratory conditions. However, if the device is to be used in the 'real world' it has to be stable against atmospheric and thermal influences. In order to compare the adhesion of the MgF_2 coating on plane and structured surfaces, we applied the Scotch test described in [15]. The coated grating is not impaired and there is no significant decrease in the transmission signal. In contrast the thin MgF_2 film on the plane PC surface is completely destroyed. As a qualitative result we know that the MgF_2 adhesion to PC is improved by structuring the surface.

We also put the coated gratings together with the bare gratings on a hot plate and tempered them to test their resistance to heat. The bare gratings disappear at a temperature of 170°C due to surface tension forces, whereas the coated grating is stable and keeps its antireflection properties up to a temperature of 200°C (measured on the surface of the hot plate). At higher temperatures the surface becomes diffuse but even heating up to 300°C does not destroy the grating completely.

In a preliminary test we put coated gratings on the outside of a car windscreen for two weeks. Measurement of the reflectivity shows that driving several hundred kilometres through sunny as well as rainy weather did not attack the structure in a serious way.

6. Conclusions

In this paper we have presented experimental results on our investigations on coated submicrometre gratings. We have focused on their broadband antireflection characteristics for solar energy applications. Reflection and transmission measurements show that with such a treatment of the surface, the photon losses due to reflection are reduced by at least 3% compared to the untreated surface. The coating gratings are also more resistant to heat compared to bare gratings and the MgF_2 coating exhibits a better adhesion to the PC substrate than MgF_2 film on a plane unstructured substrate. Coating gratings can thus be using normal procedures without affecting their good transmission characteristics.

The coated gratings themselves reduce the unwanted (and sometimes dangerous) visual brightness of solar panels by a factor of ten for normal incidence. If this is not sufficient, superimposed macroscopic textures of the surface (on a millimetre scale) can diffuse the remaining part of the incoming light which does not enter the device. The angular dependence of the reflectance of the coated gratings is weak up to about 40°, so that these textures do not give rise to significantly higher reflection losses.

The lifetime of such a coated grating is still an open question. Nevertheless, the tests described above such as the Scotch test, heating and some preliminary lifetime tests, give good reasons to be optimistic.

Acknowledgments

The authors are grateful to K. Knop in our laboratories and to H. Rudigier of Balzers AG for helpful discussions. We thank our colleagues at Paul Scherrer

Institute Zürich for their contributions. Special thanks go to R Stutz for his very important assistance in the various fabrication steps. C. Heine gratefully acknowledges financial support from Balzers AG.

References

[1] MACLEOD, H. A., 1986, *Thin-film Optical Filters*, second edition (New York: Macmillan).
[2] RAGUIN, D., and MORRIS, G. M., 1993, *Appl. Optics*, **32**, 1154.
[3] RAGUIN, D., and MORRIS, D., 1993, *Appl. Optics*, **32**, 2582.
[4] GAYLORD, T. K., BAIRD, W. E., and MOHARAM, M. G., 1986, *Appl. Optics*, **25**, 4562.
[5] GLYTIS, E. N., and GAYLORD, T. K., 1992, *Appl. Optics*, **32**, 4459.
[6] MOTAMEDI, M. E., SOUTHWELL, W. H., and GUNNING, W. J., 1992, *Appl. Optics*, **31**, 4371.
[7] ENGER, R. C., and CASE, S. K., 1983, *J. opt. Soc. Am.*, **73**, 1113.
[8] ONO, Y., KIMURA, Y., OHTA, Y., and NISHIDA, N., 1987, *Appl. Optics*, **26**, 1142.
[9] WILSON, S. J., and HUTLEY, M. C., 1982, *Optica Acta*, **29**, 993.
[10] GRANN, E. B., MOHARAM, M. G., and POMMET, D. A., 1995, *J. opt. Soc. Am.* A, **12**, 333.
[11] SOUTHWELL, W. H., 1991, *J. opt. Soc. Am.* A, **8**, 549.
[12] HEINE, C., and MORF, R. H., 1995, *Appl. Optics*, **34**, 2476.
[13] MORF, R. H., 1995, *J. opt. Soc. Am.* A, **12**, 1043.
[14] MENZ, W., and BLEY, P., 1993, *Mikrosystemtechnik für Ingenieure* (Weinheim: VCH Verlagsgesellschaft mbH).
[15] PULKER, H. K., 1985, *Coatings on Glass, Thin Films Science and Technology*, 62nd imprint (Amsterdam: Elsevier).

Paper IV

Submicron gratings with dielectric overcoat: performance and stability

C. Heine R. H. Morf and M. T. Gale

Paul Scherrer Institute
Badenerstrasse 569, CH-8048 Zürich, Switzerland
Tel. +41 1 492 63 50   Fax +41 1 491 00 07

1. Introduction

Submicron gratings show increasing potential in applied optics, often presenting attractive alternatives to thin film technology solutions. Gratings on light-weight plastic materials can replace heavy and expensive glass devices. Embossing techniques can be used for cheap mass production. The coating of gratings with thin films leads to additional degrees of freedom for component design. For practical applications, it is important not only to investigate the possibilities of such structures, but also the limiting factors such as fabrication considerations and stability properties.

In the first part of this paper we discuss stability aspects of surface-relief submicron grating structure overcoated with a thin dielectric film. Measurements on a broadband antireflection structure are presented. We also give an interpretation of the results of our measurements. The second part describes an experiment which shows that the symmetry of the grating can strongly be influenced using directional evaporation. In the third part we propose a new kind of polarizer and discuss fabrication possibilities.

High frequency surface-relief gratings can exhibit broadband antireflection characteristics. This has been investigated over several years in theoretical [1] as well as experimental [2,3] work. Recently, we reported on the realization of a broadband antireflection (BAR) structure for solar energy applications [4,5]. It consists of a lamellar surface grating in a polycarbonate (PC) substrate with a dielectric thin film overcoat. Coating the grating structure with a thin MgF_2 layer is one essential step to achieve the excellent broadband antireflection performance shown by these devices. A practical problem is that for evaporating MgF_2, the best coating results are obtained when the substrate temperature is relatively high, ~200°C [6]. At this temperature PC starts to flow and the gratings disappear due to surface forces. The dielectric has therefore to be deposited on the cold PC substrate and the mechanical properties have to be investigated.

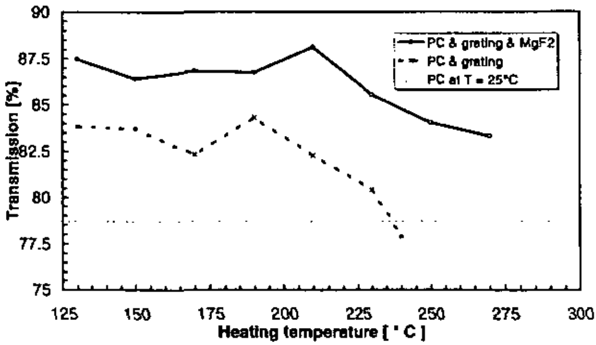

Fig. 1: Measured transmission of bare and MgF_2 coated gratings after heating. The angle of incidence was 45° and the measurement wavelength 800 nm. Coated gratings not only have better antireflection performance but are also stable up to higher temperatures.

2. Stability of thin film coated gratings

a) Temperature:

We have investigated the stability of bare surface gratings and the BAR structures as a function of temperature. Only the front side of the devices was structured. The transmission performance was measured before and after tempering them for several minutes on a hot plate, with a small distance between hot plate and PC-foil in order to avoid separation problems. The temperatures given correspond to the temperatures at the hot plate.

Figure 1 shows the measured transmission of E-polarized light (E-vector perpendicular to grating vector) for an angle of incidence of 45°. The transmission of the device with the bare grating starts to decrease at temperatures higher than 190°C (measured on the hot plate). This coincides with a disappearance of the grating as visible to the naked eye. The MgF_2 coated structure not only shows better transmission, but also withstands significantly higher temperatures. The coating appears to stabilize the grating which, in contrast to a bare grating, does not disappear. At higher temperatures, parts of the polycarbonate started to become dull.

b)Adhesion:

The evaporation of MgF_2 was performed on the cold substrate. In order to test adhesion on the surface, we used the tape test, applying a strip of adhesive tape to the surface and removing it again [5]. Figure 2 shows the measured transmission for E-polarized light at normal incidence. Shown is the transmission as a function of wavelength for coated, structured PC-foils (continuous line and dots) and coated unstructured PC-foils (cross symbols). Measurements were performed before applying the tape test and afterwards. For the unstructured but MgF_2 overcoated PC-foil, we see that the transmission is the same as for the uncoated PC-foil (broken line) - the MgF_2 coating was completely lifted off. For the structured PC foils, the tape test had no significant effect on the transmission performance. This can be explained by the roughness of the surface on a scale which does not give rise to straylight, but helps to improve MgF_2-PC adhesion. In addition, the structure may relax the intrinsic tensions at the boundary of the two materials and thus lead to higher stability.

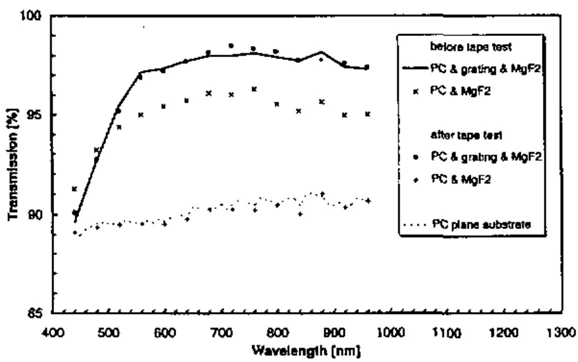

Fig. 2: Transmission of coated substrates before and after tape test. The measurements show that MgF_2 deposited on cold unstructured substrates is lifted off the surface when a tape test is applied, leading to a significant reduction in transmission. By contrast, the test applied on coated gratings did not have an effect on the transmission performance. The MgF_2-films adheres well to the structured substrate.

c) Conclusion: The experiments show that:

- a grating in PC is (temperature) stabilized by a thin film coating of MgF_2.
- MgF_2 shows better adhesion to the substrate if the latter is structured.

This can be important for applications in optics in two very different ways. The first point opens the possibility to apply antireflection structures onto substrates by hot transfer ("melting"), including application onto curved substrates such as lenses. We have 'melted' thick PC-foils (up to now without BAR-structure) on BK7 glass and were not able to separate them without damaging the glass surface. The second point opens the possibility to coat substrates which may not be heated. Provided there is possibility to etch a submicron grating structure into this substrate, thin films evaporated onto the cold substrate cab be expected to exhibit good adhesion.

The BAR-structures are intended to be used outdoors for solar energy applications. Handling the tempered devices gave us the impression that the MgF_2 coating stability is increased after tempering them up to 210°C. This can be due to a better contact between substrate and coating as it is the case when MgF_2 is deposited on hot substrates. The tempered structures are also less sensitive to finger prints. An exposure of the structures to extreme weather conditions over several months will give insight in medium range lifetime properties.

3. Non-symmetric gratings:

Light coupling and light trapping are two other interesting applications for submicron gratings. Depending on the application, it is favorable to use non-symmetric- rather than symmetric gratings. Light which couples into diffraction orders will be totally reflected at the surface opposite to the structure and impinge again on the grating. According to the reciprocity theorem, part of the light will couple to an outgoing zero order wave. This effect limits the coupling efficiency. The effect can be reduced with a nonsymmetric grating geometry such as blazed gratings. Light trapping in solar cells was improved by use of such structures [4]. A nonsymmetric grating (see inset of Figure 3)can be realized by means of directional evaporation of a dielectric at an angle not perpendicular to the grating surface. *Using rigorous calculations*, we found grating geometries having a high ratio of the first transmission orders (T_{+1}/T_{-1}).

In order to demonstrate this effect, we coated the PC-gratings in such a way on both the front and the backside of the PC-foil (see Figure [3] inset). The transmission measurements were performed with light incident at an angle of 45° (plane of incidence parallel to the grating vector). The second measurement was taken after turning the grating by 180° around an axis normal to the surface. This introduces no difference for a symmetric grating. By contrast, we measured a strong coupling effect not found in the first measurement (see Figure 3). This can only be explained by the introduced asymmetry of the coating.

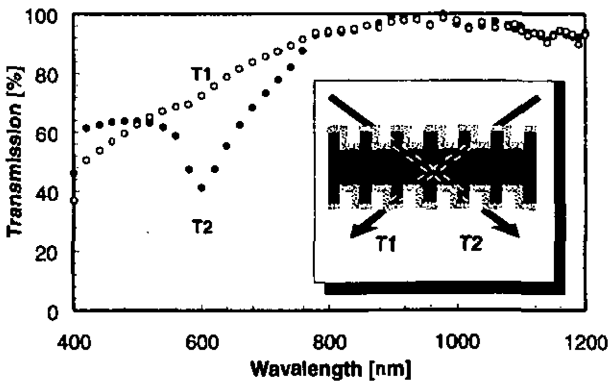

Fig. 3: Transmission spectrum for asymmetric grating structure. T1 and T2 are the measured spectra for off-axis illumination upon rotating the grating by 180°.

4. Other types of thin film coated gratings:

The use of high frequency gratings is a well known approach to realize polarizing components. We propose a dielectric polarizer based on submicron gratings and materials commonly used in thin film technology. It consists of a TiO_2 grating on a SiO_2 substrate, overcoated with MgF_2 (Figure 4, inset). The outer MgF_2/air grating will act as antireflection grating for the H-polarization and improve the polarizer's performance. It is surprising to find that the polarizing performance is excellent for a wavelength at which the first order of transmission is already evanescent and the first order of reflection just starts to be non-propagating. Therefore, moderate grating periods have to be used, which can be realized by holographic techniques. It is clear that in this region, rigorous diffraction theory has to be used to calculate the efficiencies. Figure 4 shows the transmission for the H-polarization (H-vector perpendicular to grating vector) as well as the inverse polarization contrast ratio (inverse PCR) which is the ratio of the transmitted energy of H- and E-polarization. The calculations were performed with the method described in Ref. [7]. Note that solely the grating period, which can be realized very accurately, determines the wavelength of optimum polarization performance.

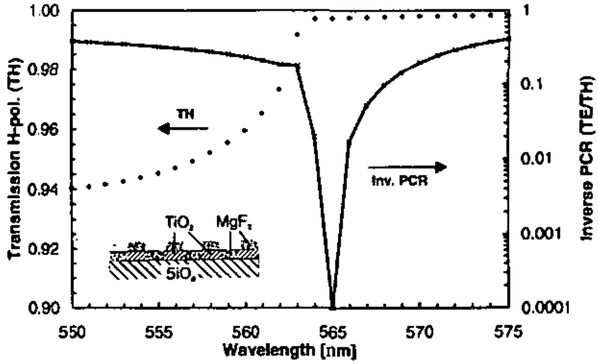

Fig 4: With usual thin film materials and the appropriate grating period an excellent polarizer can be realized, as rigorous calculations show.

5. Conclusions

Thin dielectric films on submicron gratings present a simple and effective possibility to manipulate their optical properties such as reflectivity, polarization selectivity or symmetry of coupling to diffraction orders. Our tests on BAR-structures showed that mechanical properties of microstructures on polycarbonate can be significantly improved by the additional thin film coating. Similarly, adhesion of coating materials to the substrate can be improved by structuring the substrate.

References

[1] E. B. Grann, M. G. Moharam, and D.A. Pommet, "Optimal design for antireflection tapered two-dimensional subwavelength grating structures", *J. Opt. Soc. Am. A.* **12**, 333-339, (1995).

[2] S.J. Wilson and M.C. Hutley, "The optical properties of 'moth eye' antireflection surfaces", *Opt. Act.*. **29**, 993-1009, (1982).

[3] R. C. Enger and S. K. Case, "High-frequency holographic transmission gratings in photoresist", *J. Opt. Soc. Am.* **73**, 1113-1118, (1983).

[4] C. Heine and R.H. Morf, "Submicrometer gratings for solar energy applications", *Appl. Opt.* **34**, 2476-2482, (1995).

[5] C. Heine, R.H. Morf, and M.T. Gale, "Coated submicron gratings for broadband antireflection in solar energy applications", *submitted to J. Mod. Opt in October1995.*

[6] H.A. Macleod, "Thin-Film optical Filters", 2nd ed., p 390 *(Macmillan, New York, 1986).*

[7] R. H. Morf, "Exponentially convergent and numerically efficient solution of Maxwell's equations for lamellar gratings", *J. Opt. Soc. Am. A.* **12**, 1043-1056, (1995).